

Metal Nanowires: Synthesis, Processing, and Structure-Property Relationships in the
Context of Flexible Transparent Conducting Films

by

Aaron R. Rathmell

Department of Chemistry
Duke University

Date: _____

Approved:

Benjamin J. Wiley, Supervisor

Stephen L. Craig

Jie Liu

Michael J. Therien

Dissertation submitted in partial fulfillment of
the requirements for the degree of Doctor
of Philosophy in the Department of
Chemistry in the Graduate School
of Duke University

2013

ABSTRACT

Metal Nanowires: Synthesis, Processing, and Structure-Property Relationships in the
Context of Flexible Transparent Conducting Films

by

Aaron R. Rathmell

Department of Chemistry
Duke University

Date: _____

Approved:

Benjamin J. Wiley, Supervisor

Stephen L. Craig

Jie Liu

Michael J. Therien

An abstract of a dissertation submitted in partial
fulfillment of the requirements for the degree
of Doctor of Philosophy in the Department of
Chemistry in the Graduate School of
Duke University

2013

Copyright by
Aaron R. Rathmell
2013

Abstract

The demand for flat-panel televisions, e-readers, smart-phones, and touch-screens has been increasing over the past few years and will continue to increase for the foreseeable future. Each of these devices contains a transparent conductor, which is usually indium tin oxide (ITO) because of its high transparency and low sheet resistance. ITO films, however, are brittle, expensive, and difficult to deposit, and because of these problems, alternative transparent electrodes are being studied. One cheap and flexible alternative to ITO is films of randomly oriented copper nanowires. We have developed a synthesis to make long, thin, and well-dispersed copper nanowires that can be suspended in an ink and coated onto a substrate to make flexible transparent films. These films are then made conductive by annealing in a hydrogen atmosphere or by a solution processing technique that can be done in air at room temperature. The resulting flexible transparent conducting films display transparencies and sheet resistance values comparable to ITO.

Since it is well known that copper oxidizes, we also developed a synthesis to coat the copper nanowires with a layer of nickel in solution. Our measurements indicated that copper nanowires would double their sheet resistance in 3 months, but the sheet resistance of cupronickel nanowire films containing 20 mole% nickel will double in about 400 years. The addition of nickel to the copper nanowires also gave the film a

more neutral grey appearance. The nickel coating can also be applied to the copper nanowires after the film is formed via an electroless plating method.

To further optimize the properties of our transparent conductors we developed a framework to understand how the dimensions and area coverage of the nanowires affect the overall film properties. To quantify the effect of length on the sheet resistance and transmittance, wires with different lengths but the same diameter were synthesized to make transparent conducting films and finite-difference time-domain calculations were used to determine the effect of the nanowire diameter on the film's transmittance. The experimental data and calculations were then incorporated into random resistor network simulations that demonstrated that wires with an aspect ratio of 400 or higher are required to make a network that transmits >90% of visible light while maintaining a sheet resistance below $100 \Omega \text{ sq}^{-1}$.

These properties, and the fact that copper and nickel are 1000 times more abundant than indium or silver, make copper and cupronickel nanowire films a promising alternative for the sustainable, efficient production of transparent conductors.

Dedication

To my child(ren), never stop learning and never stop pursuing your dreams. I love you!

Contents

Abstract	iv
List of Tables	x
List of Figures	xi
Acknowledgements	xviii
1. Introduction	1
1.1 Indium Tin Oxide	3
1.2 Conducting Polymers	4
1.3 Graphene	5
1.4 Carbon Nanotubes	7
1.5 Metal Nanostructures	9
1.5.1 Thin Metal Films.....	9
1.5.2 Nanoscale Metal Grids.....	10
1.5.3 Metal Nanowires.....	13
1.5.3.1 Silver Nanowires.....	13
1.5.3.2 Copper Nanowires	14
1.6 Summary.....	15
2. Structure Property Relationship for Nanowire Films.....	16
2.1 Size-Dependent Electrical Resistivity of Metal Nanowires	16
2.2 Size-Dependent Optical Properties of Metal Nanowires.....	21

2.3 Effects of Nanowire Width and Length on the Properties of Transparent Conducting Films	27
3. Nanowire Synthesis	36
3.1 Silver Nanowires	36
3.2 Copper Nanowires	45
3.2.1 Ethylenediamine Capped Copper Nanowires.....	45
3.2.2 Nickel Coated Copper Nanowires	54
3.2.3 Hexadecylamine Capped Copper Nanowires.....	59
3.3 Gold Nanowires.....	60
4. Making Transparent Conductors.....	72
4.1 Introduction.....	72
4.2 Methods for Making Transparent Conductors.....	72
4.2.1 Drop Casting.....	72
4.2.2 Filtration.....	72
4.2.3 Spin Coating.....	73
4.2.4 Spray Coating.....	74
4.2.5 Meyer Rod Coating.....	75
5. Metal Nanowire Transparent Electrodes.....	77
5.1 Gold Nanowire Transparent Electrodes	77
5.2 Silver Nanowire Transparent Electrodes.....	78
5.2.1 Longer Silver Nanowires in Transparent Electrodes.....	84

5.3 Copper Nanowire Based Transparent Electrodes.....	85
5.3.1 Copper Nanowire Transparent Electrodes.....	85
5.3.2 Cupronickel Nanowire Transparent Electrodes.....	93
5.3.3 Film-Processable Copper Nanowire Networks.....	105
5.3.4 Nickel can be Directly Deposited onto CuNW Films Through Electroless Plating.....	108
6. Summary and Conclusion	112
Appendix A.....	114
References	113
Biography.....	133

List of Tables

Table 1: Arrhenius plot data for Cu, Ag, 4:1 Cu:Ni, and 1:1 Cu:Ni nanowire films. ...100

List of Figures

Figure 1: Forecast of transparent conductors based on applications.....	1
Figure 2: Images of A) a flexible display, B) flexible phones, and C) solar panels incorporated into a tent.....	2
Figure 3: A) Structure of PEDOT:PSS B) Plot showing the transmittance (%) vs. sheet resistance for ITO films, commercially available PEDOT:PSS, and in situ PEDOT:PSS...	5
Figure 4: A) Cartoon image of graphene, where the black balls represent carbon atoms and the blue balls represent hydrogen atoms. B) Plot of sheet resistance vs. transmittance for graphene films.....	6
Figure 5: A) Cartoon of a carbon nanotube. B) Plot of sheet resistance vs. transmittance comparing various CNT film properties.....	7
Figure 6: A) SEM image of a metal nanogrid with line widths of 120 nm. B) Illustration of a metal nanogrid showing “a” the main grating and “b” the secondary grating that connects grating “a”. C) Calculated optical transmittance of a 1D silver nanogrid. Transmittance is graphed vs. electrodes with a sheet resistance of 3.2 (blue) 1.6 (green) and 0.8 (blue). The inset is showing how the sheet resistance is maintained by using an area-conserving geometrical transformation, $h_1w_1/a = h_2w_2/a = h_3w_3/a$. D) Plot showing the transmittance vs. sheet resistance for various nanogrids with a line width of 120 nm.....	11
Figure 7: A) Schematic showing the effect of surface roughness on electromagnetic radiation reflectance. B) A graphical representation of Ziman’s angle and roughness-dependent specularly parameter for values of $h = 0.25, 1, \text{ and } 5 \text{ \AA}$	17
Figure 8: Plots of A) silver nanowires, B) copper nanowires, and C) gold nanowires showing the effects of diameter as a function of resistivity for both experimental and theoretical results based on Samble’s calculations. The red number on the x-axis is showing the mean-free path for the various metals.....	20
Figure 9: FDTD calculations of the absorption, scattering, and extinction efficiency of A) silver, B) copper, and C) gold nanowires vs. diameter, averaged over 400-800 nm.....	23

Figure 10: FDTD Plots of the A) conductance to extinction ratio and B) conductance to scattering cross-section for silver, copper, and gold nanowires vs. diameter.....	25
Figure 11: Experimental sheet resistance as a function of the area fraction (AF) of silver nanowires for L/D = 200 (blue, circles), 258 (red, triangles) and 275 (green, squared). For clarity, sheet resistance values for L/D = 200 and 258 are scaled by 100 and 10, respectively. Sheet resistance from the pseudo-2D simulations use effective average contact resistances between nanowires of $R_{\text{effective}} = 1.5 \text{ k}\Omega$ (dashed lines) and $2.5 \text{ k}\Omega$ (solid lines).....	28
Figure 12: Conductivity percolation scaling fits to experimental data from silver nanowire films with dimensions A) $L_{\text{nw}} = 21.65 \text{ }\mu\text{m}$, $D_{\text{nw}} = 84 \text{ nm}$, and $L/D = 258$ and B) $L_{\text{nw}} = 20.60 \text{ }\mu\text{m}$, $D_{\text{nw}} = 75 \text{ nm}$, and $L/D = 275$. Fits to both data sets yield a value of the conductivity exponent $t = 1.75$, which is consistent with contact resistance dominated transport ($R_c \gg R_{\text{nw}}$) as predicted theoretically by both Stanković ⁵⁴ and Cleri. ⁵⁵ The universal conductivity exponent for 2D networks $t \approx 1.3$ is expected to hold at densities very close to the percolation threshold.....	29
Figure 13: Sheet resistance from simulations as a function of L/D and area fraction of the rods in nanowire films using an effective average contact resistance $R_{\text{effective}} = 2 \text{ k}\Omega$ and constant $D_{\text{rod}} = 50 \text{ nm}$. The dashed line indicates the desired performance criterion $R_s \leq 100 \text{ }\Omega \text{ sq}^{-1}$ for high performance applications.	30
Figure 14: Calculated transmittance vs. simulated sheet resistance for silver nanowire films for L/D ranging between 50 and 800 with $R_{\text{effective}} = 2 \text{ k}\Omega$ and constant $D_{\text{nw}} = 40 \text{ nm}$. %T values were calculated using the empirical expression in equation 1. ⁵⁷ Dashed lines indicate desired performance criteria $\%T > 90\%$ and $R_s \leq 100 \text{ }\Omega \text{ sq}^{-1}$ for high performance applications.	33
Figure 15: Simulated sheet resistance as a function of area fraction using $R_{\text{effective}} = 2 \text{ k}\Omega$ for nanowire films comprised of bidisperse mixtures of rods with L/D = 50 (Reference) and 400 (Long). The diameter is the same for both nanowire populations ($D_{\text{Ref}} = D_{\text{Long}} = 50 \text{ nm}$), while the low- and high-aspect-ratio nanowires have lengths of 2.5 and 20 μm , respectively. The proportion of longer rods in the network is expressed as a relative area fraction, $F_{\text{Long}} = AF_{\text{Long}} / (AF_{\text{Ref}} + AF_{\text{Long}})$	35
Figure 16: A) Silver nanowire length, B) silver nanowire diameter, and C) % conversion of Ag^+ to Ag^0 vs. time for three reaction temperatures. Lower temperatures lead to the formation of longer nanowires with larger diameters.....	39

Figure 17: A) Reaction conditions for synthesizing nanowires with distinct lengths and diameters. B) SEM image of the silver nanowire product after growth for 0.3 hours at 160°C. The nanowires are 42 ± 5 nm in diameter and 3 ± 0.5 μ m in length. C) SEM image of the silver nanowire product after growth for 5 hours at 130°C. The nanowires are 85 ± 25 nm in diameter and 25 ± 5 μ m in length. The scale bar in the inset is 200 nm. 42

Figure 18: Silver nanowire length distribution graph for regularly grown silver nanowires (top) and silver nanowires grown using the successive multistep growth method (middle). The bottom SEM image is showing the longest nanowire obtained. . 44

Figure 19: Plot showing the diameter increase of silver nanowires vs. moles of silver added..... 45

Figure 20: Pictures of the reaction flask A) before the synthesis and B) after growth of CuNWs at 80 °C for 1 hr. C) SEM image of the CuNW product. The nanowires are 90 ± 10 nm in diameter and 10 ± 3 μ m in length. The inset shows CuNWs with a spherical copper particles attached at one end (scale bar = 200 nm). 47

Figure 21: XRD pattern of copper nanowires..... 48

Figure 22: A) SEM image showing copper nanorods sprouting from spherical copper seeds at a reaction time of 3.5 minutes. B) By 20 minutes the rods had grown to form longer wires. C) TEM image of two CuNWs growing out of a nanoparticle. D) A selected area electron diffraction pattern (SAED) from the nanowire shown in E) indicates the nanowire grew along the [110] direction..... 50

Figure 23: A) CuNW diameter (nm) versus EDA concentration (moles L⁻¹). Error bars show one standard deviation for 16-40 measurements. B) CuNW length (μ m) versus EDA concentration (moles L⁻¹). Error bars show one standard deviation for 7-10 measurements. An EDA concentration of 0.13 M was ideal for growing the longest, thinnest wires, presumably because EDA selectively capped the sides of the wires. Higher concentrations of EDA may have capped the ends as well as the sides, leading to shorter, fatter wires..... 53

Figure 24: SEM image showing the average length (20 ± 5 μ m) and diameter (52 ± 17 nm) of copper nanowires..... 54

Figure 25: A-C) Energy dispersive x-ray spectroscopy images of a copper nanowire coated with 54 mole % nickel. D) Copper nanowires before coating. The nanowires had

a length of $28.4 \pm 7.1 \mu\text{m}$ and a diameter of $75 \pm 19 \text{ nm}$. E) After the copper nanowires were coated with nickel to a concentration of 54 mole %, the diameter of the wires increased to $116 \pm 28 \text{ nm}$. The insets of D & E show the cross sections of the copper nanowire and cupronickel nanowire respectively. F & G) TEM images of the polycrystalline cupronickel nanowires with a grain size of 10 nm.	57
Figure 26: A) SEM and B) TEM images of copper nanowires synthesized by Xia and coworkers. The inset in A) shows the copper nanowire solution.	60
Figure 27: A & B) TEM images showing AuNWs. C) HRTEM image showing the single crystal lattice structure.	61
Figure 28: TEM image showing the polymer strands of the white gel and AuNWs within those strands after heating at 60°C	62
Figure 29: Cartoon image showing the OA complexed metal nanowire growth.....	63
Figure 30: TEM images of Au nanoparticles using A) AuCl and B) Au ₂ S in the reaction while under nitrogen. C & D) TEM images of the AuCl reaction when O ₂ was introduced during the last 6 hours of the reaction.....	66
Figure 31: TEM images of AuNWs synthesized in different solvents. A) hexane, B) heptane, C) toluene, and D) chloroform.	69
Figure 32: TEM images of AuNWs made with different alkylamines. A&B) DDA, C&D) TDA, E&F) HDA, and G&H) ODA.	71
Figure 33: Schematic of the spray coating process.	74
Figure 34: CuNW ink before and after Meyer rod coating.	76
Figure 35: Diagram of the AuNW densely aligned monolayer formation.	78
Figure 36: Plot showing transmittance vs sheet resistance for networks of randomly oriented AgNWs as transparent electrodes.	79
Figure 37: Plot of sheet resistance vs time for AgNWs heated at 200°C showing a gradual decrease in sheet resistance followed by a gradual increase as the nanowires turn to droplets seen in the SEM image in the inset.	80

Figure 38: Cartoon representation of the Au galvanic displacement reaction to improve the nanowire junction resistance. 81

Figure 39: A) Schematic of the RTA technique used to weld the AgNWs. The junctions have a nanoscale gap (shown in red) due to a layer of PVP which allows extremely high local heating to occur because of the strong field concentration. B) Top view SEM image of AgNW junctions before welding and C) after welding. Scale bars are 200 nm and 500 nm respectively.....82

Figure 40: Finite element simulations of optical heat generation at the silver nanowire junctions during the nanowire welding process. A) A cross-sectional view of the heat generation in a 2 nm gap between two silver nanowires before heating, B) once the recrystallization begins, and C) after the recrystallization is complete. 83

Figure 41: Plot of sheet resistance vs transmittance comparing the longer AgNWs to previous one-pot syntheses of AgNWs and ITO..... 84

Figure 42: A) A bent CuNW film ($25 \Omega \text{ sq}^{-1}$ and 83% transparent) completing an electrical circuit with a battery pack and a LED. B) Plot of current versus voltage for $40 \Omega \text{ sq}^{-1}$ CuNW films and C) $42 \Omega \text{ sq}^{-1}$ ITO, demonstrating their maximum current carrying capacity. D) Current vs. time plot for films of CuNWs ($40 \Omega \text{ sq}^{-1}$) and ITO ($42 \Omega \text{ sq}^{-1}$) with an applied voltage of 1.5 V over 24 hours demonstrates the relative stability of CuNW films over time. The inset of E shows a visual comparison of ITO ($10 \Omega \text{ sq}^{-1}$) and CuNW ($75 \Omega \text{ sq}^{-1}$) films, both 88% transparent, backlit by an iPhone display..... 86

Figure 43: A & B) Dark field optical microscope images showing uniformly dispersed networks of CuNWs that are 90 and 85% transparent with sheet resistances of 186 and $30 \Omega \text{ sq}^{-1}$, respectively. C & D) Corresponding SEM images of the CuNW films from A & B showing the average length ($20 \pm 5 \mu\text{m}$) and diameter ($52 \pm 17 \text{ nm}$) of the CuNWs..... 88

Figure 44: A Plot of transmittance (550nm) vs. amount of CuNWs (g m^{-2}) in a CuNW film. 89

Figure 45: A) Plot of transmittance (at a wavelength of 550 nm) vs. sheet resistance for films of CuNWs and ITO. Error bars show one standard deviation for 5 measurements. B) Plot of transmittance vs. wavelength for ITO ($42 \Omega \text{ sq}^{-1}$) and films of CuNWs with different nanowire densities. C) Plot of sheet resistance vs. number of bends of CuNW films (85% transparent) and ITO on PET. Inset shows the radius of curvature before (10 mm) and after bending (2.5 mm). D) Plot of sheet resistance vs. time for CuNW films (89, 86, and 82% transparent from top to bottom) exposed to air for 42 days..... 90

Figure 46: A) Plot of specular transmittance ($\lambda = 550 \text{ nm}$) vs. sheet resistance for films of copper nanowires, cupronickel nanowires, and ITO on glass (the light blocked by the glass was subtracted). Error bars show one standard deviation for five measurements. B) A plot of specular transmittance vs. number density of nanowires shows the effect of increasing wire diameter on the film's transmittance. C) Graph comparing the absorbance, reflectance, diffuse transmittance, and specular transmittance ($\lambda = 550 \text{ nm}$) of ITO and nanowire films with different nickel contents. D) Plot of resistivity vs. nickel content for cupronickel nanowires and bulk cupronickel alloys. Error bars show one standard deviation for five measurements. 94

Figure 47: Plot of sheet resistance vs. the inverse of the effective nanowire thickness. The slope gives the resistivity of the nanowire networks. Error bars show one standard deviation for five measurements. 96

Figure 48: A) A Plot of sheet resistance vs. time for films of silver nanowires, copper nanowires, and cupronickel nanowires stored at 85°C . B) An Arrhenius plot of $\ln(k)$ vs. 1000 T^{-1} illustrates the temperature-dependent stability of the nanowire films. C) Plot of transmittance vs. sheet resistance for cupronickel nanowire films annealed in various atmospheres. All error bars show one standard deviation of five measurements. 98

Figure 49: A & B) Camera images of nanowire films ($\%T = 87\%$) on a black background and a white backlit display show the nanowire films change from a reddish-orange to grey color with increasing amounts of nickel. C) Plot showing a quantitative comparison of color on a Hunter color scale. D) Plot of transmittance vs. wavelength for ITO ($11 \Omega \text{ sq}^{-1}$), copper nanowires, and cupronickel nanowires with different nickel contents. The nanowire films all have a sheet resistance of $60 \Omega \text{ sq}^{-1}$ 103

Figure 50: Plot of sheet resistance vs. number of bends for copper nanowires, 4:1 Cu:Ni nanowires, 1:1 Cu:Ni nanowires, and ITO films on PET. Error bars show one standard deviation for five measurements. 105

Figure 51: A) Camera image showing a CuNW thin film being cleaned in glacial acetic acid. B and C) TEM images showing the removal of copper oxide using acetic acid. ... 106

Figure 52: SEM images of CuNWs A) before and B) after pressing at 160 bar. 107

Figure 53: Plot of transmittance vs sheet resistance comparing films that were annealed in a hydrogen environment and cleaned in acetic acid. 107

Figure 54: A) Camera image showing a copper nanowire film immersed in the nickel plating bath after nickel has been deposited on the lower half of the slide. B) Plot of Nickel percentage vs. time in minutes the CuNW film remains in the nickel plating bath. 108

Figure 55: SEM images of A) CuNWs and B) 20% Ni coated CuNWs showing the diameter change without major morphological changes.....109

Figure 56: A) Plot of sheet resistance vs. transmittance for film processable CuNW and 20% Ni CuNW films. B) A modified Arrhenius plot of $\ln(k)$ vs. T showing the temperature-dependent stability of the nanowire films..... 110

Figure 57: Plot of sheet resistance vs. transmittance comparing electrodes made with CuNWs, NiCuNWs, AgNWs, CNT, graphene, and ITO. 112

Acknowledgements

I would like to thank my graduate advisor, Dr. Benjamin Wiley, whose guidance and mentorship were invaluable to me. He has given me the freedom to pursue various projects without objection, and his questions, feedback, and expectation of nothing less than completion have pushed me and helped me to grow as a researcher and scientist.

I would also like to thank my group members – those who have moved on, those in the quagmire, and those just beginning – for their support, feedback, and friendship. I have been blessed to work with so many brilliant and talented people.

I would not be in graduate school if it was not for my undergraduate advisor, Dr. Edward Rajaseelan. He saw a potential in me that I didn't even know was there, and encouraged me to become a better student and scientist.

I would like to thank my family and friends. They have loved, encouraged, and supported me throughout my entire life.

Lastly, I would like to thank my wife, Emily. Through her love and support I was able to accomplish all that I have done. Without her, this would have been so much harder. I love you!

1. Introduction

Transparent conductors (TCs) are a necessary component in flat-panel televisions, e-readers, smart-phones, smart-glass, touch-screens, organic light emitting diodes, and organic solar cells. From 2009 to 2012 the revenues made with transparent conductors doubled, and it is expected to double again by 2016 (Figure 1).¹ Typically,

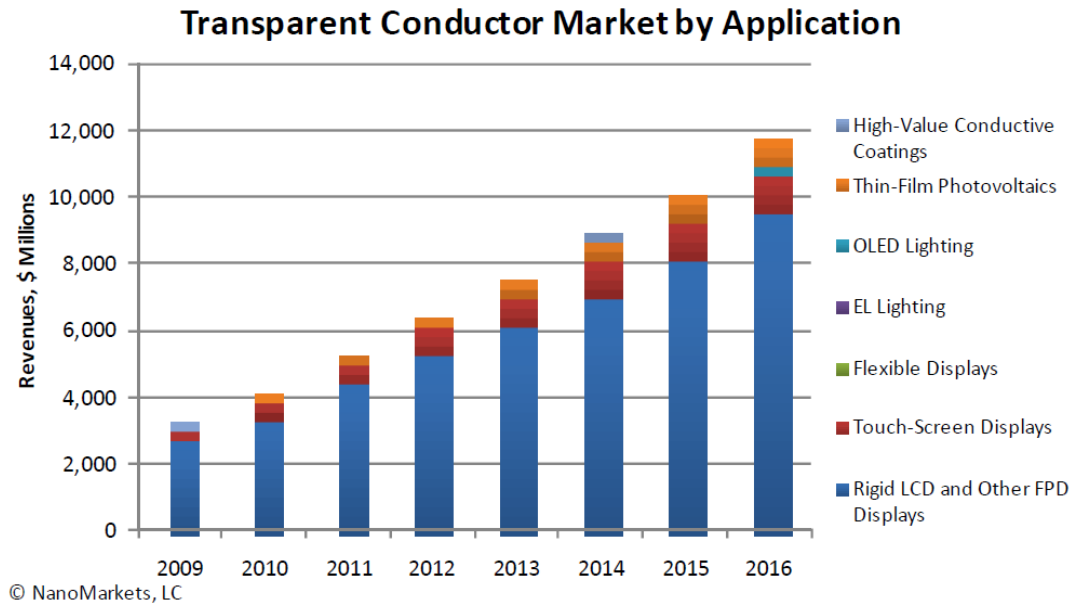


Figure 1: Forecast of transparent conductors based on applications.¹

the material of choice has been indium tin oxide (ITO) because of its low sheet resistance ($\sim 10 \Omega \text{ sq}^{-1}$) and high optical transparency ($\sim 90\%$). ITO has limitations, however, and alternatives are being sought that can handle the rapidly expanding market and the push towards light-weight and flexible electronics (Figure 2). Imagine being able to



Figure 2: Images of A) a flexible display, B) flexible phone, and C) solar panels incorporated into a tent.²⁻⁴

carry an e-reader in something the size of a pen and simply unrolling it like a window blind when you want to use it, or not having to worry about dropping your phone, because there is nothing breakable in it anymore. The military could use similar technologies by turning the tarps of their tents into solar panels, which could then power their equipment. In order to make these ideas a reality we need to find a cheap, flexible, and easily scalable alternative to ITO.

My research over the past four years has focused on using copper nanowires as the replacement to ITO. During the past four years I have developed and modified the copper nanowire reaction to meet our changing needs, first by scaling the reaction up,⁵ then by modifying it to produce longer and thinner wires.⁶ These wires were then incorporated into transparent electrodes using a new ink solution.⁶ Then to improve the color and the oxidation resistance of the copper nanowire films, I developed a method to coat the nanowires with nickel.⁷ To get insights on how to further improve the nanowire electrodes we started collaborations with theoretical and computational scientists,^{8,9} and

by coupling their simulations with our experimental results we discovered the specific properties of wires that are necessary in order to produce films whose properties are equal to or better than the properties of ITO film. We are currently developing new methods to make the films conductive without using hydrogen gas, as well as continuing our efforts to make longer and thinner nanowires that one day might be incorporated into films that can outperform ITO.

This dissertation comprises 5 chapters. Chapter 1 gives a brief overview of the transparent electrode market, paying special attention to the alternatives to ITO. Chapter 2 discusses how the structure of the nanowires directly impacts the properties of the nanowire film by using theoretical and simulated models in conjunction with our own experimental evidence. Chapters 3-5 then show how to make the nanowires and then process them into transparent electrode films.

1.1 Indium Tin Oxide

Indium tin oxide (ITO) is the dominant transparent conductor currently on the market, with sales predicted to be around \$7 billion for 2013.¹ While ITO was being studied over the last several decades,¹⁰ it was found that ITO could transmit 90% of visible light while having a sheet resistance of $10 \Omega \text{ sq}^{-1}$, making it ideal for transparent conductors. ITO has its drawbacks however. It is brittle and easily cracks due to its ceramic nature, and ITO films are very expensive because of the scarcity of indium

(~\$700 kg⁻¹) and the chemical vapor deposition process.¹¹ During deposition, only 30% of the ITO vapor is deposited onto the substrate at a linear coating rate of ~0.01 m sec⁻¹, which is about 1000 times slower than newspaper printing.¹¹ Motivated by the problems associated with ITO and an increasing demand for transparent conductors, especially in the liquid crystal displays (Figure 1), alternative transparent conductors are being investigated. I will briefly discuss the possibility of using conducting polymers, graphene, carbon nanotubes, and various metal nanostructures as possible replacements to ITO before focusing on films made from randomly oriented metal nanowires.

1.2 Conducting Polymers

Intrinsically conducting polymers (ICP) are one alternative to ITO and their transparent and conductive properties have greatly improved since their discovery in 1977.^{12, 13} ICP offer three major advantages to ITO: 1) they are flexible, 2) they can be printed from solution allowing nearly all of the material to be deposited onto the substrate, which 3) reduces the processing costs compared to ITO.¹⁴ There are many different types of ICPs of which poly-(3,4-ethylenedioxythiophene) poly(styrenesulfonate) (PEDOT:PSS) is the most promising (Figure 3A).¹⁴ The electronic

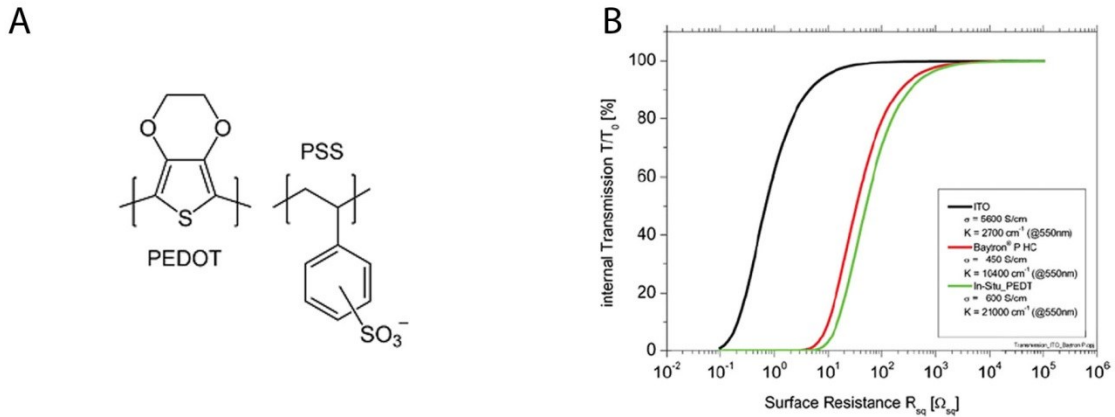


Figure 3: A) Structure of PEDOT:PSS B) Plot showing the transmittance (%) vs. sheet resistance for ITO films, commercially available PEDOT:PSS, and *in situ* PEDOT:PSS.¹⁴

conductivity of the polymer comes from the positively charged doping in PEDOT. The PSS portion has two important roles; first it stabilizes the positive charges in the PEDOT polymer and second it helps to solubilize the polymer in an aqueous solution. Together PEDOT:PSS found applications in various antistatic products from photographic films to textiles, gloves, and several others. By changing the ratio of PEDOT to PSS the ICP can become more or less conductive. Figure 3B shows the transmittance verses sheet resistance for commercial PEDOT:PSS, *in situ* PEDOT:PSS, and ITO. While the polymer is a transparent conductor, it does not match the properties of ITO.

1.3 Graphene

Graphene is a layer of sp^2 hybridized carbon (Figure 4A) that has shown

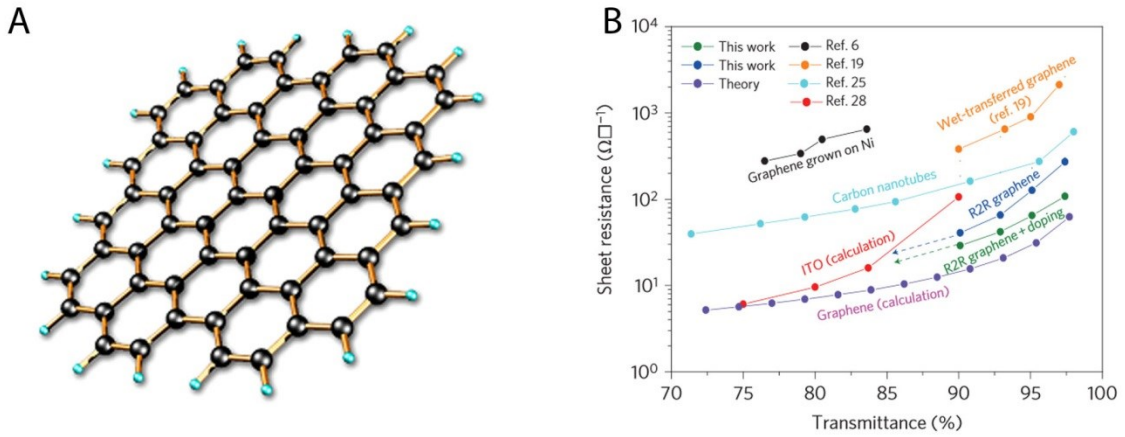


Figure 4: A) Cartoon image of graphene, where the black balls represent carbon atoms and the blue balls represent hydrogen atoms.¹⁵ B) Plot of sheet resistance vs. transmittance for some of the best results to date.¹⁶

electrical, optical, and mechanical properties that are similar to, or better than, ITO.^{16, 17}

There are several ways to obtain a transparent conducting film of graphene including exfoliation, chemical vapor deposition (CVD), and reduction of graphene oxide.

Recently, researchers were able to make 30 inch films that were ~90% transparent with a sheet resistance of 30 Ω sq⁻¹ (Figure 4B) using a CVD method.¹⁶ However, making graphene via a CVD process has its drawbacks. First, graphene is grown at 1000°C in a hydrogen environment for 30 minutes. Second, graphene sheets are grown on a copper substrate that must be etched away in subsequent steps. Finally, in order to be useful the graphene sheets need to be transferred whole and without any defects to the substrate of interest, even the smallest defect could have negative impacts on its performance. So although graphene films have shown great mechanical, optical, and

electrical properties, the high processing temperatures, high copper consumption, and the chemical vapor synthetic method may hinder their use in some products.

1.4 Carbon Nanotubes

Carbon nanotubes (CNT) are sheets of graphene rolled up into a tube with a diameter on the nanometer scale and a length that can be anywhere from a few micrometers to millimeters (Figure 5A).^{10, 18-25} When these tubes, either single-walled or

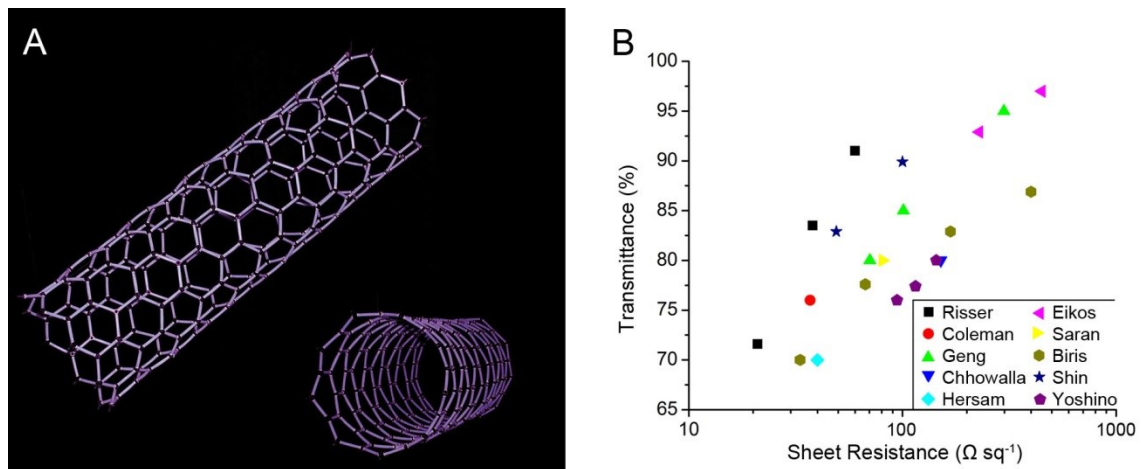


Figure 5: A) Cartoon of a carbon nanotube. B) Plot of sheet resistance vs. transmittance comparing various CNT film properties.^{25, 26}

few-walled,²⁶ are randomly distributed onto a surface in sufficient quantities, they can form transparent conducting films that are flexible, optically transparent, and conductive. Researchers have shown that CNTs can be dispersed in various aqueous solutions which can take advantage of current roll-to-roll setups already being utilized in industry.

However, CNTs also have their drawbacks. Depending on the chiral vector, the CNT will either be metallic or semi-conducting. Ideally transparent conductors would be made of all metallic CNTs, but most CNT reactions will yield a mixture of metallic and semi-conducting tubes in a ratio of 1:2.¹⁰ CNTs also tend to form bundles or ropes, especially when the tubes have long lengths. The attractive van der Waals force in highly crystalline CNTs is strong enough to make separating the CNTs nearly impossible. Several methods to prevent the CNTs from forming have been investigated. First the CNTs can be functionalized, but by adding functional groups to the sides of the CNT the conjugated sp^2 structure is disrupted making the film less conductive. Second, various solvents can help keep the tubes dispersed, but the most effective solvents, N-Methyl-2-pyrrolidone and N,N-dimethylformamide, are toxic. Finally, CNTs can be dispersed in water with an amphiphilic surfactant or dispersant, but unless the surfactant is removed, the CNT film will lose some of its conductivity. Finally, CNTs need to be grown at high temperatures using CVD processes. As can be seen by Figure 5B, transparent conductors made with CNTs have properties very similar to ITO, but not yet equivalent to it.

1.5 Metal Nanostructures

Metals are highly conductive, but bulk metals are obviously not transparent..

There are three ways to make a transparent metal film 1) a piece of metal could be fashioned so that it is extremely thin (<10 nm), which will allow light to pass through the sample while maintaining electrical conductivity; 2) A grid could be etched or grown onto a substrate allowing the electrical charge to be carried through the metal grid and light to pass through the holes, and 3) metal nanowires can be randomly distributed onto a surface and as long as the nanowires were in sufficient contact with one another, the charge could be carried through the connected wires and light could be passed through the random holes in the network.

1.5.1 Thin Metal Films

Metal films can be made transparent if they are fabricated in such a way that they are less than ~10 nm thick.^{10, 27-31} The film's resistivity can be negatively influenced by a wide variety of factors. First, the metal needs to be as pure as possible, the slightest impurity can increase the resistivity. Second, the surface needs to be smooth. If the substrate or film is not smooth, the metal film's surface roughness will increase which will cause greater surface scattering, and thus increase the resistivity. Lastly, in order to transmit as much light as possible the film needs to be as thin as possible, but as the thickness of the film decreases the thickness approaches the electron mean free path

length which, again, causes the resistivity of the metal to increase. Thin films of nickel (2-10 nm) can transmit 40-80% of visible light but the sheet resistance varies significantly over that range from 30-1200 $\Omega \text{ sq}^{-1}$.³⁰

The films are made through vacuum evaporation techniques or through sputter deposition techniques. Both of these methods require a high vacuum which can limit the size of the substrate and both have relatively small deposition rates and efficiencies. As a result of these considerations, thin metal films are not being studied as much as other possible replacements for ITO.

1.5.2 Nanoscale Metal Grids

The metal nanoscale grids developed by nanoimprint lithography techniques (Figure 6A&B) have shown the best conductivity and transmittance compared to other

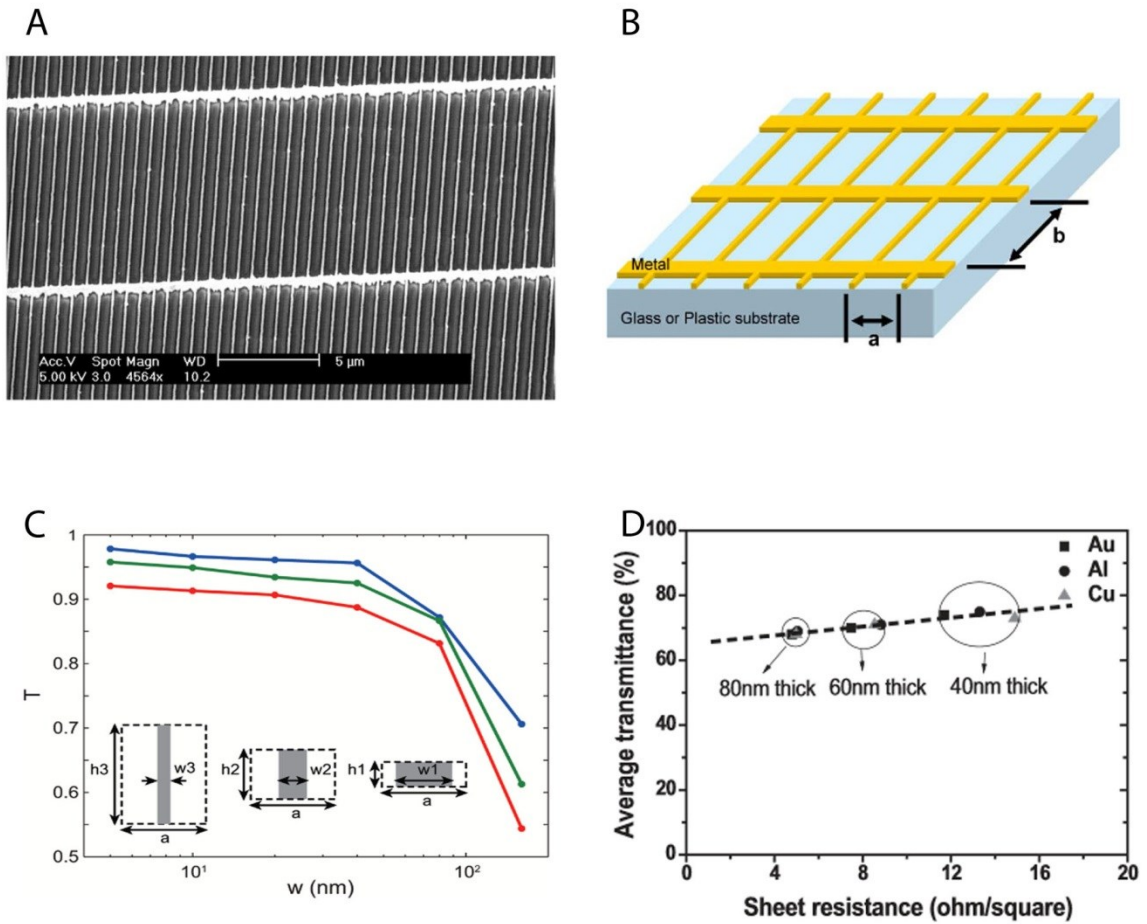


Figure 6: A) SEM image of a metal nanogrid with line widths of 120 nm.³² B) Illustration of a metal nanogrid showing “a” the main grating and “b” the secondary grating that connects grating “a”.³³ C) Calculated optical transmittance of a 1D silver nanogrid. Transmittance is graphed vs. electrodes with a sheet resistance of 3.2 (blue) 1.6 (green) and 0.8 (red). The inset is showing how the sheet resistance is maintained by using an area-conserving geometrical transformation, $h_1w_1/a = h_2w_2/a = h_3w_3/a$.³⁴ D) Plot showing the transmittance vs. sheet resistance for various nanogrids with a line width of 120 nm.³²

methods and can be made using roll-to-roll processes.^{32, 33, 35-37} The first factor to consider when making these metal grids is the line width. The line width should be

subwavelength to minimize the light scattering and reflection while allowing the most light to transmit through the grid. The second factor is the frequency of lines in mesh “a” shown in Figure (6B). Guo stated that this spacing should be sub-micrometer to collect as much current as possible from the active layer in devices such as solar cells and LEDs. The secondary grating, mesh “b,” connects all of the mesh “a” lines to ensure good electrical flow through the conductor.³³ By tuning the frequency of lines in mesh “a” and the width and height of the individual lines, the optical and electrical properties can be adjusted to the specific sheet resistances and transparencies desired. By increasing the height it is possible to decrease the sheet resistance without having a major impact on the transparency of the film. Figure 6C shows that when a theoretical film is made from thin and tall lines, the optical properties are far superior to films with short and fat lines (assuming the period, the cross sectional area of silver, and the sheet resistance are kept constant),³⁴ which is in rough agreement with Guo et al’s experimental data (Figure 6D).³² The frequency of lines in mesh “a” can also be varied to collect as much current as possible from the active layer, but as the lines become too frequent the transparency of the film decreases.

While the overall properties of the metal nanoscale grids are promising there are two disadvantages to using them. Since the grid lines often have a height on the order of 100 nm, the surface of the film tends to be extremely rough, which is not ideal for

applications with thin active layers due to the possibility of electrical shorts . While the holes in the grating provide 100% of the light to be transmitted, there is also no conductive material present in the holes to collect the current before the electrons recombine with the holes in the active layer. In order for metal nanoscale grids to be useful as the transparent conductor in solar cells and other devices that require a current collector, there needs to be an additional coating applied to the grid (graphene, conductive polymer, or a thin metal film), which will decrease the transparency even more.

1.5.3 Metal Nanowires

Networks made from randomly oriented nanowires have shown great promise in the last few years. The wires can be coated from various solutions, allowing for the possibility of large scale roll-to-roll processing at relatively low costs. The nanowire networks are highly transparent, they have a low sheet resistance, and they are mechanically flexible and stretchable. Of the many types of solution grown nanowires being studied, films of silver, copper, and gold nanowires have shown the most comparable properties to ITO.

1.5.3.1 Silver Nanowires

Silver nanowires are made using a controllable, solution-based, synthetic process called the polyol process. Controlling nanowire growth and their dimensions will play a

key factor in using the AgNWs in transparent electrodes. In Chapter 2, I use simulated and experimental data to show that wires with high aspect ratios will allow for the production of films with properties comparable to ITO. In Chapter 3, I show that by tuning reaction conditions, we can obtain nanowires with diameters from 30-70 nm and lengths from several hundred nanometers to 25 μm . I also discuss methods to selectively increase the diameter of the nanowires, and to grow nanowires with lengths up to 97 μm .³⁸

1.5.3.2 Copper Nanowires

While networks of silver nanowires have properties that are comparable to those of ITO, silver is also comparable to indium in terms of price ($\$1000 \text{ kg}^{-1}$) and scarcity.³⁹ Copper ($\rho = 17 \text{ n}\Omega \text{ m}$) is almost as conductive as silver ($\rho = 16 \text{ n}\Omega \text{ m}$), but it is 1000 times more abundant and 100 times cheaper ($\$9 \text{ kg}^{-1}$).⁴⁰ Motivated by these intrinsic advantages of copper, we developed a scalable synthesis to produce long ($>20 \mu\text{m}$), thin ($<60 \text{ nm}$), and well-dispersed copper nanowires.⁶ We then demonstrated how to disperse these wires into an ink and coat them onto various substrates to make highly conductive, flexible transparent electrodes that transmitted 85% of visible light while maintaining a sheet resistance of $30 \Omega \text{ sq}^{-1}$. Copper nanowire films with these properties were among the best solution-based transparent conductors. Based on the simulated

data in Chapter 2, and our understanding of how to control nanowire growth, copper nanowires will match the properties of ITO in the near future.

1.6 Summary

The limitations of indium tin oxide and other transparent conductors have motivated a search to find a flexible and low cost alternative that can be deposited from liquids at speeds similar to newspaper printing ($\sim 10 \text{ m sec}^{-1}$). Conducting polymers, such as PEDOT:PSS, and carbon nanotubes are two examples of such alternatives, but to date their properties do not match the properties of ITO. Films of graphene have been shown to have properties similar to ITO but due to the high temperature and other growing conditions, graphene does not seem very cost effective. Of the various metallic nanostructures, thin films, grids, and nanowire meshes, nanowire films deposited from solution offer the most promise as a realistic, cost-effective alternative to ITO.

2. Structure Property Relationship for Nanowire Films

If we are to use random networks of nanowires in transparent electrodes, it is important to know how the length and diameter of a metal nanowire affects the transmittance and sheet resistance of a transparent conducting film. A simple functional relationship between the dimensions of the nanowire and the properties of the film would be very helpful in guiding the design of nanowire-based transparent electrodes. Obtaining such a relationship is complicated by the fact that (1) the intrinsic electrical and optical properties of metal nanowires are nonlinearly dependent on nanowire diameter and (2) the conductivity of nanowire films are nonlinearly dependent on the density and dimensions of nanowires. It is only recently that researchers have been able to simulate the relationship between nanowire dimensions and film properties and compare their results to relevant experimental results.

2.1 Size-Dependent Electrical Resistivity of Metal Nanowires

When the dimensions of a metal wire or film become small relative to the mean free path of an electron, the electrical resistivity of the sample increases. The first exact models for predicting how much the resistivity increases per decrease in dimension according to the electron theory of metals is attributed to Fuchs (1938) for the case of films,⁴¹ and later Dingle (1950) extended this theory to wires.⁴² These theories have and continue to be attractive to experimentalists because they depend on only two

parameters: (1) the ratio of the sample dimension d to the bulk mean free path λ_{∞} , and (2) an angle-independent parameter p that gives the probability that an electron incident upon the surface will be specularly reflected (i.e., not exhibit a decrease in drift velocity).

Recognizing that the reflection of electromagnetic radiation from a surface depends to a great extent on the incident angle to and roughness of that surface (see Figure 7A), Ziman (1960) developed an angle and roughness-dependent specularity

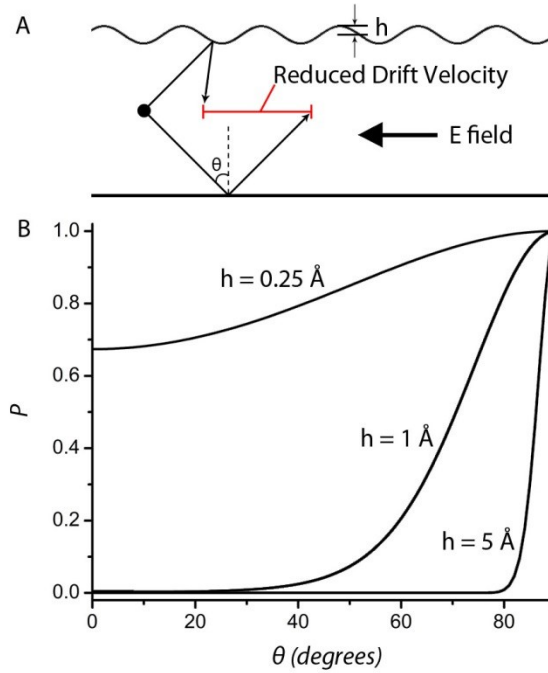


Figure 7: A) Schematic showing the effect of surface roughness on electromagnetic radiation reflectance. B) A graphical representation of Ziman's angle and roughness-dependent specularity parameter for values of $h = 0.25, 1,$ and 5 \AA .

parameter of the form given by equation (1), where θ is the angle of incidence relative to

$$p(\theta) = \exp[-(4\pi h / \lambda_e)^2 \cos^2 \theta] \quad (1)$$

the surface normal, h is the root mean square surface roughness, and λ_e is the Fermi wavelength of an electron.^{43, 44} Figure 7B plots equation (1) for various values of h . For an atomically smooth surface ($h \approx 0.03$ nm), electron reflection is mostly specular, with p ranging from 0.6 to 1 as the angle of incidence increases from 0 to 90 degrees. With an h on the order of the λ_e (≈ 0.5 nm), however, reflection from the surface is entirely diffuse below angles of 80 degrees. Soffer (1967) incorporated this parameter into a model for how resistivity of thin films depended on surface roughness.⁴⁵ Sables (1982) extended this theory to wires, and showed that this new model gave better agreement with theoretical results for thin films.⁴⁶ For example, to fit temperature-dependent experimental data with the Fuchs model, it proved necessary to introduce a temperature-dependent p or a temperature-dependent $\rho \propto \lambda_e$, both of which have no physical basis. In contrast, the Soffer model shows excellent agreement with experimental data over a wide range of temperatures without requiring a temperature-dependent $\rho \propto \lambda_e$ or h to fit the data.

Given this long history of theoretical development, it is interesting to note that it is only within the last few years that experimental data has become available to test the Soffer-Sables model of resistivity for nanowires. This is because testing this theory requires performing electrical measurements on nanowires with a roughness of about one tenth the Fermi wavelength of an electron, ~ 0.03 nm. Such experiments were

recently performed by Kotov,⁴⁷ Peddetti,⁴⁸ and Krstic⁴⁹ for gold, copper, and silver nanowires. Their data is plotted along with data from electrodeposited and lithographically-defined⁵⁰ nanowires in Figure 8. Model fits to the

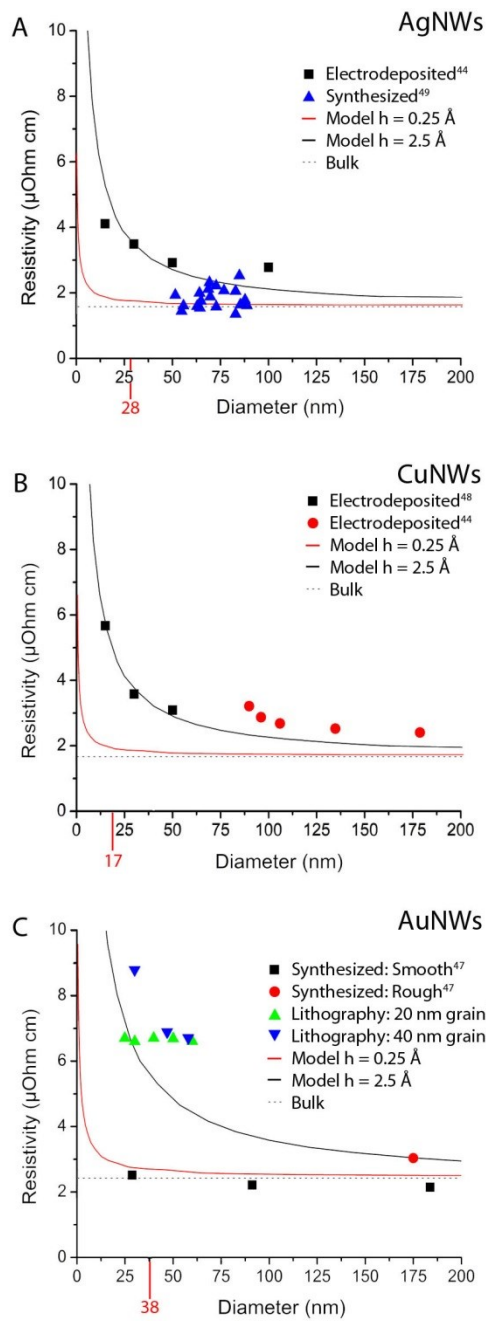


Figure 8: Plots of A) silver nanowires, B) copper nanowires, and C) gold nanowires showing the effects of diameter as a function of resistivity for both experimental and theoretical results based on Samble's calculations. The red number on the x-axis is showing the mean-free path for the various metals.

electrodeposited and lithography-defined silver, copper, and gold nanowires show that they are likely quite smooth, with a surface roughness of about 0.3 nm. However, this small surface roughness is large relative to the Fermi wavelength of an electron (0.5 nm), and subsequently these nanowires show enhanced resistivities at dimensions 2-6 times the bulk mean free path. In contrast, solution-grown gold and silver nanowires with atomically smooth surfaces exhibit resistivities comparable to the bulk, even at dimensions equivalent to or below the bulk mean free path of an electron.

The fact that atomically smooth metal nanowires exhibit very little enhancement in their resistivity is a very exciting and important development for those working in the nanowire field. What this means for transparent conducting films is that one can utilize atomically smooth nanowires with smaller diameters without significantly degrading the resistivity of the film. To come to a fuller understanding of the impact of nanowire diameter on the electro-optical performance of transparent conducting films, however, we will now examine the optical properties of nanowires.

2.2 Size-Dependent Optical Properties of Metal Nanowires

To facilitate the discussion of the effect of width on the optical properties of nanowires, we have calculated the absorption and scattering cross-sections of nanowires composed of silver, copper, and gold, for diameters between 10 nm and 300 nm. We felt the need to perform these calculations because we cannot find a comparably

convenient set of data in the literature. The absorption and scattering cross-sections of the nanowires were calculated with the finite-difference time-domain method using the Meep software package.⁵¹ The experimental dielectric dispersion data of silver, copper, and gold was used in the calculation to obtain an optical response.⁵² Two orthogonal polarization states of the normally incident plane-wave light were considered, in which the electric field was parallel or perpendicular to the cylinder axis. The nanowires were assumed to be infinitely long, yielding an effective cross-section with units of meters. To obtain the dimensionless efficiency, we divided the 1D optical cross-sections by the nanowire width. The dimensionless absorption (C_{abs}), scattering (C_{scat}) and extinction ($C_{\text{ext}} = C_{\text{abs}} + C_{\text{scat}}$) efficiencies, averaged over the wavelength range 400 – 800 nm, are plotted for silver, copper, and gold in Figure 9A-C.⁵³

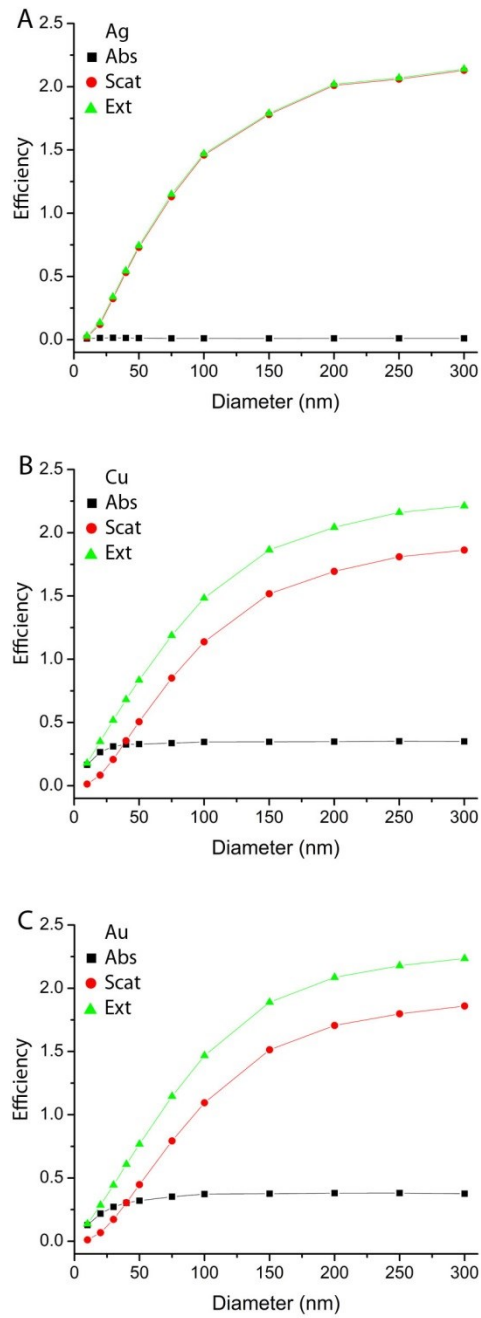


Figure 9: FDTD calculations of the absorption, scattering, and extinction efficiency of A) silver, B) copper, and C) gold nanowires vs. diameter, averaged over 400-800 nm.

There are several important points to take away from Figure 9A-C. The first and most obvious point is that, for all nanowires, nanowires with large diameters are more efficient at blocking light than nanowires with smaller diameters. For example, the extinction efficiency doubles as the nanowire diameter is increased from 50 to 100 nm. This fact is not at all surprising, as it is well known that objects become more efficient at scattering light as their dimensions approach the wavelength of light. Indeed, the calculated data shows the majority of the increase in the extinction is due to an increase in scattering, and the slope of the increase decreases once the nanowire diameter reaches 200 nm, about half the wavelength of blue light.

It is also interesting to note that nanowires of all three metals have about the same extinction coefficient for diameters greater than 100 nm because all three metals have similar scattering efficiencies. In contrast, Ag has a lower extinction coefficient than either Cu or Au for diameters smaller than 100 nm because Ag absorbs less light. The lower absorption of Ag is due to the fact that the interband absorption edge of Ag lies at a wavelength of about 350 nm, outside of the plotted wavelength range (400 – 800 nm), whereas Cu and Au absorb light with wavelengths shorter than about 550 and 500 nm, respectively. For a 10 nm wire, these differences in interband absorption between metals lead to a $C_{\text{ext}} = 0.03$ for Ag, 0.14 for Au, and 0.18 for Cu.

It has often been hypothesized that films of nanowires with smaller diameters will transmit more light at a given sheet resistance than nanowires with larger diameters, but this hypothesis has as yet not been thoroughly tested.^{54, 55} We have tried to gain some insight into whether this is in fact true by plotting $\sigma_{DC}A/\sigma_{ext}$ versus nanowire diameter in Figure 10A. Here σ_{DC} is the DC conductivity of the metal adjusted

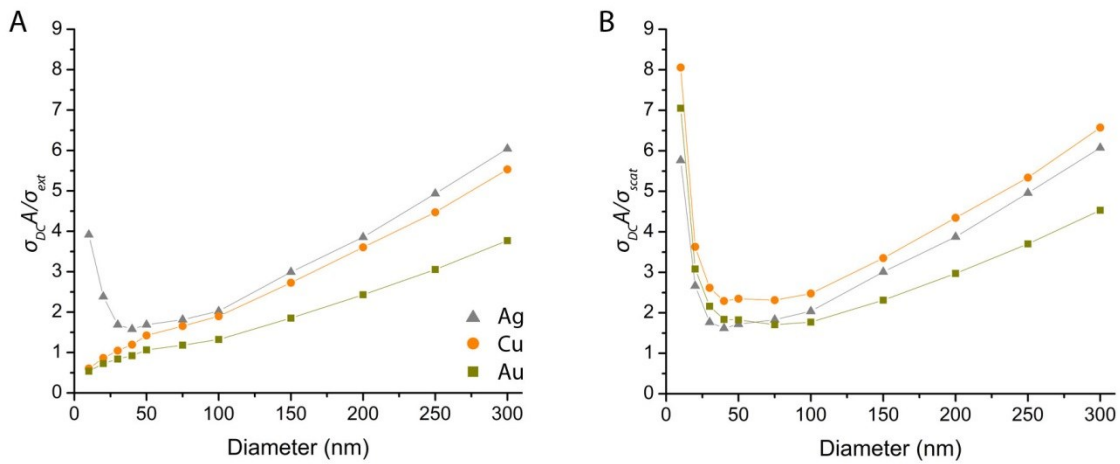


Figure 10: FDTD Plots of the A) conductance to extinction ratio and B) conductance to scattering cross-section for silver, copper, and gold nanowires vs. diameter.

for size using Sambles's equation 13 in reference 45 and $h = 0.03$ nm (atomically smooth).^{46, 47} A is the cross-sectional area of the nanowire, and σ_{ext} is the extinction cross-section of the nanowires. The quantity $\sigma_{DC}A/\sigma_{ext}$ is basically the conductance to extinction ratio; higher values denote better performance.

Figure 10A shows that for copper and gold, nanowires with larger diameters are better suited for transparent conductive films. Intuitively, this makes sense because the amount of light blocked by large wires should scale with diameter d , whereas the

conductance will scale with d^2 . This calculated result is supported by the fact that metal grids consisting of lines 10- μm -wide exhibit sheet resistances of $\sim 10 \Omega \text{ sq}^{-1}$ at a transmittance of 95%, values which are comparable to or exceed some of the best results reported for films of nanowires or ITO. In contrast to Au and Cu, the conductance to extinction ratio for Ag nanowires starts to improve for diameters smaller than about 30 nm. The higher conductance to extinction ratio for Ag nanowires is due to the fact that Ag nanowires of this size scatter very little light, and Ag does not absorb much light in this wavelength range. Cu and Au nanowires of this size also scatter very little light, but because they absorb about 16 times more light than silver, one cannot obtain improved performance by going to smaller nanowire diameters.

Although the properties of Ag nanowires start to improve as their diameter is reduced below 30 nm, the higher resistivity of these nanowires prevents them from matching the properties of nanowires several hundred nanometers in diameter. It's worth emphasizing that we have assumed that the nanowires will be atomically smooth, and thus their resistivity will rise to the lowest extent that can reasonably be expected. We note that in practical applications the nanowires may not be atomically smooth, and thus they might exhibit even higher resistivities at small sizes. However, as there are not many resistivity measurements of nanowires in this size range, let alone measurements

of their properties in transparent conducting films, the true properties of nanowires in this sub-30-nm size range remains uncertain.

Minimizing the light diffusely scattered from the nanowires, which results in haze, is a major concern for display applications. Thus we also plotted the ratio of the conductance to the scattering cross-section vs. nanowire diameter in Figure 10B. On this plot copper nanowires exhibit the least haze, which corresponds well with experimental results that show haze from Cu nanowire films is between 1.5 and 4%, while that for Ag nanowire films is about 10%.^{7, 56} This plot also shows that only the 10 nm nanowires will have less haze than nanowires hundreds of nanometers in diameter

2.3 Effects of Nanowire Width and Length on the Properties of Transparent Conducting Films

Recently Winey and coworkers simulated for the first time the sheet resistance of thin-film metal nanowire networks as a function of the nanowire dimensions, areal density, and size-dispersity.⁹ These simulations were fit to experimental results and an effective average contact resistance between two silver nanowires, $R_{c_effective}$, was determined that enabled the simulations to quantitatively predict experimental behavior. In their simulations, $R_{c_effective}$ was the only free variable (Figure 11), their

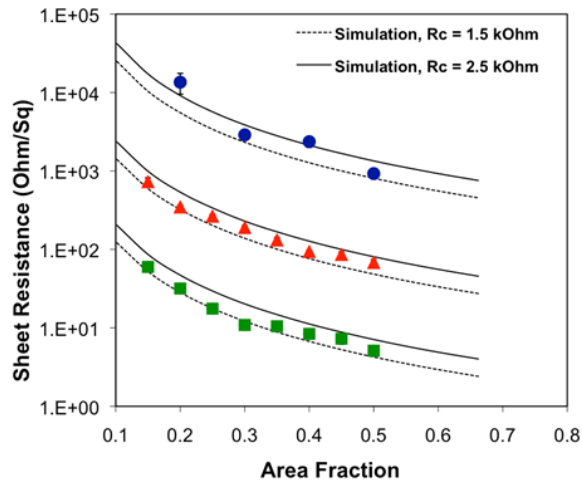


Figure 11: Experimental sheet resistance as a function of the area fraction of silver nanowires for $L/D = 200$ (blue, circles), 258 (red, triangles) and 275 (green, squared). For clarity, sheet resistance values for $L/D = 200$ and 258 are scaled by 100 and 10 , respectively. Sheet resistance from the pseudo-2D simulations use effective average contact resistances between nanowires of $R_{c_effective} = 1.5 \text{ k}\Omega$ (dashed lines) and $2.5 \text{ k}\Omega$ (solid lines).⁹

results indicated that they could capture the influence of nanowire dimensions and area fraction on sheet resistance with their simulations. In these simulations, they assume that $R_c / R_{nw} \rightarrow \infty$ and make the case that for these silver nanowire films the assumption is credible because the quality of the fit is good and the percolation conductivity exponent is 1.75 (Figure 12). The initial assumption was made because typically there

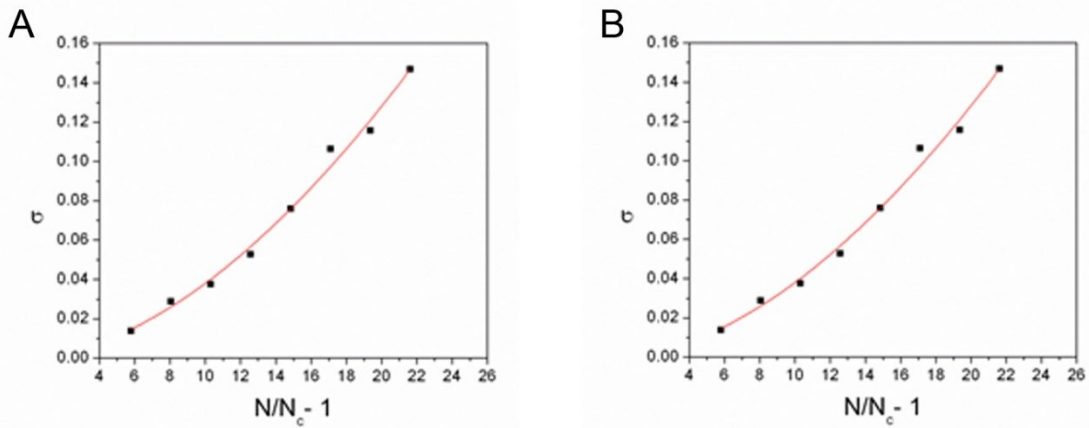


Figure 12: Conductivity percolation scaling fits to experimental data from silver nanowire films with dimensions A) $L_{nw} = 21.65 \mu\text{m}$, $D_{nw} = 84 \text{ nm}$, and $L/D = 258$ and B) $L_{nw} = 20.60 \mu\text{m}$, $D_{nw} = 75 \text{ nm}$, and $L/D = 275$. Fits to both data sets yield a value of the conductivity exponent $t = 1.75$, which is consistent with contact resistance dominated transport ($R_c \gg R_{nw}$) as predicted theoretically by both Stanković⁵⁷ and Cleri.⁵⁸ The universal conductivity exponent for 2D networks $t \approx 1.3$ is expected to hold at densities very close to the percolation threshold.⁹

is a large amount of surfactant on the surface of the wires and the wires do not conform to one another very well, which causes small contact areas. This assumption will start to falter as the average distance between nanowire contacts increases (Resistance = $\rho \cdot \text{length}/\text{area}$). The parameter $R_{c_effective}$, however, can be considered as a lumped parameter that can account for any non-idealities within the system. Furthermore, the conductivity exponent is consistent with theories reported by both Stanković⁵⁷ and Cleri⁵⁸ that point toward transport that is dominated by contact resistance.

The simulations were best fit to experimental results when $R_{c_effective}$ was between 1.5 and 2.5 k Ω (Figure 11). It is important to point out that the same $R_{c_effective}$ range fit all three experimental data sets with $D_{nw} = 50$ nm – 84 nm, which shows that $R_{c_effective}$ has only a minimal sensitivity to diameter change across a narrow range. For their simulations, an $R_{c_effective} = 2$ k Ω was applied to show how the aspect ratio (L/D) and area fraction (AF) affect the sheet resistance in silver nanowire films (Figure 13).

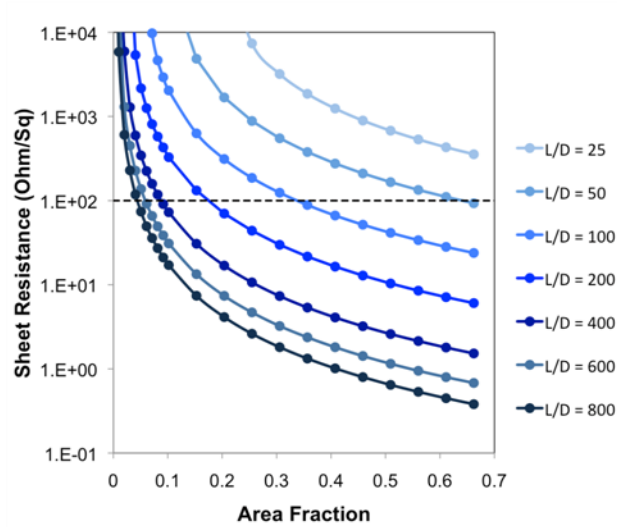


Figure 13: Sheet resistance from simulations as a function of L/D and AF of the rods in nanowire films using an effective average contact resistance $R_{c_effective} = 2$ k Ω and constant $D_{rod} = 50$ nm. The dashed line indicates the desired performance criterion $R_s \leq 100 \Omega \text{ sq}^{-1}$ for high performance applications.⁹

A broad range of aspect ratios, $L/D = 25-800$, was used in the nanowire network simulations, where all the wires had a $D_{wire} = 50$ nm and various lengths ($L_{wire} = 1.25 - 40 \mu\text{m}$). As can be seen in Figure 13, the sheet resistance followed three stages for each L/D which is typical to percolative behavior: (1) very resistive network at low nanowire

densities ($AF = 0.01$ when $L/D = 800$), (2) rapid decrease in sheet resistance in the critical region in the vicinity of the percolation threshold, and (3) weakening network dependence at high nanowire densities when the networks are well established.⁹

The sheet resistance is highly dependent on the aspect ratio. Figure 13 shows that the sheet resistance changes by over three orders of magnitude from an L/D of 25 to 800. These simulations show that an L/D of 100 is needed for applications that allow a maximum sheet resistance of $100 \Omega \text{ sq}^{-1}$ and that in order to optimize the properties of metal nanowire transparent conductors very high L/D 's should be pursued.

The aspect-ratio effect on sheet resistance in Figure 13 shows high aspect ratio wires can form percolative networks at lower densities. Pike and Seager showed that for widthless 2D sticks, the critical number density of sticks (N_c) required to form a percolated network is inversely proportional to L_{stick} ($N_c \propto 5.71/L_{stick}^2$).⁵⁹ This shows that longer stick lengths will be able to make networks with less sticks resulting in higher conductivities at lower densities, which is consistent with the findings in Figure 13. The finding that $L/D > 100$ is required for $R_s \leq 100 \Omega \text{ sq}^{-1}$ at modest nanowire densities is also consistent with our recent experimental results,⁸ where we observed best performances for silver nanowire films with an $L/D = 182$ and 375.

Figure 13 also shows the importance of L/D at high area fractions. De et al.⁵⁴ observed the conductivity of dense silver nanowire networks transitions from

percolative to “bulk-like” behavior with increasing thickness. The conductivity eventually became constant for thick films plateauing around 8% of the bulk conductivity of silver. Winey’s simulations show that for a dense nanowire network the minimum sheet resistance is highly dependent on the aspect ratio of the nanowires. Their contact-resistance dominated system shows that the sheet resistance of nanowire films made with wires that have lower aspect ratios will plateau roughly three orders of magnitude higher than films made with wires that have higher aspect ratios. These results are expected since there is a high penalty for additional contacts⁶⁰ and the number of contacts per rod is proportional to number of rods.^{57, 58}

Transparent conductors must display both low sheet resistances and high optical transparencies. Adjusting both of these properties has proven to be difficult. In order to increase the transmittance of the film, the area fraction of the wires needs to be decreased, but as the area fraction is decreased the sheet resistance starts to increase. Because of these interdependencies, the metal nanowire transparent conductor field needs a theoretical framework for predicting how nanowire properties and network structure affect both of these parameters to guide future experimental work. We recently studied the experimental and FDTD simulated optical properties of silver nanowire films, reporting linear dependence of network transmittance to area coverage of nanowires for a given nanowire diameter.⁵³ We showed that the optical properties are

independent of the nanowire length and found that the area fraction (AF) and the optical transmittance at $\lambda = 550$ nm can be related by:

$$\%T = 1 - \exp(-a_1 AF) \quad (2)$$

where a_1 is a fitting parameter that accounts for the diameter, wavelength-dependent optical properties, and the effects of holes in the network. Winey used this expression ($a_1 = 87$) and combined it with their simulated sheet resistance values using $R_{c_effective} = 2$ k Ω , and constructed Figure 14. This plot predicts how both the $\%T$ and sheet resistance

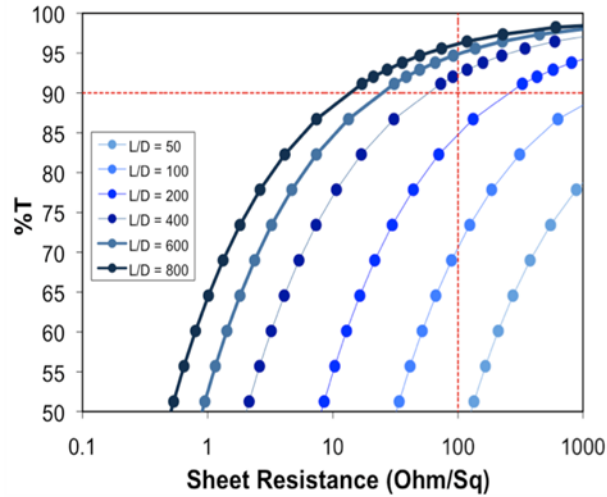


Figure 14: Calculated transmittance vs. simulated sheet resistance for silver nanowire films for L/D ranging between 50 and 800 with $R_{c_effective} = 2$ k Ω and constant $D_{nw} = 40$ nm . $\%T$ values were calculated using the empirical expression in equation 1.⁵³ Dashed lines indicate desired performance criteria $\%T > 90\%$ and $R_s \leq 100 \Omega \text{ sq}^{-1}$ for high performance applications.⁹

depend on the nanowire length (at fixed $D_{nw} = 40$ nm) and area fraction and is the first fully calculated plot of $\%T$ vs. sheet resistance in thin-film nanowire networks (each point on the curve represents a specific area fraction).

Figures 13 & 14 demonstrate that high uniform L/D nanowires are the most promising candidates to replace ITO. However, most nanowire syntheses very rarely yield monodispersed nanowires. To show the effect of non-uniform nanowire lengths, Winey and coworkers simulated a wire network using a bi-disperse distribution of lengths. They used a set of reference wires with an $L/D = 50$ ($L_{Ref} = 2.5$ μm and $D_{Ref} = 50$ nm) and longer rods with an $L/D = 400$ ($L_{Long} = 20$ μm and $D_{Long} = D_{Ref}$) in various proportions expressed as a relative area fraction, $F_{Long} = AF_{Long} / (AF_{Ref} + AF_{Long})$. The proportion of wires was varied between $F_{Long} = 0$ (monodisperse; $L/D = 50$) and 1 (monodisperse; $L/D = 400$). They used an $R_{c_effective} = 2$ k Ω for the wire junctions and continued the assumption of $R_{nw} = 0$. Figure 15 shows a plot of the sheet resistance as a

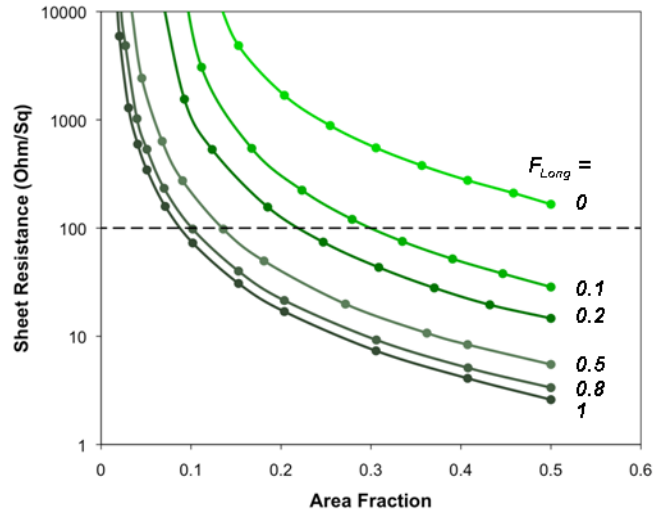


Figure 15: Simulated sheet resistance as a function of area fraction using $R_{c_effective} = 2$ k Ω for nanowire films comprised of bidisperse mixtures of rods with $L/D = 50$ (Reference) and 400 (Long). The diameter is the same for both nanowire populations ($D_{Ref} = D_{Long} = 50$ nm), while the low- and high-aspect-ratio nanowires have lengths of 2.5 and 20 μm , respectively. The proportion of longer rods in the network is expressed as a relative area fraction, $F_{Long} = AF_{Long} / (AF_{Ref} + AF_{Long})$.⁹

function of the total area fraction for $F_{Long} = 0, 0.2, 0.5, 0.8$ and 1 for these bidispersed wire networks. When only 10% of the wires were long, the sheet resistance dropped by almost an order of magnitude, and as the fraction of long wires continued to increase, the simulated film's sheet resistance decreased. Figure 15 also shows that if a small amount of shorter wires are mixed in with longer wires, the impact on the film's sheet resistance is relatively small.

3. Nanowire Synthesis

The fact that metal nanowires can be grown in liquid solutions at low temperatures makes them particularly easy to commercialize because solution-phase syntheses are orders of magnitude less capital-intensive and easier to scale than vapor-phase processes. It is remarkable to note that methods for the solution-phase growth of metal nanowires without a template did not exist ten years ago, but now there are hundreds of different syntheses for producing metal nanowires in solution, and about a dozen companies producing and selling metal nanowires for a variety of applications. All solution-phase syntheses of nanowires are similar in that they require a reducing agent to convert metal ions into metal, and a capping agent to direct anisotropic assembly of the metal atoms into nanowires. This section will highlight some of the synthetic processes capable of producing metal nanowires from silver, copper and gold with lengths, widths, and yields well-suited for use in transparent conducting films.

3.1 Silver Nanowires⁸

The polyol synthesis of silver nanowires developed by Sun, Xia and co-workers in 2002 represents one of the earliest syntheses suitable for scalable production of metal nanowires, and variations of it are widely used for commercial production of silver nanowires for transparent conducting films.⁶¹⁻⁶³ This synthesis involves the reduction of silver ions by hot ethylene glycol (EG) in the presence of polyvinylpyrrolidone (PVP), a

polymeric capping agent. Typically the EG is preheated to the desired temperature (~150 °C) before adding solutions containing the dissolved silver precursor (usually AgNO₃) and PVP (a molecular weight of 55,000 seems to work best).

Heating of the ethylene glycol generates glycolaldehyde, which in turn reduces the silver ions to atoms. The atoms then agglomerate to form nuclei. At a small size, the nuclei crystal structure will fluctuate between a single-crystalline, single-twinned, or a multiply twinned decahedral morphology. As the nuclei grow, the amount of energy required to break the bonds in the nuclei and modulate its morphology becomes greater than the thermal energy available. At this point the nuclei become stuck in a given morphology, and are then called seeds. Generally a high-yield of the multiply twinned seeds are observed due to the ability of twinning to increase the coverage of the lowest-surface-energy, (111) facets. Silver atoms preferentially add to the faces of the decahedra, leading to their elongation into nanorods. PVP is then thought to preferentially adhere to the sides of the nanorods, leaving their ends open to further atomic addition. This leads to the rapid anisotropic growth of nanowires to form nanowires.

For consistently high yields of high-aspect-ratio silver nanowires, the starting EG should contain very low concentrations of Fe and Cl species, which are common contaminants. One source for high purity EG is J.T. Baker, which conveniently puts the

lot analysis for Cl and Fe on the label. Before using the EG in the reaction, it must be doped with a controlled amount of Fe and Cl (for example, with about 5 μM of $\text{Fe}(\text{NO}_3)_3 \cdot 9\text{H}_2\text{O}$ and 0.22 mM of NaCl). If no Cl is added, the silver seeds will rapidly agglomerate into spheroids. Although it's not entirely clear how the Cl ions prevent aggregation of seeds, one possibility is that the Cl ions coordinate to the surface of the seeds, imbue them with negative charge, and thus electrostatically stabilize them against aggregation. However, if the reaction is performed in air, the coordination of Cl ions to the silver decahedra will assist in their oxidative dissolution. One way to prevent this is to add Fe species. Although it is again not entirely clear how a small amount of Fe can prevent oxidative dissolution, one possibility is that reduction by glycolaldehyde keeps the iron species in the divalent state, and these divalent iron species act as oxygen scavengers.

Previous work has shown that the reducing power of EG increases with temperature, and that this effect is due to the temperature-dependent oxidation of ethylene glycol to glycolaldehyde, the reducing agent.⁶⁴ The temperature-dependent reducing power of EG is apparent in Figure 16A, which clearly shows nanowire growth

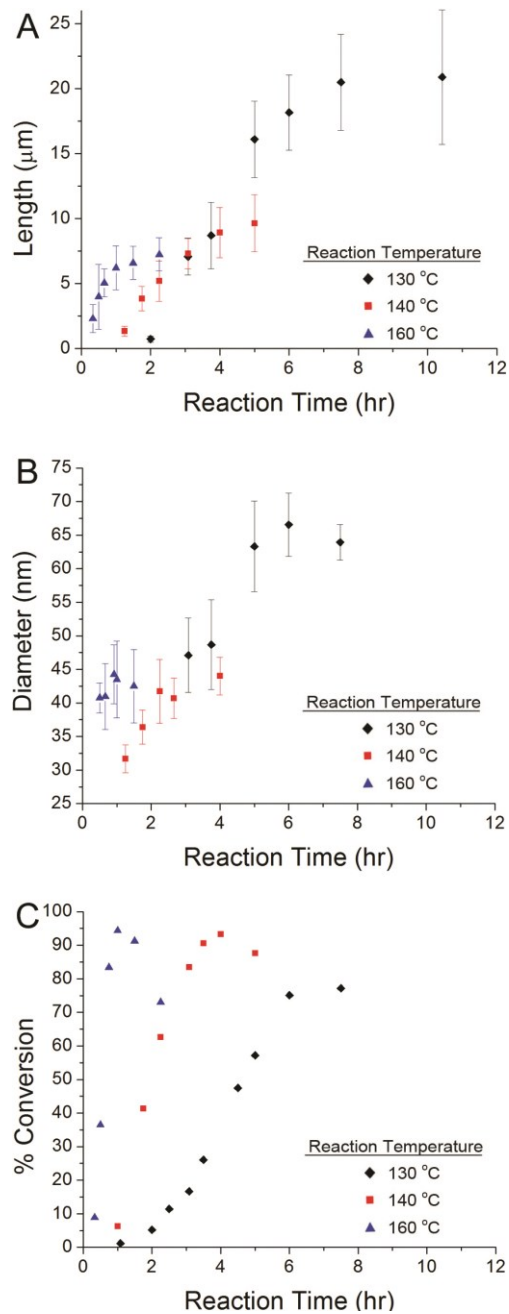


Figure 16: (A) Silver nanowire length, (B) silver nanowire diameter, and (C) % conversion of Ag^+ to Ag^0 vs. time for three reaction temperatures. Lower temperatures lead to the formation of longer nanowires with larger diameters.⁵³

occurs more rapidly at higher temperatures. For example, nanowires grew to a length of 5 mm at 160°C within 30 minutes, but it took two hours for them to reach the same length at a reaction temperature of 140 °C. Figure 16A & B illustrate that longer nanowires with larger diameters could be produced at lower reaction temperatures. For example, the longest nanowires that could be obtained at 160°C were 7.5 μm in length and 45 nm in diameter, while those produced at 130°C could reach lengths of over 20 μm, with diameters of 65 nm.

It is hypothesized that the reason the nanowires grew longer and wider at lower temperatures was because the nucleation rate was lower at lower reaction temperatures, leaving more silver precursor per nuclei. To test this hypothesis, the percent conversion of Ag^+ to Ag^0 vs. reaction time (Figure 16C) were measured and plotted. This plot confirms the reduction rate was greater at higher reaction temperatures, which in turn likely supported a higher nucleation rate. Not surprisingly, the time at which the maximum percent conversion was reached roughly corresponds to the time at which nanowires stopped growing. Given that both high and low temperature reactions produced roughly the same mass of reduced silver, but wires of different lengths, we conclude that the higher temperature reactions contained a higher number density of nanowires, and thus a higher density of nanowire nuclei (five-fold twinned decahedra) must have formed during the nucleation stage of the reaction.^{65, 66}

The decrease in the percent conversion seen at the very end of the high-temperature reactions could be due to settling and aggregation of the wires, as well as etching by nitric acid. Acid is generated during the reduction of silver ions by glycolaldehyde through equation (3). The greater rate of reduction at higher



temperatures likely resulted in a more acidic environment, and thus a greater etching rate. Using a pH strip, we measured the 160°C reaction to have a pH = 4 at 30 minutes, and pH = 2 at 2 hours. The reaction also gave off a reddish-brown gas similar in color to the NO gas given off by nitric acid; this gas had a pH = 1. If the reaction was allowed to run for long times (>1.5 hours) at 160°C, a large clump of silver formed at the bottom of the reaction flask. As this clumping did not occur as readily at 130°C, it seems likely that the aggregation of the nanowires at high temperatures and long reaction times is induced by the in situ generation of acid.

Knowing the effect of temperature and reaction time on the growth rate of the nanowires, we could judiciously select reaction conditions to produce nanowires with distinct lengths and diameters. An example set of reaction conditions for obtaining nanowires with nine different lengths and diameters is given in Figure 17A. In some

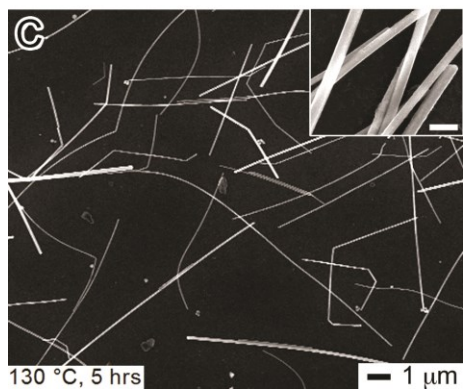
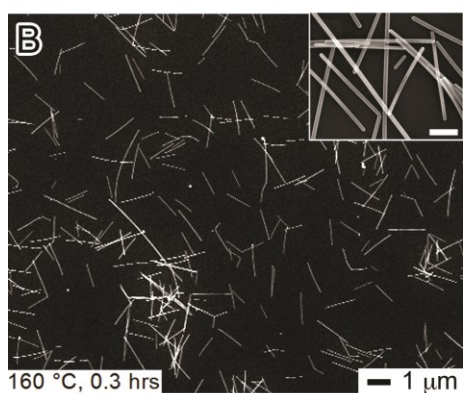
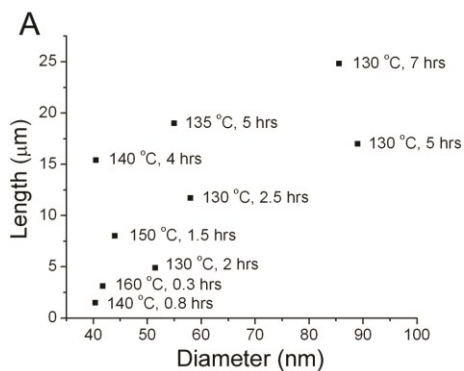


Figure 17: (A) Reaction conditions for synthesizing nanowires with distinct lengths and diameters. (B) SEM image of the silver nanowire product after growth for 0.3 hours at 160°C. The nanowires are 42 ± 5 nm in diameter and 3 ± 0.5 μm in length. (C) SEM image of the silver nanowire product after growth for 5 hours at 130°C. The nanowires are 85 ± 25 nm in diameter and 25 ± 5 μm in length. The scale bar in the inset is 200 nm.⁵³

cases, the reaction procedure was modified to obtain fewer nuclei, and thus nanowires with larger diameters. For example, the reaction was heated at a lower temperature (e.g. 120°C) during the nucleation stage of the reaction (first 5 minutes), and then brought up to a higher temperature (e.g., 130°C for 7 hours) to induce nanowire growth. Figure 17B & C show SEM images of some of the shortest, skinniest nanowires and longest, fattest nanowires respectively.

Based on Figure 14 it would be beneficial to be able to grow nanowires that have an even higher aspect ratio. Recently Ko and coworkers have developed a method using the as synthesized nanowires that were previously described above as “seeds” for longer nanowires called the successive multistep growth method.³⁸ In this method the starting nanowires from an 8 mL reaction are concentrated down to 1 mL and heated to 95°C to decrease the temperature difference before they are added to the reaction flask. Next, 5 mL of ethylene glycol is heated at 151.5°C for 1 hour while stirring. Then a copper additive solution is injected into the flask and allowed to heat for 15 minutes, followed by the addition of a PVP/ EG solution, similar to Xia and coworker’s synthesis.⁶⁷ The starting nanowires are then added to the flask and 1.5 mL of a AgNO₃ solution is injected at a rate of 0.1 mL min⁻¹. To further increase the length of the nanowires, this process is repeated using the newly lengthened nanowires for each repetition. By

running 7 iterations of this process they were able to obtain wires as long as 500 μm (Figure 18).

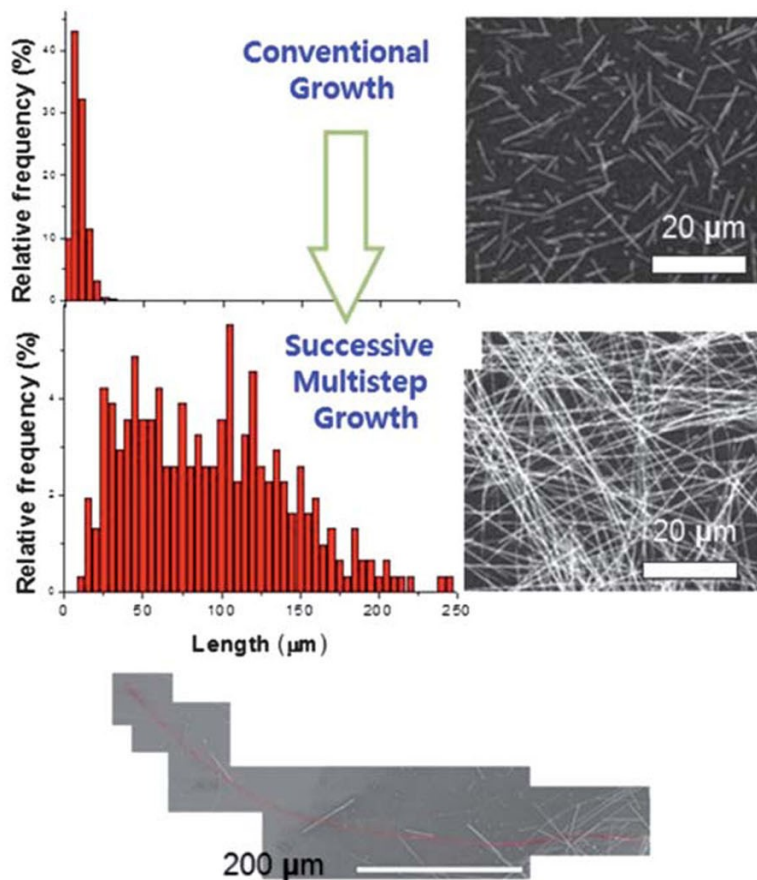


Figure 18: AgNW length distribution graph for regularly grown AgNWs (top) and AgNWs grown using the successive multistep growth method (middle). The bottom SEM image is showing the longest nanowire obtained.³⁸

We can also change the diameter of AgNWs by reducing additional silver onto the sides of the nanowire. AgNWs were put into a flask with ammonium hydroxide and ammonium tartrate, mild reducing agent, and stirred following a modified Zhang

reaction.⁶⁸ Silver nitrate was then slowly injected into the reaction solution over several hours to increase the diameter of the wires, (Figure 19), following equations 4 & 5.

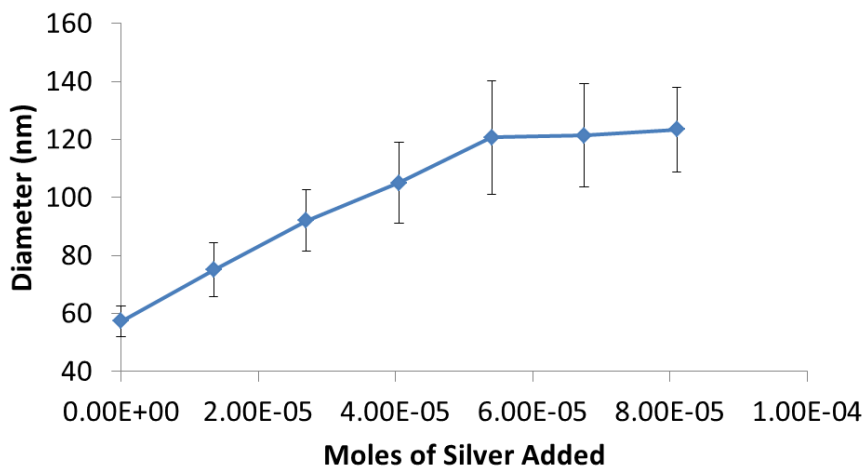
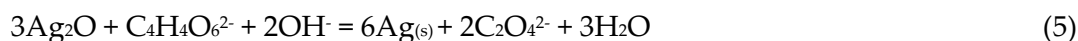
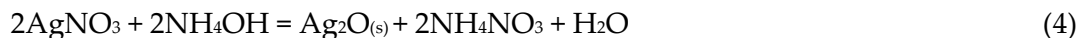


Figure 19: Plot showing the diameter increase of silver nanowires vs. moles of silver added



3.2 Copper Nanowires

3.2.1 Ethylenediamine Capped Copper Nanowires^{5, 6}

Zeng and coworkers developed one of the first scalable solution based synthesis of copper nanowires in 2005.⁶⁹ In this synthesis, copper ions are reduced by hydrazine in a basic solution containing ethylenediamine following equation 6. In a



typical synthesis all of the reagents are added together and placed in a water bath set at 60°C while stirring. After 15 minutes to 15 hours the copper products were collected and washed. The resulting copper nanowires were 90-120 nm in diameter and 40-50 μm long (aspect ratio = 350-450).

In our own work,⁵ we used the approach Zeng and coworkers used with a few modifications. To start we scaled the reaction up by 100 times to show the potential for large scale synthesis. In our reaction NaOH (2000 mL, 15M), Cu(NO₃)₂ (100 mL, 0.2M), EDA (30 mL), and hydrazine (2.5 mL, 35 wt%) were added to a reaction flask and heated at 80 °C for 60 minutes. The solution went from a royal blue (Figure 20A), indicative of

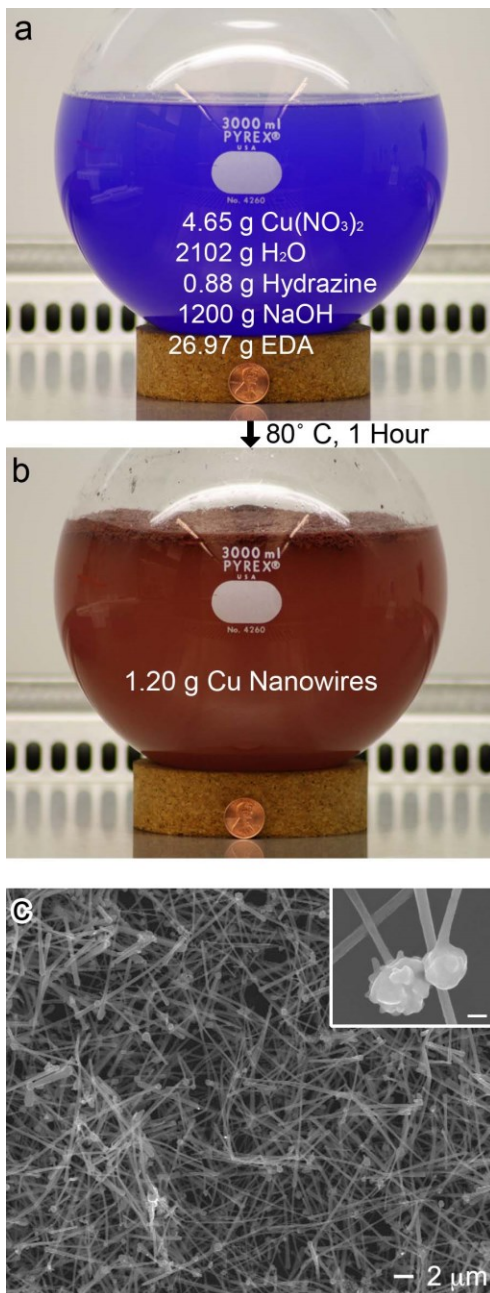


Figure 20: Pictures of the reaction flask A) before the synthesis and B) after growth of CuNWs at 80 °C for 1 hr. C) SEM image of CuNW product. The nanowires are 90 ± 10 nm in diameter and 10 ± 3 μm in length. The inset shows CuNWs with a spherical copper particles attached at one end (scale bar = 200 nm).⁵

the square planar $\text{Cu}(\text{OH})_4^{2-}$ complex,⁷⁰ to a reddish brown color indicative of CuNW formation (Figure 20B) after 20 minutes. After the reaction, the CuNWs were washed with a 3 wt% aqueous solution of hydrazine, and stored in the same hydrazine solution at room temperature under an argon atmosphere to minimize oxidation.⁶⁹

Figure 20C shows a scanning electron microscope (SEM) image of the reaction product, consisting of CuNWs with a diameter of 90 ± 10 nm, and a length of 10 ± 3 μm . An x-ray diffraction pattern of this nanowire product confirms that the nanowires are FCC copper (Figure 21). The inset image shows a close up of the wires, in which it

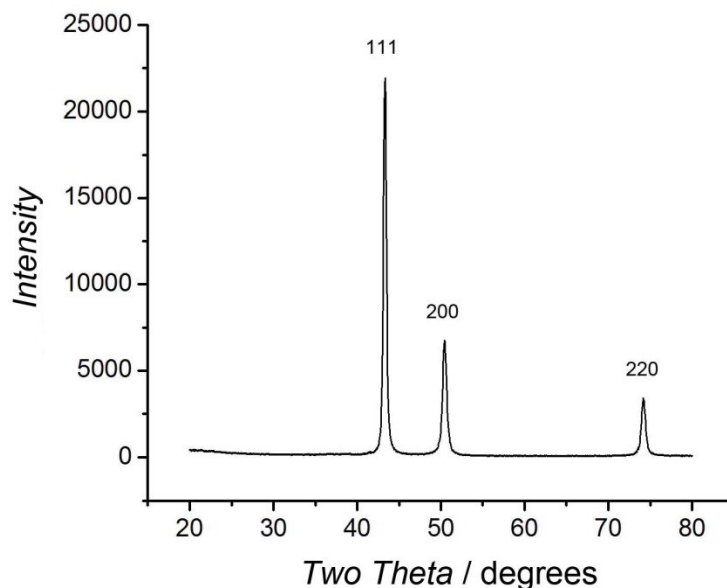


Figure 21: XRD pattern of copper nanowires

appears spherical nanoparticles are attached to one end of the nanowires. We could observe many similar wires with spherical nanoparticles attached at one end, but

initially it was not clear if the wires grew from the spherical nanoparticles, or if the spherical nanoparticles formed at the ends of the nanowires in the later stages of growth. These spherical particles at the ends of CuNWs were not previously observed in the work of Zeng et al.

To determine if CuNWs did indeed grow from spherical seeds, we stopped the CuNW reaction at different times and examined the products with electron microscopy. These reactions were performed at a scale that was one hundred times smaller than that shown in Figure 20 with one-half the concentration of $\text{Cu}(\text{NO}_3)_2$ and EDA. As with the scale up reaction, the reaction color was initially blue, but became cloudy at 0.5 min., and clear at 2.5 min. The reaction mixture stayed clear until approximately 3 min. into the reaction, at which time we observed the first copper precipitate suspended in the solution. SEM images of this precipitate (Figure 22A) revealed CuNWs 100 ± 10 nm in

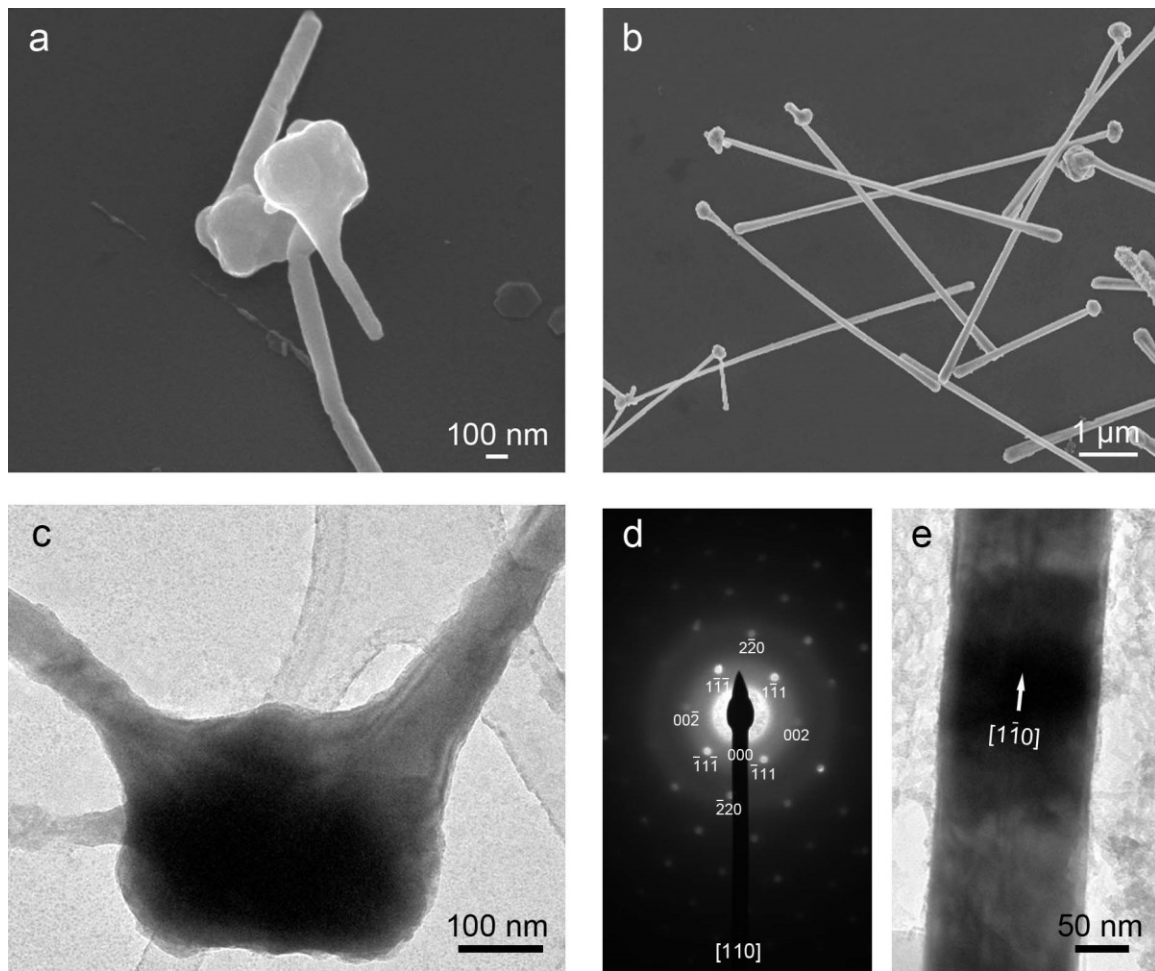


Figure 22: A) SEM image showing copper nanorods sprouting from spherical copper seeds at a reaction time of 3.5 minutes. B) By 20 minutes the rods had grown to form longer wires. C) TEM image of two CuNWs growing out of a nanoparticle. D) A selected area electron diffraction pattern (SAED) from the nanowire shown in E) indicates the nanowire grew along the $[1\bar{1}0]$ direction.

diameter and less than $1\ \mu\text{m}$ in length growing out of spherical nanoparticles. After reacting for 20 minutes (Figure 22B), wires grew to be $6 \pm 1\ \mu\text{m}$ in length, and were still attached to the spherical nanoparticles. The reaction was stopped after 60 minutes, at

which time the CuNWs were $10 \pm 3 \mu\text{m}$ in length, which was consistent with the length observed for the wires in the large-scale reaction. These images definitively show that CuNWs grew from spherical seeds. This growth mechanism has not been previously observed for CuNWs, and is further unique among all known solution-based syntheses of metal nanowires. The growth of Pt nanowires (PtNWs) from large, spherical aggregates of nanoparticles is somewhat similar in that both nanowires grow from spherical nanoparticles.^{71, 72} The growth mechanisms differ in that hundreds of PtNWs grow from spherical aggregates in a structure similar to a sea urchin, where in the case of Cu, only one or two wires typically grow from a single seed.

To gain insight into the reason why CuNWs grew from spherical seeds, we examined the seed-nanowire interface with transmission electron microscopy (TEM). Figure 22C shows two CuNWs 70 nm in diameter that grew out of a spherical nanoparticle. The lack of any sharp difference in contrast between the nanoparticle and nanowire suggests the seed-wire interface consists of a single crystal. Figure 22D shows a selected area electron diffraction (SAED) pattern from the nanowire shown in Figure 22E. This pattern indicates the electron beam is oriented along the [110] zone axis, and that the nanowire grew along the $[1\bar{1}0]$ direction. We obtained the same SAED pattern from several nanowires, suggesting that the nanowires preferentially lay with a (110) facet in contact with the substrate.

The CuNWs grew via atomic addition to (110) planes, which have the highest-surface energy among the low-index facets of copper and all other fcc metals.⁷³⁻⁷⁵ Single-crystalline nanostructures of Pb,^{76, 77} Al,⁷⁸ and Ag⁷⁹ also grow via atomic addition to the (110) planes, but single-crystalline nanostructures of Au,^{80, 81} Pt,^{71, 72} and Rh⁸² grow via atomic addition to (111) planes. The lack of correlation between the surface energy of a metal and the direction of anisotropic growth in solution suggests that other forces besides surface energy drive anisotropic growth.

The addition of EDA to the reaction solution is necessary to promote anisotropic growth of CuNWs. When EDA was not added to the reaction, only spheres with diameters ranging from 125-500 nm were present after 1 hour. The amine groups of EDA allow it to bind to the surface of copper nanostructures in solution. If EDA binds preferentially to the side facets of the CuNWs, this could cause preferential growth along the axial [110] direction. To examine the role of EDA as a possible director of anisotropic growth in the reaction, we studied the effect of EDA concentration on the diameter and length of the nanowires (Figure 23). As the concentration of EDA was

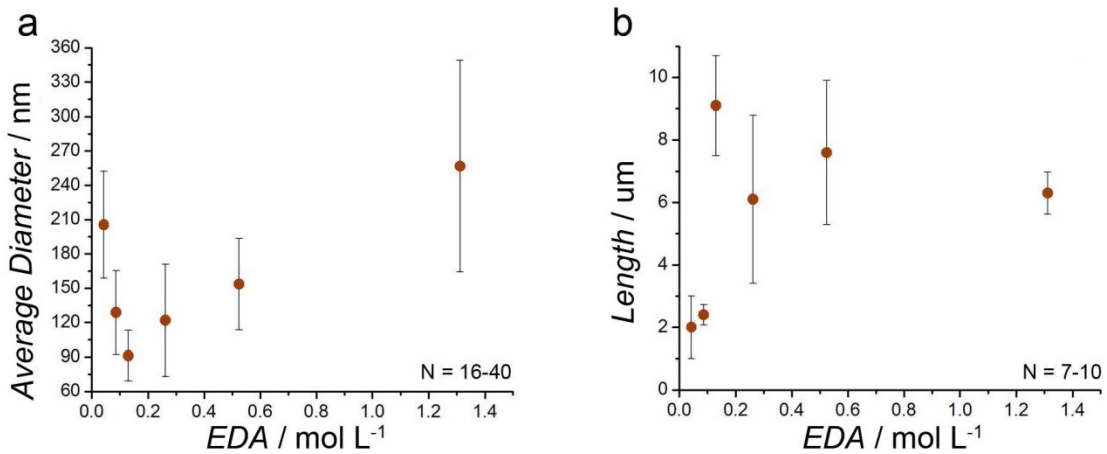


Figure 23: A) CuNW diameter (nm) versus EDA concentration (moles L⁻¹). Error bars show one standard deviation for 16-40 measurements. **B) CuNW length (μm) versus EDA concentration (moles L⁻¹).** Error bars show one standard deviation for 7-10 measurements. An EDA concentration of 0.13 M was ideal for growing the longest, thinnest wires, presumably because EDA selectively capped the sides of the wires. Higher concentrations of EDA may have capped the ends as well as the sides, leading to shorter, fatter wires.

increased from 0.04 M (the minimum necessary for formation of nanowires) to 0.13 M, the diameter of the nanowires decreased from 205 nm to 90 nm, while the length increased from 2 μm to 9 μm. Increasing the concentration of EDA further to 1.31 M increased the diameter by a factor of about three (260 nm) and decreased the length to 6 μm. This data suggests that low concentrations of EDA preferentially cap the sides of the wire, leading to anisotropic growth of long, thin nanowires. Higher concentrations of EDA may cause capping of wire ends as well as the sides, leading to shorter wires with larger diameters.

In an effort to make longer, thinner copper nanowires we developed a new synthesis.⁶ In our new synthesis, we heated the reaction mixture only a short time (about 3 minutes at 80 °C) in order to induce reduction of copper ions (as indicated from a change in the reaction color from blue to clear). PVP was then added to this mixture to prevent the CuNWs from aggregating, and this mixture was quickly cooled in an ice bath. This process allowed the CuNWs to grow at a lower temperature, which could have reduced the initial amount of copper seed particles and rate of copper reduction, resulting in a longer ($20 \pm 5 \mu\text{m}$), thinner ($52 \pm 17 \text{ nm}$) morphology (Figure 24).

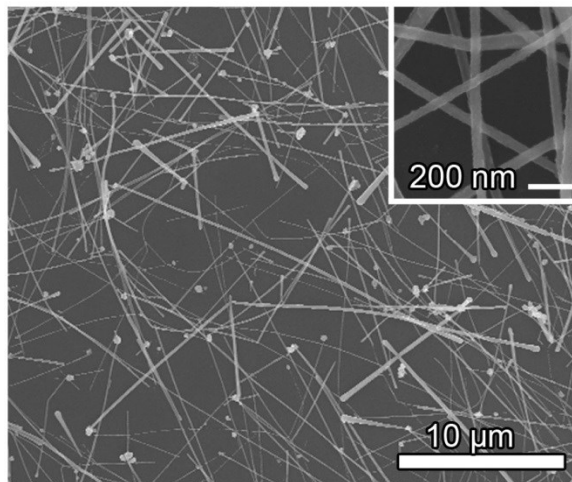


Figure 24: SEM image showing the average length ($20 \pm 5 \mu\text{m}$) and diameter ($52 \pm 17 \text{ nm}$) of copper nanowires.

3.2.2 Nickel-Coated Copper Nanowires⁷

Copper nanowires have excellent properties when they are made into transparent electrodes, but they have two problems that hinder their practical

implementation: (1) copper oxidizes, and (2) copper is reddish-orange in color, which is an undesirable characteristic for displays.

Alloying copper with nickel makes it grey in color and highly resistant to oxidation. For these reasons, cupronickel is widely used in coinage (the U.S. nickel is a 3:1 Cu:Ni alloy), as well as salt-water marine applications (boat hulls, propellers, ect.). There is only one previous paper that describes the production of copper nanowires with a nickel coating in a “one-pot” synthesis.⁸³ In this work, the nanowires were 200-300 nm in diameter, with the outer 20-30 nm consisting primarily of nickel. Although this work represents a good first step, the diameters of these nanowires are too large to be suitable for use in high-performance transparent conductive films, and the nanowires could be produced only at one copper to nickel ratio (13:7); other ratios produced spikey, spherical particles.

Copper nanowires, were synthesized in a manner similar to that which was reported previously.⁶ The nanowires were stored at a copper nanowire concentration of 1.4 mg mL^{-1} in an aqueous solution containing polyvinylpyrrolidone (PVP, 1 wt %) and diethylhydroxylamine (1 wt %). Cupronickel nanowires were synthesized by adding the copper nanowire stock solution (0.732 mL) to a 20 mL scintillation vial containing a solution (1.32 mL) of PVP (2 wt %) in ethylene glycol, a given amount of a solution containing $\text{Ni}(\text{NO}_3)_2 \cdot 6\text{H}_2\text{O}$ (0.1M) in water (157, 78.7, 39.3, or 15.7 μl for nanowires

containing 54, 34, 20, 10% Ni, respectively), and hydrazine (132 μ L, 35 wt %). This mixture was vortexed for 15 seconds and heated at 120 °C for 10 minutes without stirring. During the heating step, the copper nanowires aggregated and floated to the top of the solution. As the Ni reduced onto the copper nanowires, they became darker in color. After heating for 10 minutes, the solution was removed with a pipette, and the nanowires were dispersed in a solution containing PVP (1 wt %) and hydrazine (3 wt %).

Figures 25A-C show energy dispersive x-ray spectroscopy images of a copper

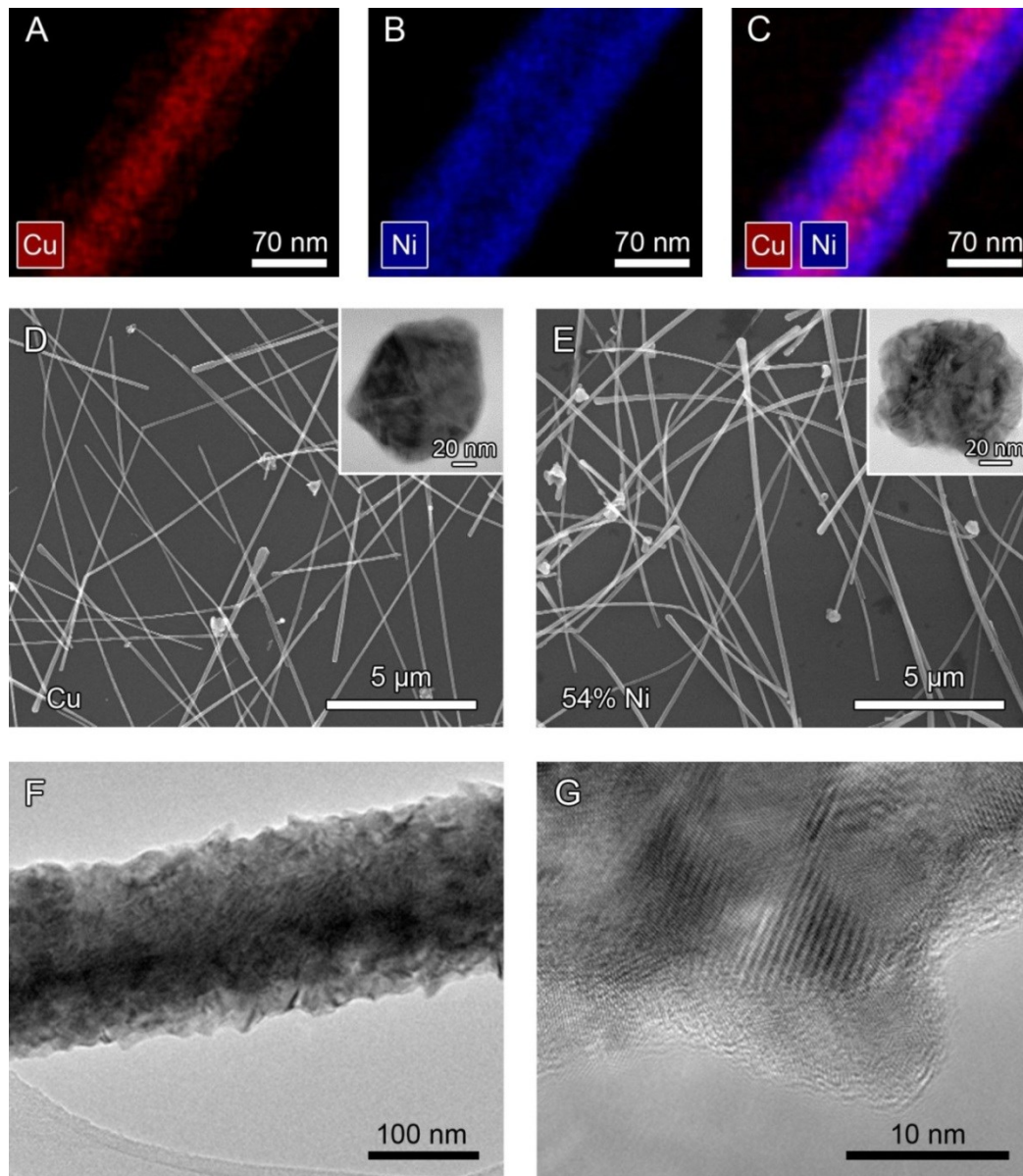


Figure 25: A-C) Energy dispersive x-ray spectroscopy images of a copper nanowire coated with 54 mole % nickel. D) Copper nanowires before coating. The nanowires had a length of $28.4 \pm 7.1 \mu\text{m}$ and a diameter of $75 \pm 19 \text{ nm}$. E) After the copper nanowires were coated with nickel to a concentration of 54 mole %, the diameter of the wires increased to $116 \pm 28 \text{ nm}$. The insets of D & E show the cross sections of the copper nanowire and cupronickel nanowire respectively. F & G) TEM images of the polycrystalline cupronickel nanowires with a grain size of 10 nm .⁷

nanowire coated with nickel to a content of 54 mole % (roughly 1:1 Cu:Ni). As shown in panel A, copper is present not only in the core of the wire, but also diffuses into the nickel shell, creating a shell composed of a cupronickel alloy. Since copper and nickel are completely miscible in all proportions, it is not surprising that these two elements interdiffuse after the nickel coating to form a nanowire consisting of a cupronickel alloy. Figure 25D shows the copper nanowires before coating; these nanowires had an average length of $28.4 \pm 7.1 \mu\text{m}$ and an average diameter of $75 \pm 19 \text{ nm}$. The inset is a TEM image of a microtomed cross-section of a copper nanowire, showing that it has a 5-fold twinned crystal structure and a pentagonal cross-section similar to silver nanowires synthesized in ethylene glycol.^{65, 66} After coating to a wire composition of 54 % Ni, the diameter of the nanowires increased to $116 \pm 28 \text{ nm}$ (Figure 25E). A TEM cross-section of a microtomed cupronickel nanowire in the inset of Figure 25E shows the five-fold twinned crystal structure became distorted and more randomly polycrystalline after alloying. It is not entirely clear why this transformation in the crystal structure took place, but this image seems to suggest that the diffusion of nickel into the copper nanowire caused a rearrangement of the copper atoms, and a conversion of the original five-fold twinned crystal structure into one that is characterized by small, random

crystal domains. TEM images (Figure 25F & G) of the 1:1 Cu:Ni nanowires show that the nickel coating is polycrystalline with a grain size on the order of 10 nm.

3.2.3 Hexadecylamine Capped Copper Nanowires

Mohl and coworkers recently developed a new method to synthesize copper nanowires.⁸⁴ They found that hexadecylamine will preferentially bind to the (100) facets, which, when combined with the reducing agent, glucose, allows copper to add to the (111) facets and form nanowires similar to the silver nanowire synthesis. This synthesis is also similar because the copper nanowires that are formed have a five-fold twinning pattern that is parallel to the nanowire.

A typical synthesis starts by mixing 21 mg of $\text{CuCl}_2 \cdot 2\text{H}_2\text{O}$, 50 mg of glucose, 180 mg of hexadylamine, and 10 mL of water in a capped vial at room temperature overnight.^{84, 85} The vial is then heated in an oil bath to 100°C for 6 hours while stirring. As with the ethylenediamine capped copper nanowire reaction, as the reaction progressed the color of the solution went from blue to red signifying that Cu^{2+} was reduced to Cu^0 (inset of Figure 26). The nanowires had an average diameter of 24 ± 4

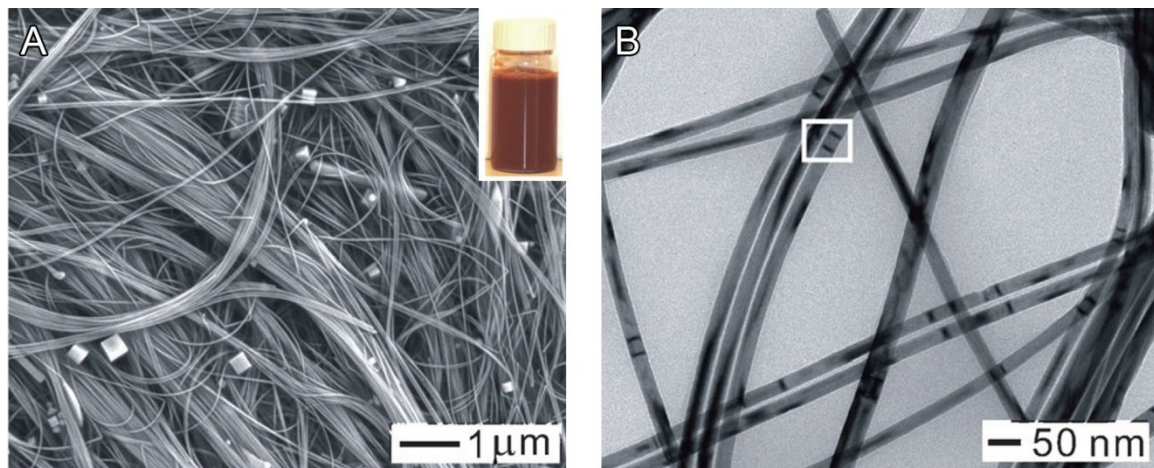


Figure 26: A) SEM and B) TEM images of copper nanowires synthesized by Xia and coworkers. The inset in A) shows the copper nanowire solution.⁸⁵

nm and lengths ranging from tens of micrometers to hundreds of micrometers. The SEM images in Figure 26 show that the wires are aligned in parallel, most likely due to the hydrophobic tail of the hexadecylamine that is covering the nanowires.

3.3 Gold Nanowires

The solution-based synthesis of gold nanowires is surprisingly simple and easily scalable. The basic approach requires chloroauric acid (HAuCl_4) to be dissolved in oleylamine (OA) and allowed to sit at 25-85°C for 2-30 hours.^{81, 86-89} The resulting nanowires are <2 nm in diameter and anywhere from a few hundred nanometers to almost 10 micrometers in length (Figure 27). In this synthesis oleylamine

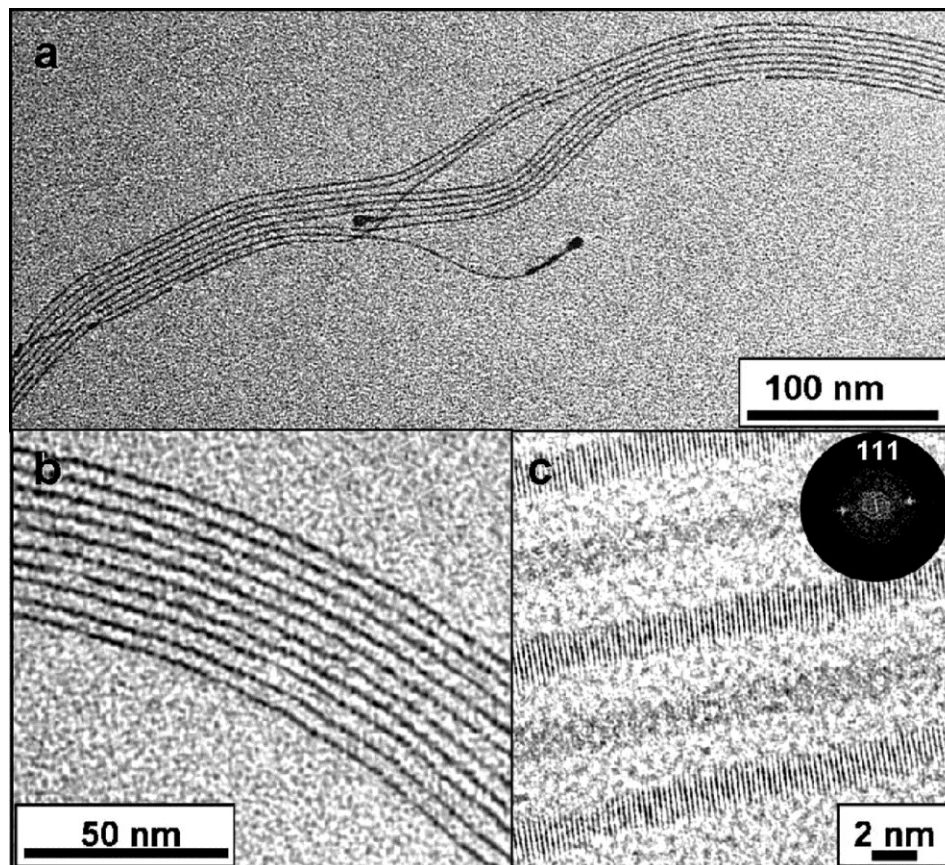


Figure 27: A&B) TEM images showing AuNWs. C) HRTEM image showing the single crystal lattice structure.⁸⁸

acts as the reducing agent, the solvent, and the capping agent. Adjusting the OA/Au volume ratio (0.2-2.2) allows for control over the length of the wires from 10 nm to 4 μ m.

In a typical synthesis H₂AuCl₄ is dissolved in OA by means of sonication at room temperature until the color of the solution turned to an intense orange color, which indicates the formation of a Au³⁺ OA complex. Then the solution is left on the benchtop for at least 24 hours, during which time the solution initially turns to a pale yellow,

indicative of Au^{3+} being reduced to Au^+ , and then the solution gradually turns red as Au^+ is reduced to Au^0 . In order to speed the process up the reaction can be heated,^{88, 89} silver nanoparticles can be added to act as a catalyst,⁸¹ or additional reducing agents such as ascorbic acid⁸⁶ or triisopropylsilane (TIPS)⁹⁰ could be added to the reaction.

Several different mechanisms have been proposed for how AuNWs form. In one such growth mechanism, OA is thought to bind to Au^+ and form an ordered mesostructure which appears to be a white gel.⁸¹ Figure 28 shows a TEM image of the white gel with AuNWs within the polymer strands after it was heated at 60 °C. As Au^+

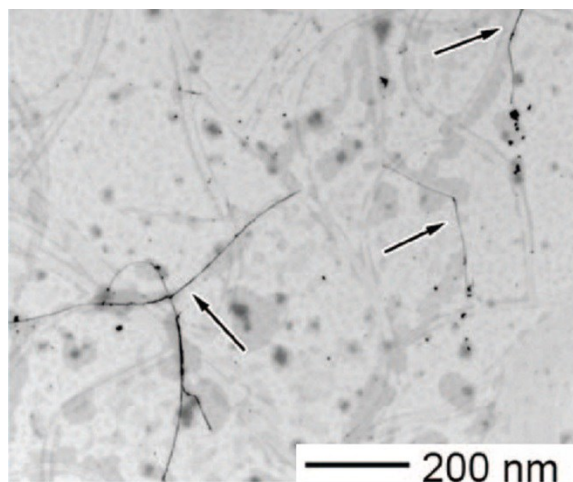


Figure 28: TEM image showing the polymer strands of the white gel and AuNWs within those strands after heating at 60 °C.⁸¹

OA complexes come together they form small crystals with different surface energies for each of their facets. The different surface energies will allow for different OA packing

densities which help guide the growth of the AuNW⁸⁸ (Figure 29 shows a cartoon of this idea⁹¹).

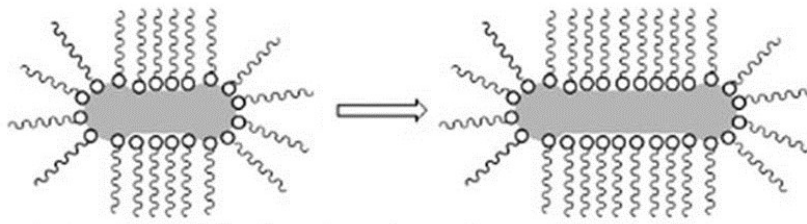


Figure 29: Cartoon image showing the OA complexed metal nanowire growth.⁹¹

Small angle X-ray scattering data further shows that the Au⁺ OA assemblies are separated by 4.7 nm which is roughly the width of a bilayer of OA.⁸⁷

Ravishankar and coworkers proposed a growth mechanism in which Au particles coalesce to form nanowires. The beginning particles are roughly the same diameter as the resulting nanowires, and the nanowires show defects that are seen in oriented-attachment processes. In this process, two particles will fuse together through (111) facets to form a single particle that is single crystalline for maximum energy reduction or a particle with a coherent twin boundary with slightly less energy reduction.

In order for the particles to come together, the OA must first be removed from the facets with the lower binding energy. Calculations using density functional theory suggest that amines will strongly bind to high-index ridge surfaces and then to the 100}

and (111) facets with (100) having a higher binding energy. These calculations also point out that the (100) facets will have more bound amines than (111) facets.⁹² Since the binding energy of an amine on gold is on the order of physisorption, Ravishankar hypothesizes that a surface reaction with ascorbic acid might be able to remove the capping agent from the (111) facets allowing two particles to come together.

When particles coalesce the surface of the new structure is typically not smooth. To account for the smoothness of the AuNWs the smoothing process was proposed. In this process the different chemical potentials associated with the concave and convex regions of the wire leads to smoothing by atomic diffusion, which occurs on the nanosecond timescale.⁸⁶ While this mechanism could be true for all gold nanowire syntheses, this particular synthesis requires the use of ascorbic acid, a reagent that most other syntheses do not use. This reaction also produces nanowires with branching, which is also not usually seen in other methods.

Mourzina and coworkers found that the growth of AuNWs is dependent upon the amount of atmospheric oxygen present.⁹³ When they performed the reaction under a nitrogen environment, only Au particles were formed. By saturating the solution with O₂, they were able to obtain AuNWs with an incredible aspect ratio of ~4000 (diameter = 2 nm and length = 8 μm).

HRTEM images revealed that Au nanoparticles with twin boundaries were the first Au⁰ species to form and as the reaction progressed over 30 hours thin wires formed. The defects in the particles are more susceptible to oxidative etching by O₂/Cl⁻.⁹⁴⁻⁹⁸ To determine the effect of the etchants, experiments were carried out using AuCl and Au₂S in an inert atmosphere. Under nitrogen, only particles were formed with both precursors. When O₂ was introduced to the reactions, the reaction with AuCl gradually formed nanowires while the reaction with Au₂S did not (Figure 30). In fact, the reaction

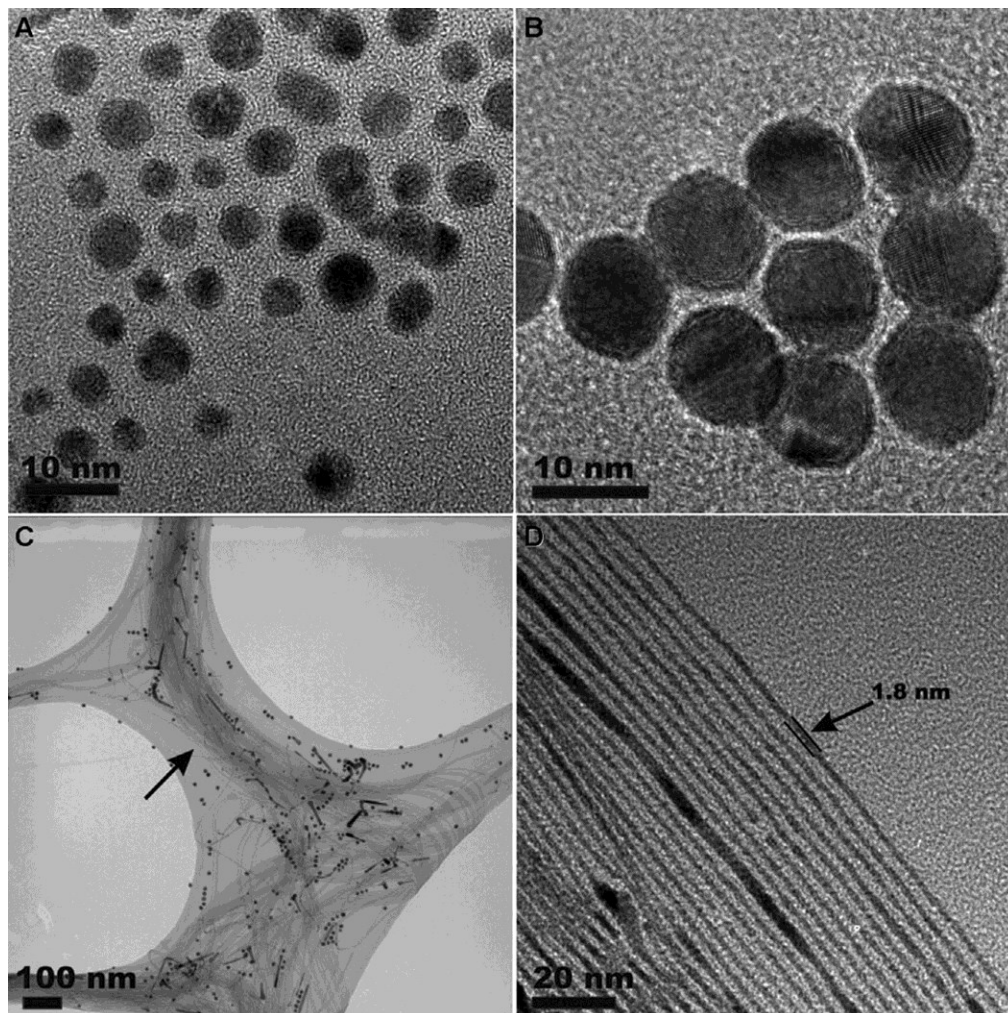


Figure 30: TEM images of Au nanoparticles using A) AuCl and B) Au₂S in the reaction while under nitrogen. C & D) TEM images of the AuCl reaction when O₂ was introduced during the last 6 hours of the reaction.

with Au₂S produced nanoparticles with a larger diameter, further showing the effect of O₂. It is well known that sulfur binds strongly to gold and because of the strong binding it blocks the surface and prevents nanowire growth. However O₂ can still pass through

the sulfur layer and etch away the smaller particles. The gold can then redeposit on existing particles to make them larger.

The surface of the Au particles is stabilized by OA which also controls the rate of Au ions contacting the particle surface. Since we are seeing anisotropic growth, we know that one of the facets has to be able to shed off the OA, and because the (111) facets are lower in energy, the OA can be selectively removed during the etching process. It is thought that as the OA is removed and the exposed twinned surface is etched away, the OA on the other facets can confine the Au ions and redeposit them quicker than the etching process removes them. The continuous removal and deposition of Au will eventually reshape and elongate the nanowire resulting in a smooth single-crystalline wire.⁹³

The solvents that the AuNWs are grown can also have morphological effects on the nanowires.^{86, 89, 90, 99} Sun and coworkers showed that larger diameter nanowires, 9 nm in diameter, could be obtained by using a 1:1 mixture of OA and oleic acid.⁸⁹ As in the basic synthesis of AuNWs, the oleic acid can serve not only as the solvent but also the reducing agent and capping agent. The exact details as to why the oleic acid would change the diameter were not mentioned, but it is most likely do to the way the organic molecules cap the AuNWs.

Zhou and coworkers also studied the effect of solvent on the nanowire synthesis. In their work they also used a mixture of OA and oleic acid with HAuCl_4 , but they dissolved these components in an additional solvent. Most other syntheses that use an additional solvent use hexane.^{81, 90, 93} To show the effects of the polarity indexes of different solvents, hexane (0.06), heptane (0.2), toluene (2.4), and chloroform (4.4) were used in the synthesis. Figure 31 shows how the synthesis was affected by different

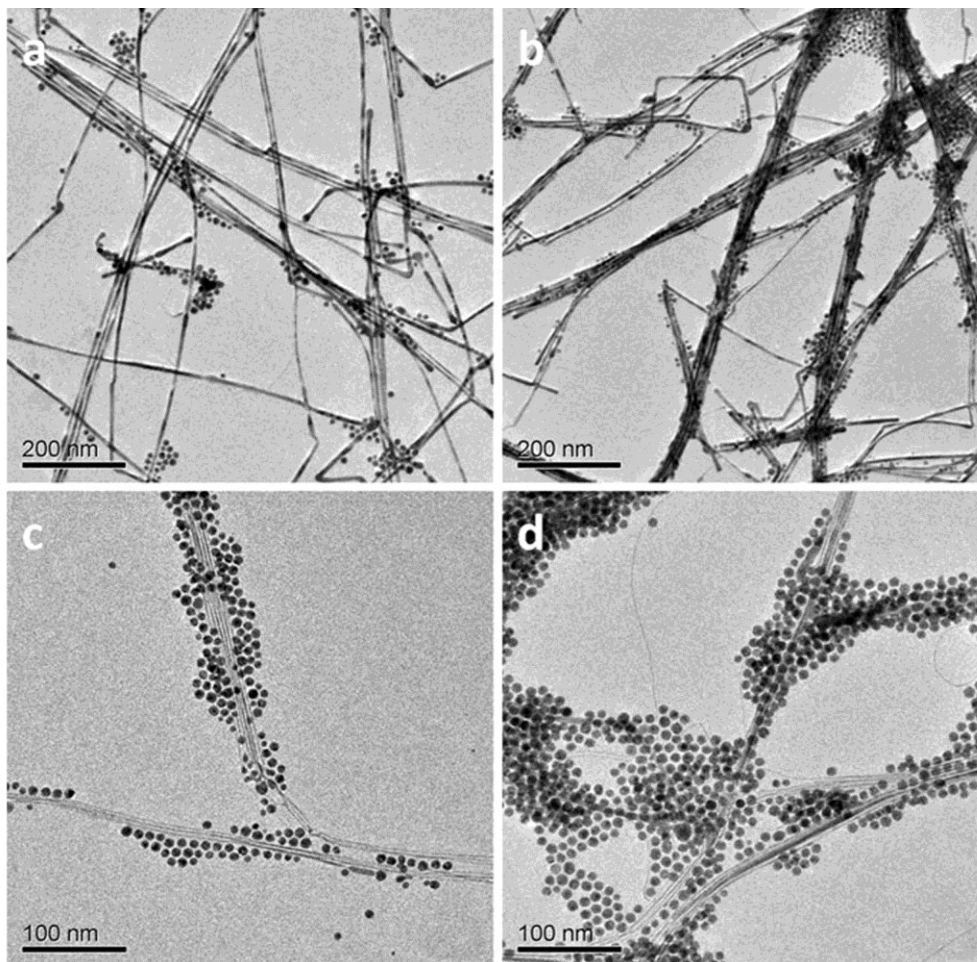


Figure 31: TEM images of AuNWs synthesized in different solvents. A) hexane, B) heptane, C) toluene, and D) chloroform.⁹⁹

solvents. Hexane and heptane produced wires with an average diameter of 7.1 and 5.9 nm respectively with hexane seemingly producing the least amount of nanoparticles. Toluene and chloroform each had significantly more nanoparticles but also thinner wires, 2.0 and 1.5 nm respectively. To explain this trend the authors attributed the effect to the solubility of HAuCl_4 . Since HAuCl_4 is a salt it is obvious that it is more soluble in

polar solvents, so in a solvent like hexane, which is very non-polar, the salt is less soluble and provides slower nucleation into particles. Since there are relatively small amounts of nuclei being formed in high non-polar solvents, there are more monomers per nucleus during the growing phase, which leads to fast growth and relatively larger wires. But as the polarity of the solvent increases, the Au salt is more soluble which allows for faster nucleation, which in turn reduces the amount of monomer that can reduce during the growth process. Thus in order to get the highest yield of nanowires, solvents that are more non-polar should be used and in order to synthesize nanowires with the thinnest diameter solvents that are more polar should be used.⁹⁹

Different alkylamines can be used as a co-reducing agent and co-stabilizer in the AuNW synthesis when paired with OA. Recently, 1-dodecylamine (DDA), 1-tetradecylamine (TDA), 1-hexadecylamine (HDA) and 1-octadecylamine (ODA) were used in the synthesis to make AuNWs. In a typical synthesis HAuCl_4 was dissolved in hexane and then mixed in a solution of OA and an alkylamine. When OA is not included in the reaction mixture, only nanoparticles formed. Figure 32 shows AuNWs

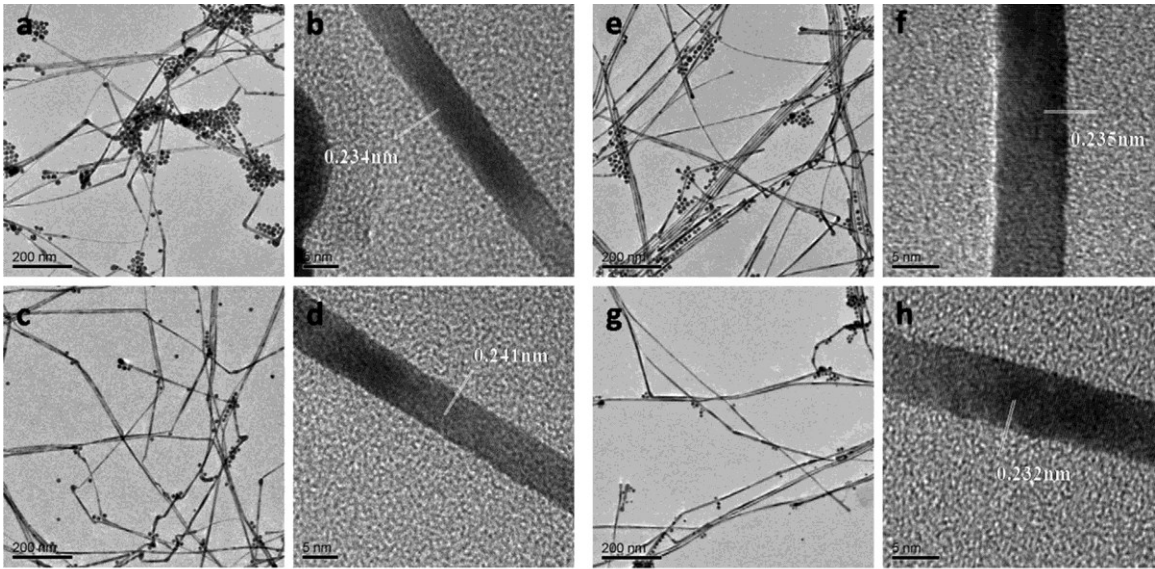


Figure 32: TEM images of AuNWs made with different alkylamines. A&B) DDA, C&D) TDA, E&F) HDA, and G&H) ODA.¹⁰⁰

made with the different alkylamines. The effect of the alkyl chain was minimal. As the length of the carbon chain increased the nanowire diameter increased slightly (DDA 6.2, TDA 6.7, HDA 6.9, and ODA 7.1 nm).¹⁰⁰

While we have some of the pieces to understand how AuNWs are formed, the full mechanism is still not entirely clear. A few plausible growth mechanisms were presented, as were different approaches to affect the dimensions of the nanowires. Using this knowledge, we can begin to tailor the size of the AuNWs and use them in various applications.

4. Making Transparent Conductors

4.1 Introduction

There are many different methods to make transparent electrodes, including spray coating, spin coating, Meyer rod coating, filtering, and dip coating. Most current efforts have been focusing on techniques similar to Meyer rod coating and spray coating because both of these types of methods are easily scalable.

4.2 Methods for Making Transparent Conductors

4.2.1 Drop Casting

One of the first methods to make transparent conductors with nanowires was by drop casting. This simple yet effective method involves dropping a volume of nanowire suspension onto a substrate and allowing it to dry in air while being agitated on a shaker.¹⁰¹⁻¹⁰⁸ The resulting nanowire meshes were randomly dispersed in the center of the droplet but formed a ring of dense wires around the edge of the droplet.

4.2.2 Filtration

Another simple and effective method of making a transparent electrode is through vacuum filtration.^{5, 38, 53, 54, 109-113} Here, a known volume of a nanowire solution is transferred to a filtering apparatus. As the vacuum pulls the solution through the filter membrane, a randomly oriented nanowire film is collected. This film can then be transferred to various substrates that have a higher affinity for the nanowires compared

to the filter membrane, including slides coated with glue, PDMS, PET and others. This method also has the added benefit that the exact concentration of wires can be determined before the film is made. By obtaining the concentration of the metal via an atomic absorbance spectrometer, knowing the dimensions of the wires, and the density of the material, the number of wires on the film can be roughly calculated. This method is not easily scalable, however, due to the limited size of the filtering apparatus and filter membrane, and it is mostly used in laboratory settings.

4.2.3 Spin Coating

Spin coating is also a technique that is mostly used in the laboratory setting and has limitations for scale up processes.¹¹⁴⁻¹²⁴ This technique requires excessive amounts of the nanowire suspension to be placed on a flat substrate and rotated at high speeds, ~250-5000 rpm, to spread the nanowire solution evenly across the substrate through centrifugal force. The thickness of the nanowire films can be adjusted by increasing (thinner films) or decreasing (thicker films) the spin rate. To obtain the most uniform films, the substrate can be functionalized with hydrophilic or hydrophobic compounds to control the wetting of the solution and the spin ramp rates can be adjusted so the material does not spin off of the substrate in only a few areas. But due to the limited size of the substrates, this process is typically used in laboratories and not in large scale processes.

4.2.4 Spray Coating

A potentially scalable method of making transparent electrodes is through spray coating. Random networks of nanowires can be sprayed from dilute suspensions in MeOH, IPA, or water using an artist's airbrush or electrostatic spray deposition.^{24, 54, 114, 125-136} During the spray process a light coating is applied to a heated substrate with each spray pass as seen in Figure 33. It is important that the substrate being coated with the

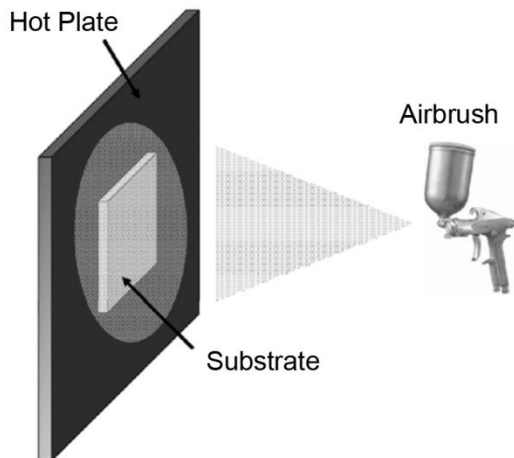


Figure 33: Schematic of the spray coating process.⁵⁵

nanowires is heated to a temperature high enough to instantly evaporate the solvent. If the solvent is not instantly evaporated, droplets will form and the nanowire mesh will not be very uniform. The concentration of nanowires in suspension is also important. If the concentration is too high, it becomes more likely for aggregates to form on the substrate and in the air brush causing clogs.

4.2.5 Meyer Rod Coating

Yi Cui demonstrated that meyer rod coating can be an effective and scalable method to make transparent films of AgNWs directly from methanol.⁵⁶ Similar groups have successfully used the same method using various alcohols to disperse their AgNWs.^{104, 137-139} Meyer rod coating can also be applied to other nanowire systems, but some metal nanowires, like copper, require a film former to prevent aggregation.^{6,7} In our case we developed an ink using nitrocellulose as a film former. To make the CuNW ink formulation, the nitrocellulose was first dissolved in acetone, which readily dissolves the polymer. Ethanol and isopropyl alcohol were added to dilute the solution of nitrocellulose in acetone, and enable the dispersion of CuNWs, which otherwise would not disperse in acetone because of their PVP-coating (PVP is not soluble in acetone). Ethyl and pentyl acetate were added to improve spreading and leveling of the ink on the plastic substrate, and toluene was added to reduce the evaporation rate. After dispersing the CuNWs into this ink formulation, it can be pipetted onto a glass or polyethylene terephthalate (PET) substrate (Figure 34A), and spread with the meyer rod to form a thin, uniform film (Figure 34B).

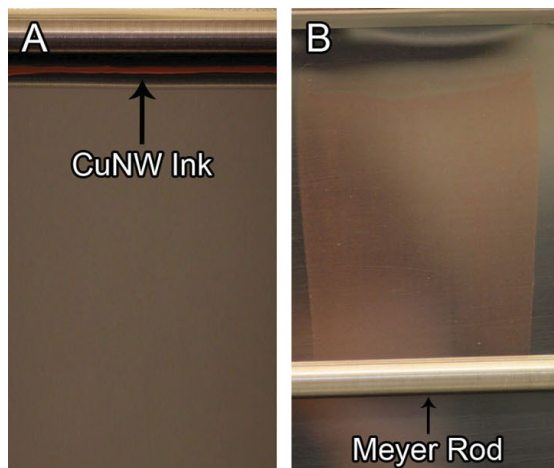


Figure 34: CuNW ink before and after Meyer rod coating.

Unfortunately, the organic film had to be removed in order for the electrode to be conductive. We allowed the ink to dry in air for about 5 minutes and then placed the film in a plasma cleaner under a forming gas atmosphere (5% hydrogen, 95% nitrogen) to remove as much of the nitrocellulose, PVP, and other organics as possible, while also avoiding oxidation of the CuNWs (which occurred if the films were plasma cleaned in air). After plasma cleaning, the films had a sheet resistance of about $20 \text{ k}\Omega \text{ sq}^{-1}$. To finish removing the nitrocellulose and anneal the wires, the films were placed in a tube furnace with a pure hydrogen atmosphere at $175 \text{ }^\circ\text{C}$. Since nitrocellulose has a low auto ignition temperature, the remaining nitrocellulose vaporized and left a highly conductive network of CuNWs on the substrate.⁶

5. Metal Nanowire Transparent Electrodes

This section describes some of the highest-performance transparent electrodes made from solution grown gold, silver and copper nanowires, and describes some of their applications in various devices.

5.1 Gold Nanowire Transparent Electrodes

AuNWs can provide resistance to oxidation and chemical stability to transparent electrodes, which is something that Ag and Cu NWs cannot do. There has only been one reported transparent electrode made with solution grown AuNWs,¹⁴⁰ most likely due to the AuNW synthesis. As was mentioned above, solution grown AuNWs are made using an *in situ* micellular structure that completely encompasses the AuNW with a layer of OA. The OA layer prevents the nanowires from touching and consequently forces them to line up parallel to one another. Researchers have recently been able to take advantage of this effect by aligning the nanowires into a monolayer at the liquid/air interface. The AuNWs, in hexane, are dropped onto a layer of diethyleneglycol (DEG) inside a Teflon container. The AuNW/hexane dispersion forms a meniscus and starts to evaporate starting from the middle of the container. As evaporation occurs the interactions between the nanowires become more favored resulting in a densely aligned monolayer of AuNWs that floats on top of the DEG (Figure 35). The film is then

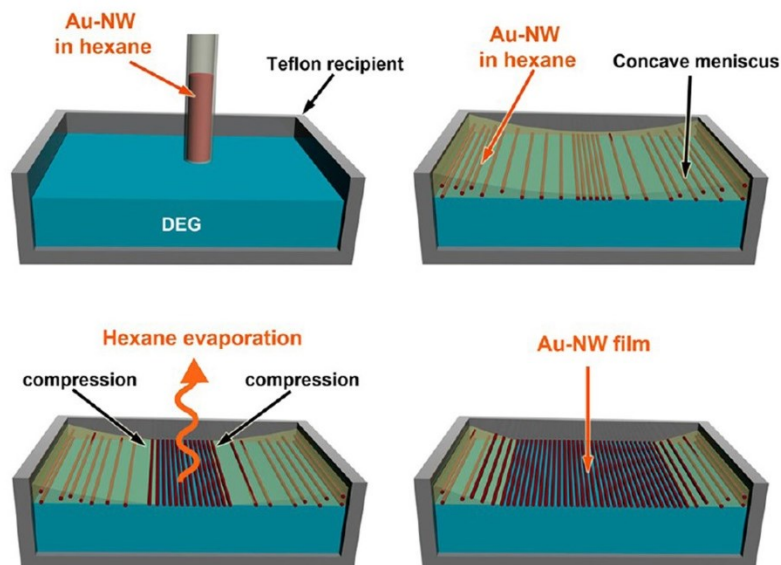


Figure 35: Diagram of the AuNW densely aligned monolayer formation.¹⁴⁰

transferred to a hydrophobic carbon coated glass slide for measurement. The lowest sheet resistance values that were obtained with this method measured between 400 and 500 $\Omega \text{ sq}^{-1}$ with a transparency of 96.5%. When multiple films of the AuNW monolayers were stacked on top of one another, the films broke and became less conductive.

5.2 Silver Nanowire Transparent Electrodes

Silver nanowire electrodes have been studied extensively. As was mentioned above, the synthesis of AgNWs is well understood and researchers can easily choose the dimensions of the nanowires that they would like to work with. The wires are very smooth, silver is the most conductive metal, and silver does not oxidize as quickly as copper, which makes working with AgNWs a logical choice. When AgNWs were first

used in electrodes they showed properties very similar to ITO as shown in Figure 36,^{54, 56,}
¹⁰¹ but the properties did not quite match the properties of commercially

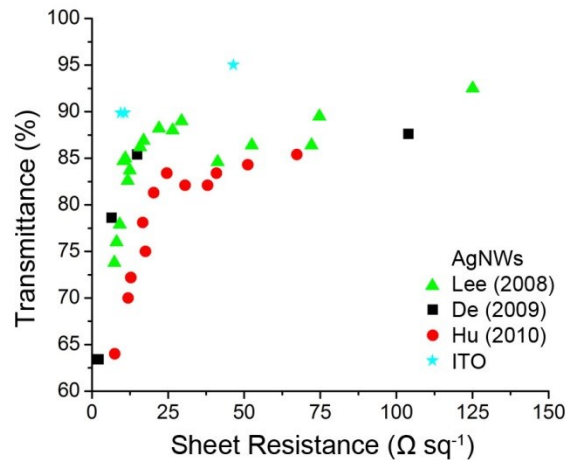


Figure 36: Plot showing transmittance vs sheet resistance for networks of randomly oriented AgNWs as transparent electrodes.^{54, 56, 101}

available ITO. To make the networks as conductive as possible, a thermal heat treatment was carried out to improve reduce the contact resistance between nanowires. During the growing process there is a thin layer of PVP on the nanowires that guides anisotropic growth. If the PVP is not removed, the junction resistance could be as high as $1 \text{ G}\Omega$,⁵⁶ and the sheet resistance of the film could be an order of magnitude higher than expected ($1\text{k}\Omega \text{ sq}^{-1}$ vs. $100 \Omega \text{ sq}^{-1}$).¹⁰¹ Heating the nanowire meshes to 200°C for 20 minutes will cause the PVP to flow and partially decompose which then allows the AgNWs to touch and possibly weld/melt together (Figure 37). If the nanowire mesh is

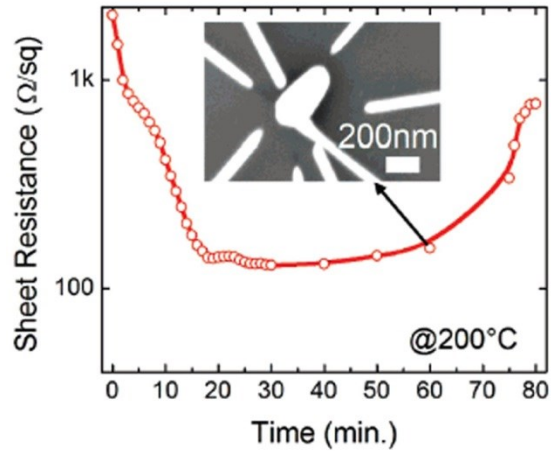


Figure 37: Plot of sheet resistance vs. time for AgNWs heated at 200 °C showing a gradual decrease in sheet resistance followed by a gradual increase as the nanowires turn to droplets seen in the SEM image in the inset.¹⁰¹

heated for 40 minutes or longer, the nanowires start to form droplets and the sheet resistance gradually increases.

Heating a nanowire mesh at 200°C is beneficial for the network but it can be detrimental to the substrate the network is on. One alternative to heating a network to increase the conductivity is to coat the AgNWs with a layer of gold, as seen in Figure 38.⁵⁶ By doing a simple galvanic replacement with H_{AuCl}₄ researchers were able

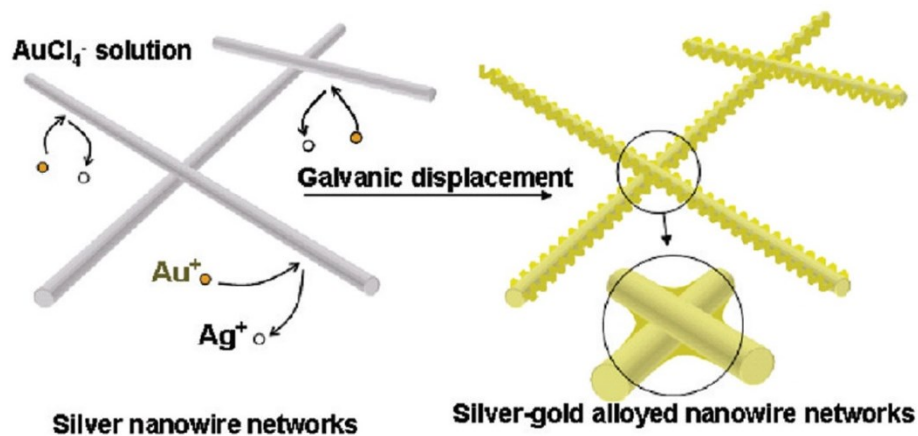


Figure 38: Cartoon representation of the Au galvanic displacement reaction to improve the nanowire junction resistance.⁵⁶

to decrease the nanowire junction resistance from 1 G Ω down to ~450 Ω .

Cui and coworkers also found mechanical pressing can decrease the sheet resistance.⁵⁶ By sandwiching their nanowire networks between two pieces of glass and using a mechanical shop press, 81GPa of pressure was applied for 50 seconds. When the sheet resistance measurements before and after pressing were compared, it was found that the sheet resistance decreased from hundreds of $\Omega \text{ sq}^{-1}$ to tens of $\Omega \text{ sq}^{-1}$ and an added benefit of pressing is the improved surface roughness. In order for these and similar films to be used in applications like LEDs, displays, etc, the surface roughness must be on the order 5 nm or less. By using this simple pressing method the average surface roughness went from 110 nm down to 47 nm.

Recently, opto-thermal heating techniques have been developed in an effort to quickly and easily improve the conductivity at nanowire junctions.¹⁴¹ AgNW networks

can be drop-cast onto various substrates, including ordinary kitchen plastic wrap, and placed in a rapid thermal annealing system (RTA) with a tungsten-halogen lamp at a power density of 30 W cm^{-2} for under 2 minutes. The nanoscale gap between overlapping AgNWs was reported to exhibit a large field enhancement when light-induced heat generation is applied to it. The heat from the RTA is localized to the nanowire junction and eventually welds the two wires together (Figure 39) without

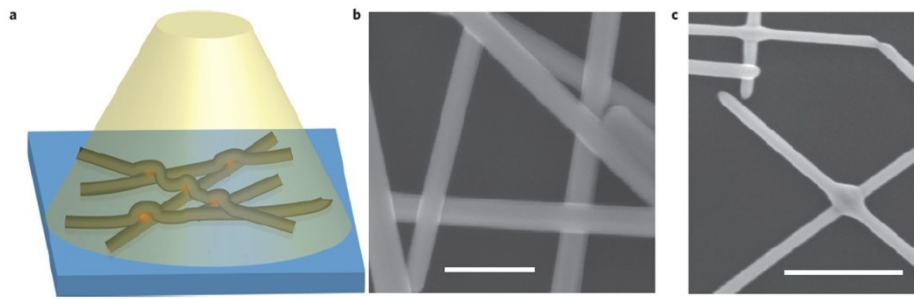


Figure 39: A) Schematic of the RTA technique used to weld the AgNWs. The junctions have a nanoscale gap (shown in red) due to a layer of PVP which allows extremely high local heating to occur because of the strong field concentration. B) Top view SEM image of AgNW junctions before welding and C) after welding. Scale bars are 200 nm and 500 nm respectively.¹⁴¹

affecting the substrate. The welds in this research are very different from annealing with a hotplate or an oven. When thermal annealing is used (15-60 seconds at 200-300 °C) the nanowires either looked like Figure 39B with no indication of welding or the wires melted and became discontinuous, whereas with optical nanowire welding, the process is self-limiting. When the junction is welded together the amount of heat generated is

greatly reduced and the welding/melting of the silver stops, which can be seen in finite element method simulations in Figure 40.¹⁴¹

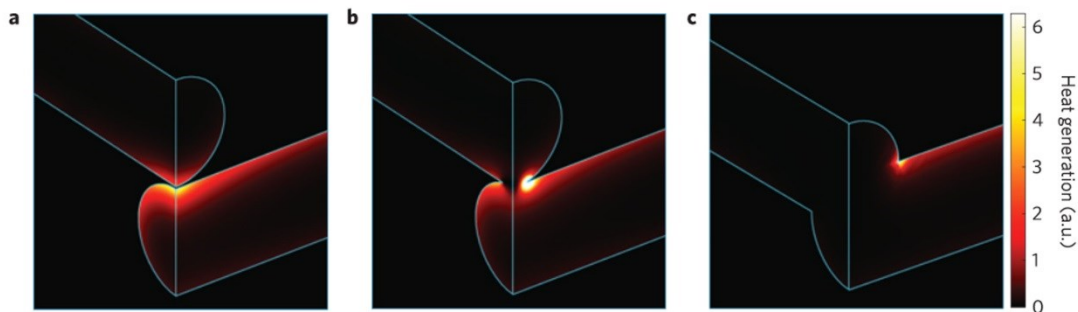


Figure 40: Finite element simulations of optical heat generation at the silver nanowire junctions during the nanowire welding process. A) A cross-sectional view of the heat generation in a 2 nm gap between two silver nanowires before heating, B) once the recrystallization begins, and C) after the recrystallization is complete.¹⁴¹

Other high-intensity pulsed light techniques have also been attracting a lot of attention recently as a method to weld nanowires together.^{104, 115, 142-145} Unlike the optical thermal heating technique described by Brongersma and coworkers which used a tungsten-halogen lamp to heat up the junctions for up to 2 minutes, these methods use xenon lamps with as much as 10 times the power of the tungsten-halogen lamp (~230 W compared to 30 W).^{104, 141} When the AgNW film is flashed, the silver absorbs the radiant energy from the lamp and converts it into thermal energy. This thermal energy can then melt/decompose the PVP allowing the nanowires to sinter together in as little as a few microseconds, which is in line with roll-to-roll processing techniques.

5.2.1 Longer Silver Nanowires in Transparent Electrodes

Using the successive multistep growth method described in Chapter 3, much longer nanowires were able to be synthesized.^{38, 146} The starting nanowires measured 10.2 μm in length with a diameter of 160 nm (aspect ratio of ~ 64). Through 7 iterations of their growth method they were able to obtain wires that still had the same diameter but with an average length of 95.1 μm (aspect ratio of 594), and one wire measuring as high as 500 μm . When these wires were made into a transparent electrode, the initial properties were not very good. In order to make them competitive they needed to be annealed in an oven at 120°C for 8 hours. Afterwards the transparent electrodes exhibited superior properties compared to other AgNW electrodes and comparable properties to ITO (Figure 41).

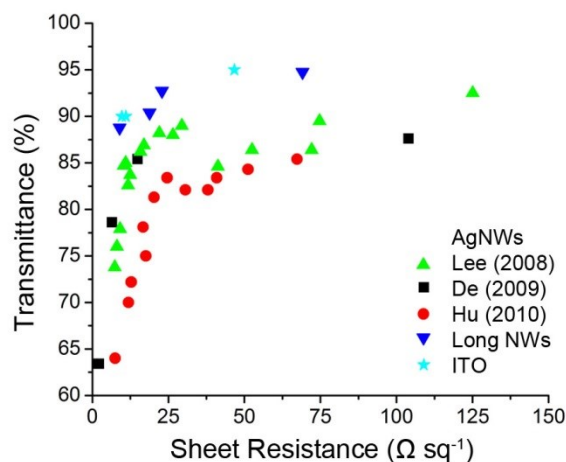


Figure 41: Plot of sheet resistance vs transmittance comparing the longer AgNWs to previous one-pot syntheses of AgNWs and ITO.^{38, 54, 56, 101}

5.3 Copper Nanowire Based Transparent Electrodes

5.3.1 Copper Nanowire Transparent Electrodes⁶

Recently we have demonstrated that CuNWs can be coated onto PET to make a highly conductive, transparent electrode. The scalable fabrication of a transparent conducting film of CuNWs on PET is particularly significant because PET is the most widely used substrate for fabrication of flexible, transparent conductive films. These films can be found in a wide array of products, including the e-ink displays used in most brands of e-readers, as well as signature pads at the grocery store checkout. To illustrate that the CuNW films can carry enough current (without oxidizing) to power display elements and lighting, while at the same time be highly flexible, we bent a film of CuNWs ($25 \Omega \text{ sq}^{-1}$ and 83% transparent) and put it into a circuit with a battery pack and a LED. As can be seen in Figure 42A, the bent film can easily carry enough current to

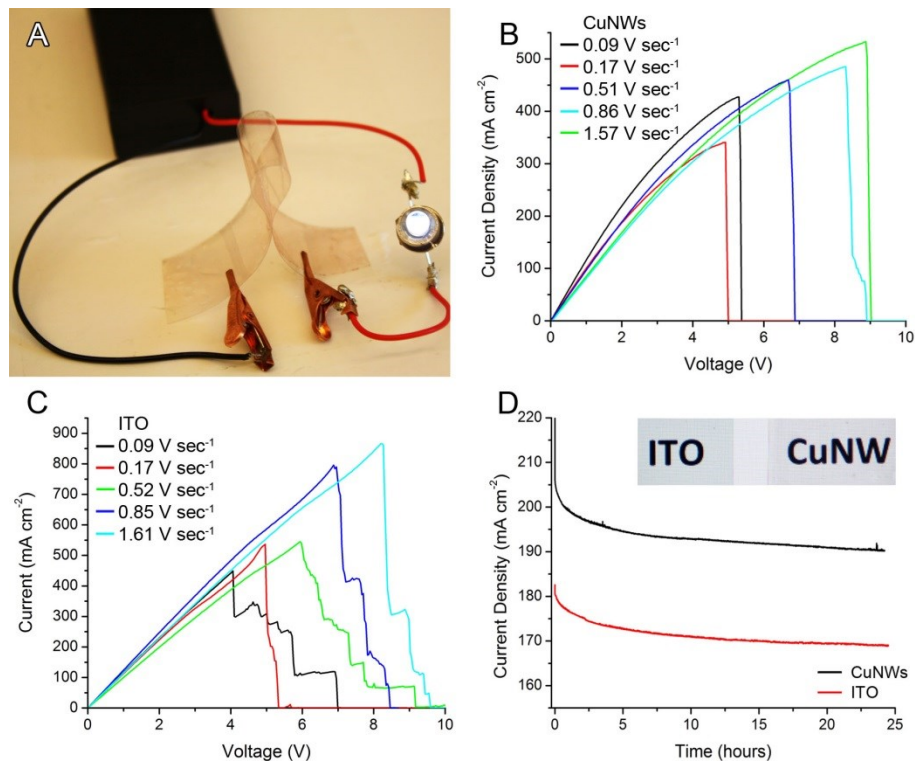


Figure 42: A) A bent CuNW film ($25 \Omega \text{ sq}^{-1}$ and 83% transparent) completing an electrical circuit with a battery pack and a LED. B) Plot of current versus voltage for $40 \Omega \text{ sq}^{-1}$ CuNW films and C) $42 \Omega \text{ sq}^{-1}$ ITO, demonstrating their maximum current carrying capacity. D) Current vs. time plot for films of CuNWs ($40 \Omega \text{ sq}^{-1}$) and ITO ($42 \Omega \text{ sq}^{-1}$) with an applied voltage of 1.5 V over 24 hours demonstrates the relative stability of CuNW films over time. The inset of E shows a visual comparison of ITO ($10 \Omega \text{ sq}^{-1}$) and CuNW ($75 \Omega \text{ sq}^{-1}$) films, both 88% transparent, backlit by an iPhone display.⁶

power the LED.

The ability to carry large currents is an attractive feature for applications of transparent conducting films in photovoltaics and lighting. To measure the maximum current carrying capacity of the CuNW film, we tested a square of film with a sheet

resistance of $40 \Omega \text{ sq}^{-1}$ at different voltage ramps. Figure 42B shows that the maximum current that can be obtained is 0.533 A cm^{-2} at a voltage ramp of 1.57 V sec^{-1} , compared to 0.866 A cm^{-2} at a voltage ramp of 1.61 V sec^{-1} for ITO (Figure 42C). This maximum current decreased to between 0.34 and 0.42 A cm^{-2} when the voltage ramp was reduced to between 0.17 and 0.089 V sec^{-1} , likely due to the fact that a slower voltage ramp increased the time available for the nanowires to melt. This lower current is enough to power 6 LEDs (similar to that in Figure 42C) at their maximum current rating. To test how the current carrying capacity of the CuNW film degraded over time in comparison to ITO, a voltage of 1.5 V was applied across CuNW and ITO films for 24 hours (Figure 42D). Both the films show a similar amount of decay over time but are still conductive after 24 hours.

Figure 43A - D show optical and SEM images of CuNW films to illustrate the

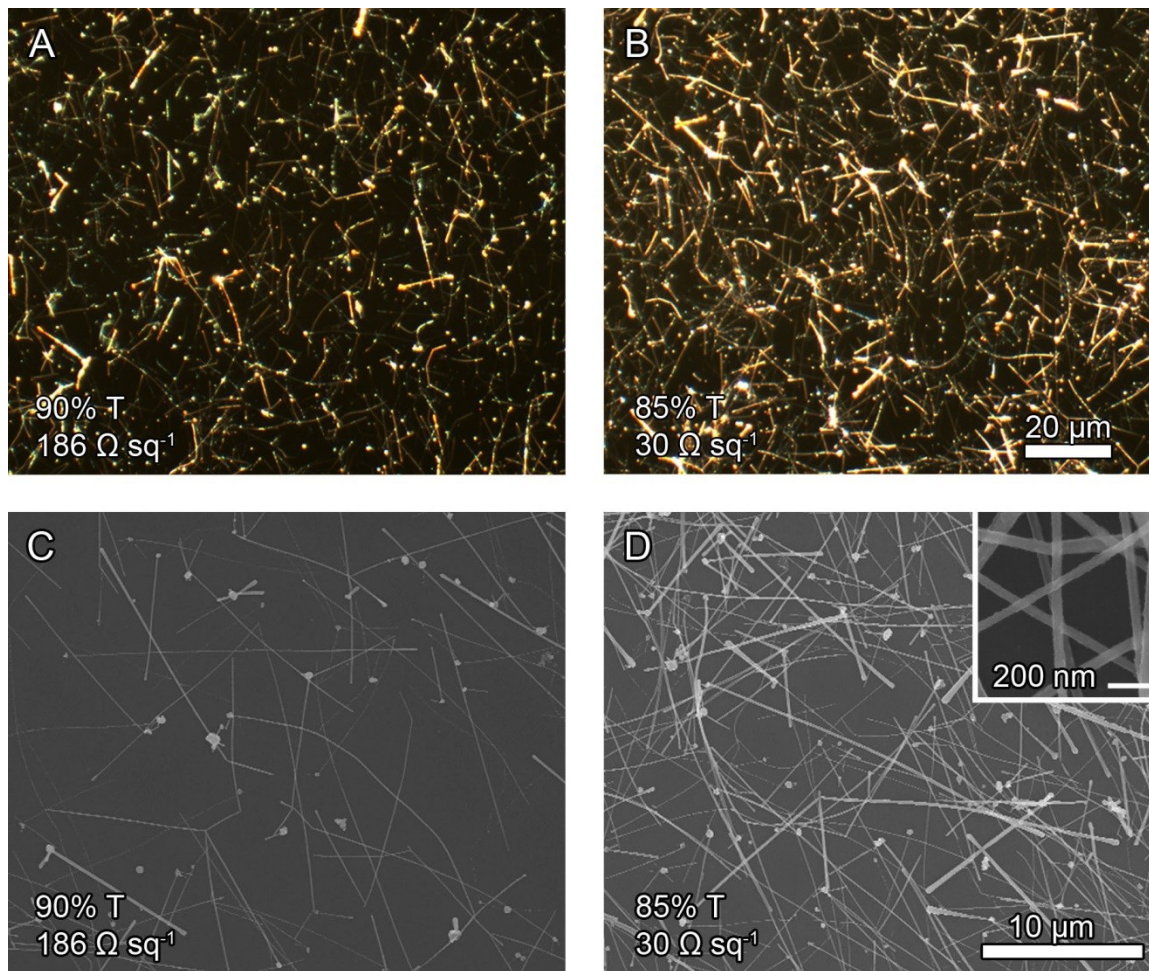


Figure 43: A & B) Dark field optical microscope images showing uniformly dispersed networks of CuNWs that are 90 and 85% transparent with sheet resistances of 186 and 30 $\Omega \text{ sq}^{-1}$, respectively. C & D) Corresponding SEM images of the CuNW films from A & B showing the average length ($20 \pm 5 \mu\text{m}$) and diameter ($52 \pm 17 \text{ nm}$) of the CuNWs.⁶

relationship between the density of nanowires on the substrate and the properties of the film. Lower densities of CuNWs (Figure 43A & C) resulted in a higher transmittance (90%) and a higher sheet resistance ($186 \Omega \text{ sq}^{-1}$). As the density of the nanowires is increased (Figure 43B & D), both the transmittance (85%) and sheet resistance decreased

($30 \Omega \text{ sq}^{-1}$). The optical and SEM images show the improved synthesis and coating process yielded films that were highly uniform (not aggregated), which, in contrast to our previous work, enabled the films to have a high transmittance and low sheet resistance. The relationship between the transmittance and amount of CuNWs used in the film is given in Figure 44. To obtain conductive films of CuNWs with a sheet

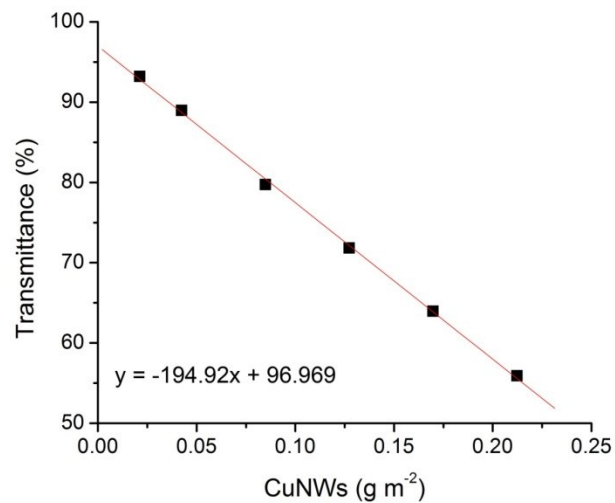


Figure 44: A Plot of transmittance (550nm) vs. amount of CuNWs (g m^{-2}) in a CuNW film.⁶

resistance of $30 \Omega \text{ sq}^{-1}$ requires only 0.06 g per m^2 of CuNWs.

The relationship between transmittance and sheet resistance for CuNW films is plotted in Figure 45A. At a sheet resistance of $\sim 50 \Omega \text{ sq}^{-1}$, the CuNW films made from

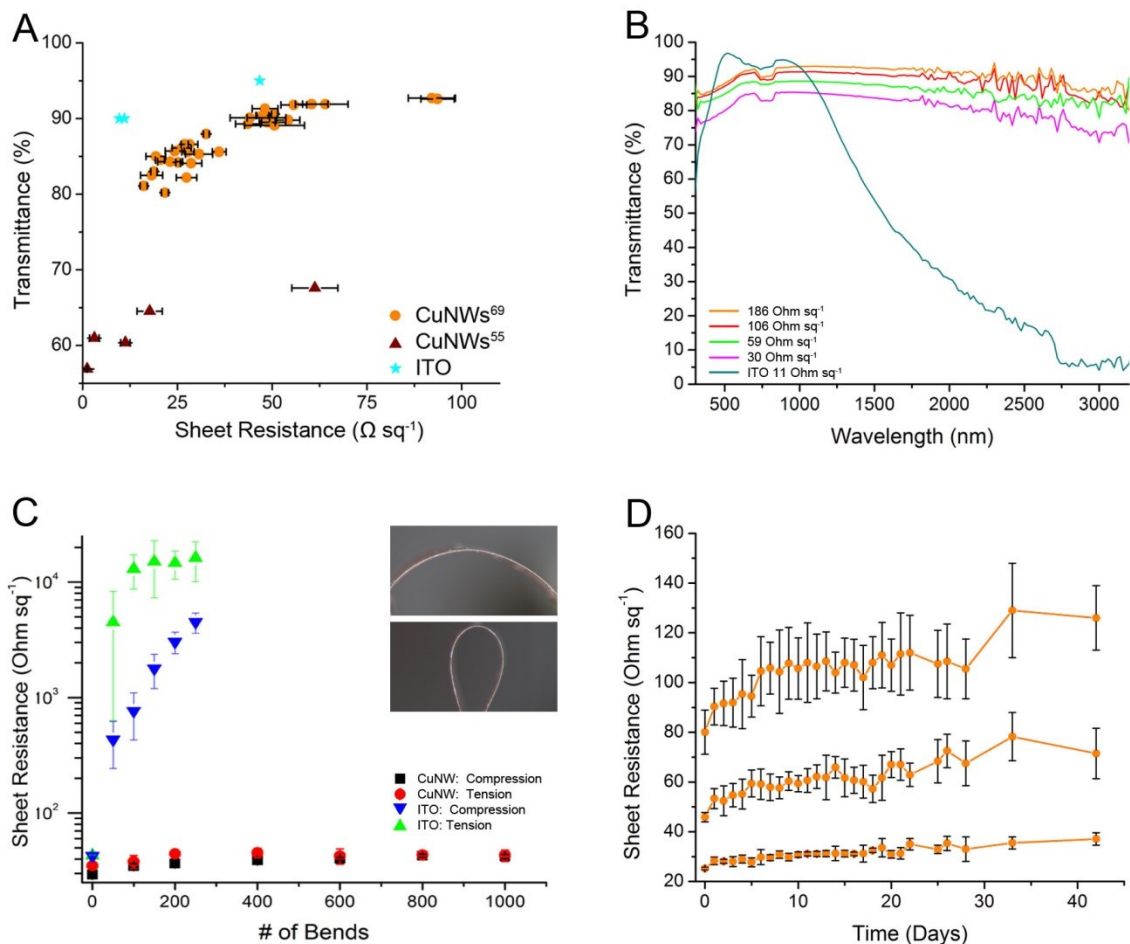


Figure 44: A) Plot of transmittance (at a wavelength of 550 nm) versus sheet resistance for films of CuNWs and ITO. Error bars show one standard deviation for 5 measurements. B) Plot of transmittance versus wavelength for ITO ($42 \Omega \text{ sq}^{-1}$) and films of CuNWs with different nanowire densities. C) Plot of sheet resistance versus number of bends of CuNW films (85% transparent) and ITO on PET. Inset shows the radius of curvature before (10 mm) and after bending (2.5 mm). D) Plot of sheet resistance versus time for CuNW films (89, 86, and 82% transparent from top to bottom) exposed to air for 42 days.

long, thin nanowires outperformed our previous short, fat, and aggregated CuNWs by almost 24% and at just 3% less transparent, they are almost as good as ITO.⁵⁻⁷

Films of ITO on glass with a sheet resistance of $45 \Omega \text{ sq}^{-1}$ are still 8% more transparent than a film of CuNWs on PET at a wavelength of 550 nm. However, ITO is only more transparent than CuNW films with the same sheet resistance at wavelengths between 400 – 1100 nm (Figure 45B). The greater transparency of CuNW films becomes especially dramatic at wavelengths greater than 1200 nm. For example, at the telecommunications wavelength of 1550 nm, the CuNW film has a transmittance of 87%, while ITO has a transmittance of 54%. Besides being useful for applications in communications, the greater transmittance of CuNW films in the infrared could be used to improve the efficiency of infrared photovoltaics.¹⁴⁷⁻¹⁴⁹

A major advantage of films of metal nanowires is that they are much more flexible than brittle films of ITO. To demonstrate the flexibility of the CuNW films, films with a transmittance of 85% were subjected to both compression and tension bending from a radius of curvature of 10 mm to a radius of curvature of 2.5 mm (Figure 45C inset). Figure 45C illustrates that the CuNW films exhibited little to no change in sheet resistance after 1000 bends. In contrast, the sheet resistance of ITO films increased by 400 times after just 250 bends.

In many of the applications in which transparent conducting films of CuNWs would be used, such as flexible displays, organic photovoltaics, and organic LEDs, there is already barrier materials in place to protect the organic component from oxygen and moisture. As copper is generally less sensitive to oxygen and moisture than these active organic components, oxidation of the CuNWs will likely not be an issue in these applications. That being said, resistance to oxidation is an advantage during manufacturing processes, as well as in applications where the CuNWs might be subjected to more corrosive conditions. In order to examine the oxidation rate of these new flexible electrodes, we left a variety of electrodes with different conductivities out in air, and periodically measured their sheet resistance. Figure 45D shows that over a period of 42 days, the conductivity of the CuNW films remained fairly constant. There was a slight increase from day 1 to day 2, but from day 2 onward the sheet resistance remained within one standard deviation. This initial increase and subsequent stability may be due to a passivating layer of Cu_2O that formed on the surface of the CuNWs.^[13] Although this is not a comprehensive test of the resistance of CuNWs to oxidation under a variety of conditions, Figure 45D illustrates that, even after plasma cleaning and annealing in hydrogen to remove the insulating organic material from the surface of the nanowires, the nanowires are fairly resistant to oxidation in air.

5.3.2 Cupronickel Nanowire Transparent Electrodes⁷

In order to overcome the two main concerns with using copper nanowires as transparent conductors, their color and the ease with which they oxidize at elevated temperatures, we coated CuNWs with nickel as described above, and used the CuNiNWs to make transparent electrodes.

A plot of the specular transmittance vs. sheet resistance for ITO and copper nanowire networks alloyed with different amounts of nickel is shown in Figure 46A.

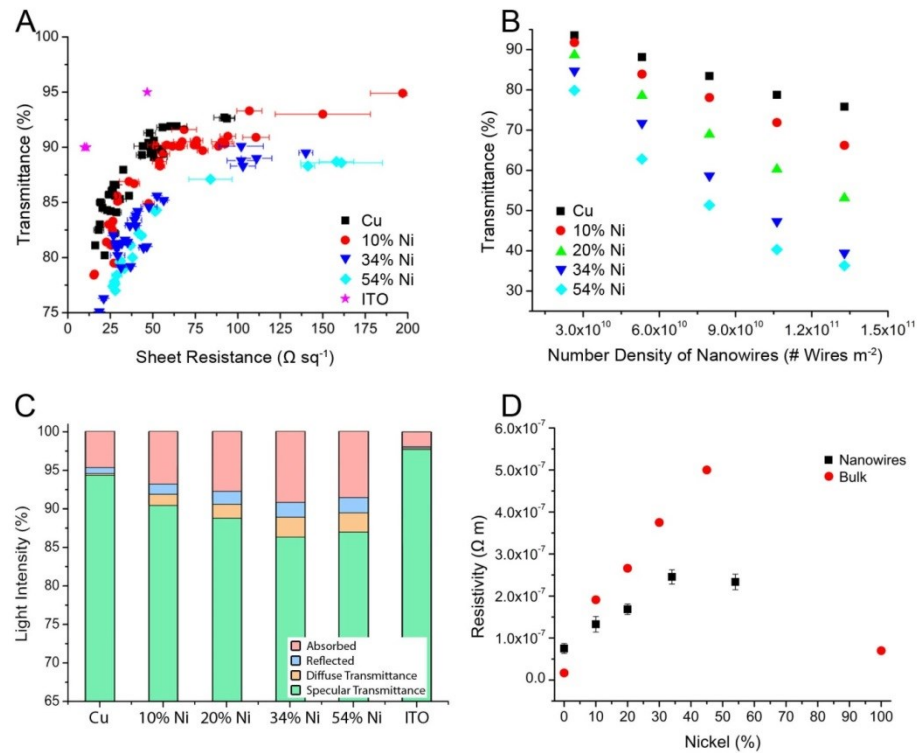


Figure 46: A) Plot of specular transmittance ($\lambda = 550 \text{ nm}$) vs. sheet resistance for films of copper nanowires, cupronickel nanowires, and ITO on glass (the light blocked by the glass was subtracted). Error bars show one standard deviation for five measurements. B) A plot of specular transmittance vs. number density of nanowires shows the effect of increasing wire diameter on the film's transmittance. C) Graph comparing the absorbance, reflectance, diffuse transmittance, and specular transmittance ($\lambda = 550 \text{ nm}$) of ITO and nanowire films with different nickel contents. D) Plot of resistivity vs. nickel content for cupronickel nanowires and bulk cupronickel alloys. Error bars show one standard deviation for five measurements.⁷

This plot illustrates that the transmittance of the networks at a given sheet resistance decreases with increasing nickel content. For example, at a sheet resistance of $60 \Omega \text{ sq}^{-1}$,

the transmittance drops from 94.4 % to 84.3 % ($\lambda = 550$ nm) as the nickel content goes from zero to 54 %. Part of this decrease in transmittance is due to the fact that the diameter of the nanowires increased from 75 nm to 116 nm after they were coated with nickel to a concentration of 54%. Figure 46B illustrates that this increase in diameter resulted in a substantial decrease in the transmittance of a nanowire film with a given number density of nanowires. In Figure 46C, we see that this decrease in transmittance was due to a combination of increased absorption, scattering, and reflectance from the nanowires. For an increase in diameter from 75 to 116 nm, the amount of light that was absorbed increased from 4.7 % to 8.6 %, and the amount of light that was scattered or reflected from the nanowires increased from 1 % to 4.5 %.

Part of the decrease in performance can also be attributed to an increase in the resistivity of the nanowires. To measure the impact of nickel content on the resistivity of the nanowires, we filtered out the nanowires to make thick (>0.5 g m⁻²) films, in which the nanowires are all highly connected. The resistance of a thick nanowire film should be proportional to the mass of the nanowires. We then converted the mass of the nanowires in the film (m) to an effective thickness (t) by dividing it by the bulk density of the metal (ρ_B) and the area of the filter (A), as illustrated in equation 7. A plot of the

$$t = \frac{m}{\rho_B A} \quad (7)$$

resistance of the films versus the effective thickness gives a line with a slope equal to the resistivity of the nanowire network (Figure 47). Figure 46D shows the resistivity of the

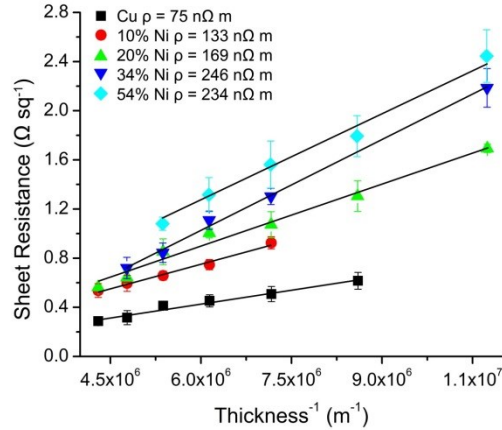


Figure 47: Plot of sheet resistance vs. the inverse of the effective nanowire thickness. The slope gives the resistivity of the nanowire networks. Error bars show one standard deviation for five measurements.⁷

copper nanowire network ($\rho = 75.1 \text{ n}\Omega \text{ m}$) is 4.4 times greater than the resistivity of bulk copper ($\rho = 16.9 \text{ n}\Omega \text{ m}$).¹⁵⁰ This increase in resistivity is perhaps due to increased resistance at the junctions between nanowires. For comparison, the resistivity of electrodeposited copper nanowires of the same diameter ($\sim 50 \text{ nm}$) is $\sim 30 \text{ n}\Omega \text{ m}$,⁴⁴ the resistivity of bulk nanotwinned copper is $17.5 \text{ n}\Omega \text{ m}$, and the resistivity of bulk nanocrystalline copper can range from $30 - 150 \text{ n}\Omega \text{ m}$ for grain sizes of $\sim 20 \text{ nm}$.¹⁵⁰ Thus, the resistivity of the nanowire network is comparable to nanocrystalline copper.

Coating the copper nanowires with nickel to a concentration of 54 mole % increased the resistivity to $234 \text{ n}\Omega \text{ m}$, 3.1 times higher than pure copper nanowires.

Causes for the relatively greater resistivity of the cupronickel nanowires likely include the intrinsically higher resistivity of nickel ($\rho = 70 \text{ n}\Omega \text{ m}$)¹⁵⁰, alloying of copper with nickel, and the polycrystalline nature of the cupronickel nanowires (the resistivity of nanocrystalline nickel with a grain size of 11 nm is $200 \text{ n}\Omega \text{ m}$).¹⁵⁰ Somewhat surprisingly, the cupronickel nanowires have a lower resistivity than the corresponding bulk alloy across all proportions.¹⁵¹ For example, the resistivity of a cupronickel alloy containing 52 mole % nickel is $500 \text{ n}\Omega \text{ m}$. The lower resistivity of the cupronickel nanowires relative to the bulk alloy is likely due to the fact that the nanowires consist of a copper-rich core and a nickel-rich shell rather than a homogeneous alloy.

Although the addition of nickel to the copper nanowires results in a lower transmittance at a given sheet resistance, it greatly improves their resistance to oxidation. To test the resistance of cupronickel nanowires to oxidation, we put films of comparable transmittance (85 – 87 %T) in an oven heated to $85 \text{ }^\circ\text{C}$, and periodically measured their sheet resistance over time. Figure 48A shows that, without any nickel

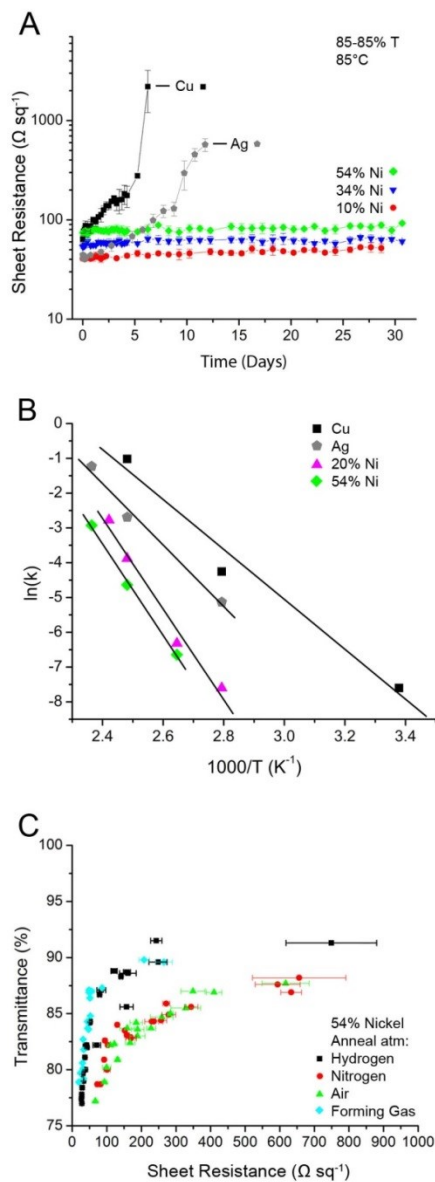


Figure 48: A) A Plot of sheet resistance vs. time for films of silver nanowires, copper nanowires, and cupronickel nanowires stored at 85°C. B) An Arrhenius plot of $\ln(k)$ vs. $1000 T^{-1}$ illustrates the temperature-dependent stability of the nanowire films. C) Plot of transmittance vs. sheet resistance for cupronickel nanowire films annealed in various atmospheres. All error bars show one standard deviation of five measurements.⁷

coating, the sheet resistance of the copper nanowire film began to increase after 1 day, and increased by an order of magnitude after 5 days. The sheet resistance of silver nanowire films increased by an order of magnitude after 13 days. In comparison, with as little as 10 % nickel relative to copper (9:1 Cu:Ni), the sheet resistance of the cupronickel nanowire film remained remarkably stable over a period of 30 days, increasing by only $10 \text{ } \Omega \text{ sq}^{-1}$ (from 30 to $40 \text{ } \Omega \text{ sq}^{-1}$). With Ni contents of 34 % or greater, the change in the sheet resistance over 30 days is so small as to be within the error of the measurement.

In order to provide an estimate of the stability of the nanowires at room temperature, we measured the normalized increase in the sheet resistance ($\Delta R/R_0$) of the nanowire films vs. time to extract a rate constant, k , at temperatures between $85 - 150 \text{ } ^\circ\text{C}$ (see **Appendix A**). We restricted our analysis to temperatures less than $150 \text{ } ^\circ\text{C}$ because at temperatures greater than $160 \text{ } ^\circ\text{C}$, a layer of Cu_2O can overgrow the NiO layer on cupronickel, and change the oxidation kinetics.¹⁵² We restricted our analysis to sheet resistance data for which $\Delta R/R_0 < 1$ because a doubling in the sheet resistance would be unacceptable for most applications. Furthermore, all the data for which $\Delta R/R_0 < 1$ could be best fit with a linear rate law, which greatly simplified the comparison between various nanowires and temperatures. Equation 8 gives the form of the

$$\Delta R/R_0 = kt + C \tag{8}$$

linear rate law used in our analysis, in which t is time (h^{-1}), and C is a constant. It was previously found that the oxidation of copper nanoparticles followed a similar linear rate law.¹⁵³

We plotted $\ln(k)$ versus $1000/T$ in Figure 48B to show that the oxidation of the nanowire films, like that of metal films and nanoparticles,¹⁵³⁻¹⁵⁵ can be described by an Arrhenius equation, given as equation 9. Here E_a is the activation energy (J mol^{-1}), R is the gas constant ($\text{J mol}^{-1} \text{K}^{-1}$),

$$\ln(k) = - E_a/R (1/T) + \ln(A) \quad (9)$$

T is the absolute temperature (K), and A is a frequency factor (h^{-1}). We determined the activation energy for the corrosion of nanowire films from the slopes of the lines in Figure 48B, and summarized these in table 1. The activation energy for the oxidation of

Table 1. Arrhenius plot data for Cu, Ag, 4:1 Cu:Ni, and 1:1 Cu:Ni nanowire films.⁷

Nanowire Composition	E_a (kJ mole^{-1})	Years to $\Delta R/R_0 = 1$ @25°C
Cu	60	0.2
Ag	73	3
4:1 Cu:Ni	108	400
1:1 Cu:Ni	109	1000

the copper nanowires (60 kJ mol^{-1}) is close to values previously obtained for copper nanoparticles (69.2 kJ mol^{-1} for $T < 200 \text{ }^\circ\text{C}$, and 54.3 kJ mol^{-1} for $T > 200 \text{ }^\circ\text{C}$).¹⁵³

The Arrhenius plot also allows us to estimate the time at which $\Delta R/R_0 = 1$ at room temperature ($25 \text{ }^\circ\text{C}$). These times, summarized in table 1, are 0.2, 3, 400, and 1000 years

for networks of copper, silver, 4:1 Cu:Ni, and 1:1 Cu:Ni nanowires, respectively.

Although using an Arrhenius plot is a generally accepted way to correlate rates of oxidation at high temperatures to those at lower temperatures,¹⁵⁵ it should be noted that these rates apply only for dry air, and may change depending on the composition of the surrounding atmosphere or matrix. Furthermore, due to their slow rate of corrosion, we cannot be certain that the activation energy for corrosion of silver and cupronickel at room temperature is consistent with the values listed in table 1. That being said, it seems likely that the activation energy for the corrosion of these metals does not vary significantly from 25 - 85 °C, and thus we can reasonably conclude that the cupronickel nanowires are about 100 times more stable than silver nanowires.

Due to their sensitivity to oxidation, copper nanowires must be annealed under a pure hydrogen atmosphere in order to reduce copper oxides and allow the nanowires to fuse at their junctions. The use of a pure hydrogen atmosphere is generally not desirable in a manufacturing environment as it introduces additional cost and safety concerns. The greater oxidation resistance of the cupronickel nanowires allows them to be annealed under a forming gas atmosphere (5 % hydrogen, 95 % nitrogen), which, unlike pure hydrogen, is not explosive. Figure 48B shows cupronickel nanowire films have similar performance when annealed under hydrogen or forming gas. The cupronickel nanowire films can even be annealed under nitrogen or air and achieve fairly good

performance, although not quite as good as if hydrogen is present as a reducing agent in the annealing atmosphere.

In addition to the issue of oxidation, alloying copper with nickel can address the issue of color. The reddish-orange color of copper nanowires is an aesthetically undesirable feature that must be addressed if they are to be used in displays. Figure 49A & B show camera images of nanowire films ($\%T = 87\%$) on a black background and

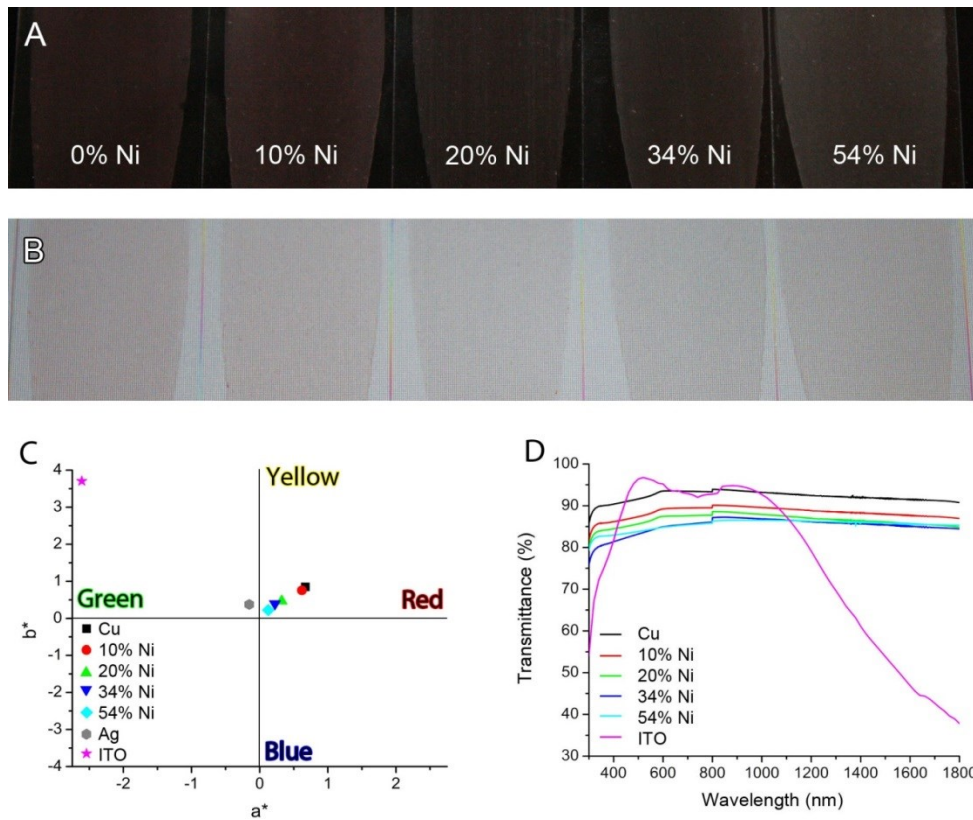


Figure 49: A & B) Camera images of nanowire films ($\%T = 87\%$) on a black background and a white backlit display show the nanowire films change from a reddish-orange to grey color with increasing amounts of nickel. C) Plot showing a quantitative comparison of color on a Hunter color scale. D) Plot of transmittance vs. wavelength for ITO ($11 \Omega \text{ sq}^{-1}$), copper nanowires, and cupronickel nanowires with different nickel contents. The nanowire films all have a sheet resistance of $60 \Omega \text{ sq}^{-1}$.

on a white backlight to simulate how they might appear in a display. The nanowire films change from a reddish color to a grey color around a nickel content of 20-30 %.

Figure 49C presents a quantitative comparison of color on a Hunter color scale. On this

scale, +a corresponds to red, -a corresponds to green, +b corresponds to yellow, and -b corresponds to blue. Surprisingly, when presented on this scale, copper appears more neutral in color than ITO, which is yellow-green in color. This can be understood by noting that the optical spectra of nanowire films are generally more flat than films of ITO, and the peak transmittance of ITO lies close to the yellow-green region of the visible spectrum (Figure 49D). The graph in Figure 49C shows that the reddish-orange color of copper gradually disappears with increasing nickel content, and the color neutrality is roughly equivalent to that of silver at a nickel concentration of 34 %.

Our previous studies have shown that, unlike ITO, copper nanowire films can retain their low sheet resistance after severe mechanical deformation.⁶ To confirm that this flexibility is retained after coating the copper nanowires with nickel, films of 20% and 54% nickel were repeatedly bent from a radius of curvature of 10 mm to a radius of curvature of 2.5. Figure 50 shows that the cupronickel films exhibited a small increase in

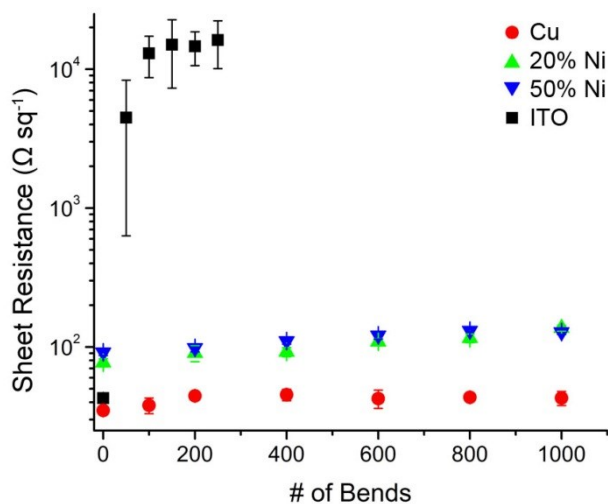


Figure 50: Plot of sheet resistance vs. number of bends for copper nanowires, 4:1 Cu:Ni nanowires, 1:1 Cu:Ni nanowires, and ITO films on PET. Error bars show one standard deviation for five measurements.⁷

sheet resistance after 1000 bends; the sheet resistance increased from 92 to 128 $\Omega \text{ sq}^{-1}$ for the 20% Ni nanowires, and 77 to 137 $\Omega \text{ sq}^{-1}$ for the 54% Ni nanowires. In comparison, the sheet resistance of the ITO film increased from 43 to 16200 $\Omega \text{ sq}^{-1}$ after 250 bends.

5.3.3 Film-Processable Copper Nanowire Networks

Copper nanowires and cupronickel nanowires have to be annealed in pure hydrogen or a hydrogen containing environment at an elevated temperature in order to become conductive. This step is highly undesirable for scaled-up roll-to-roll processes. It has been shown in the past that acetic acid can remove cupric and cuprous oxide without oxidizing the copper metal underneath the oxide layers.¹⁵⁶ To take advantage of the cleaning power of the acetic acid, we made CuNW thin films following the same

method described above, dried them, and dipped them into a beaker of glacial acetic acid, Figure 51A. The slide is pulled out of the beaker after 2 seconds, dried under

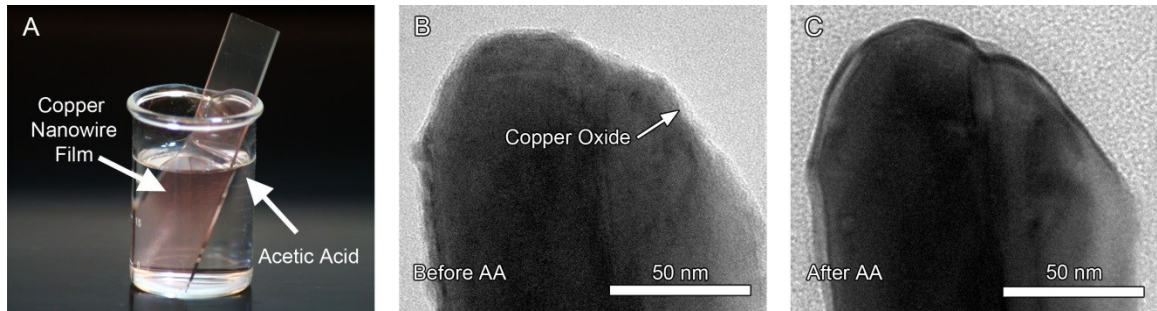


Figure 51: A) Camera image showing a CuNW thin film being cleaned in glacial acetic acid. B and C) TEM images showing the removal of copper oxide using acetic acid.

nitrogen, and further dried in a 70°C oven for 45 seconds. This process was repeated for a total of 5 times (on the fifth iteration the slide was not put in the oven) to ensure that all of the copper oxide was removed, which can be seen in the TEM images in Figure 51B & C. An added benefit of using the acetic acid to remove the oxides, was that it seemed to also remove the nitrocellulose polymer. Once the slides were cleaned, they were pressed in a mechanical press at 160 bar for 1 minute to improve the wire-wire contact which can be seen in the SEM images in Figure 52.

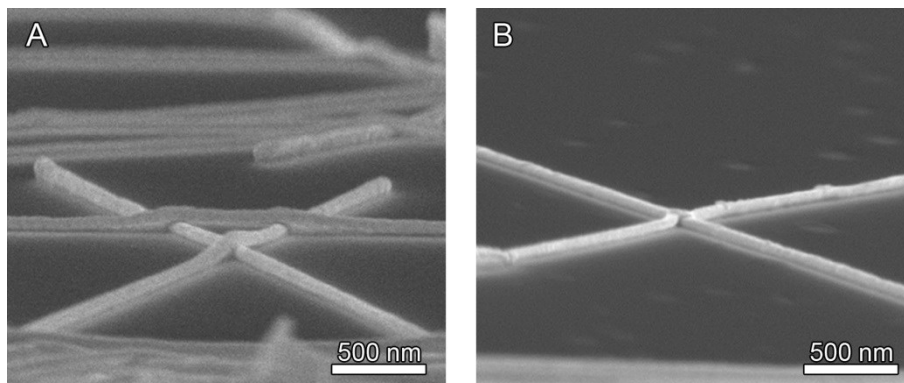


Figure 52: SEM images of CuNWs A) before and B) after pressing at 160 bar.

A plot of transmittance vs. sheet resistance comparing CuNW films that were annealed in hydrogen and films that were made conductive using acetic acid is shown in Figure 53. The films washed with acetic acid are not as conductive as films annealed in

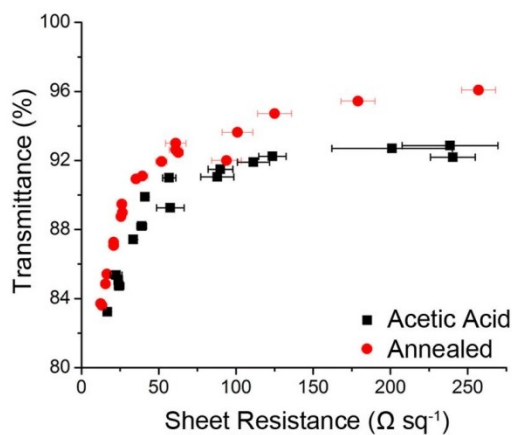


Figure 53: Plot of transmittance vs sheet resistance comparing films that were annealed in a hydrogen environment and cleaned in acetic acid.

hydrogen which may be due to the mechanical pressing. In order to obtain highly conductive nanowire junctions the wires have to be forced into contact, but if the force is

too much, the pressure will also flatten the nanowire turning it into more of a nanoribbon. A flattened nanowire will have a similar conductivity to an unflattened wire, but the increased diameter will block more light causing a shift to lower transmittances at similar sheet resistances. Further studies will need to be completed to examine this hypothesis.

5.3.4 Nickel can be Directly Deposited onto CuNW Films Through Electroless Plating

The as prepared CuNW films made using the acetic acid method can then be used as the base for nickel electroless plating.^{157, 158} The CuNW films are pretreated in a 0.5 mM Pd²⁺ for 2-4 seconds and dried under nitrogen. The film is then placed in a nickel plating solution containing Ni⁺, hydrazine, and water at 75°C (Figure 54). The

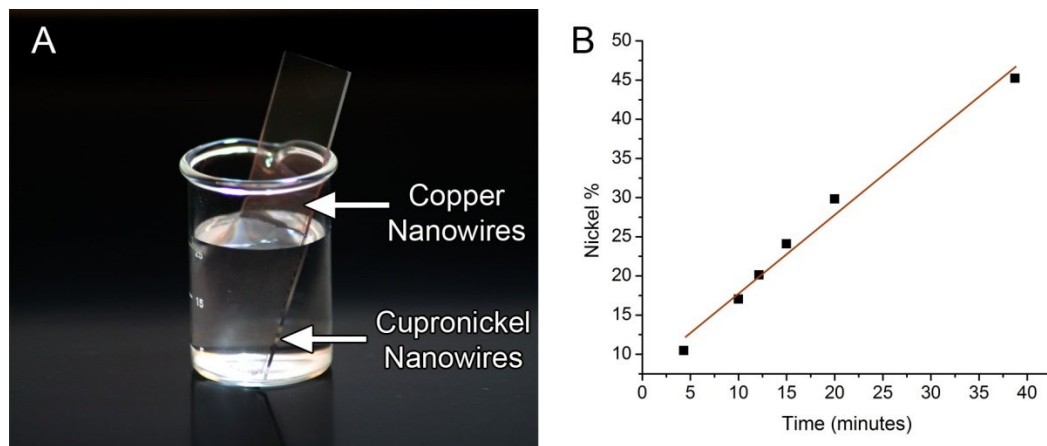


Figure 54: A) Camera image showing a copper nanowire film immersed in the nickel plating bath after nickel has been deposited on the lower half of the slide. B) Plot of Nickel percentage vs. time in minutes the CuNW film remains in the nickel plating bath.

molar ratio of nickel to copper can be adjusted by the amount of time it stays in the plating bath which is described in Figure 54B.

After nickel was coated onto copper films for 12.25 minutes, images were taken of the wires (Figure 55). The wires grew in diameter from 67 ± 15 nm to 90 ± 31 nm and

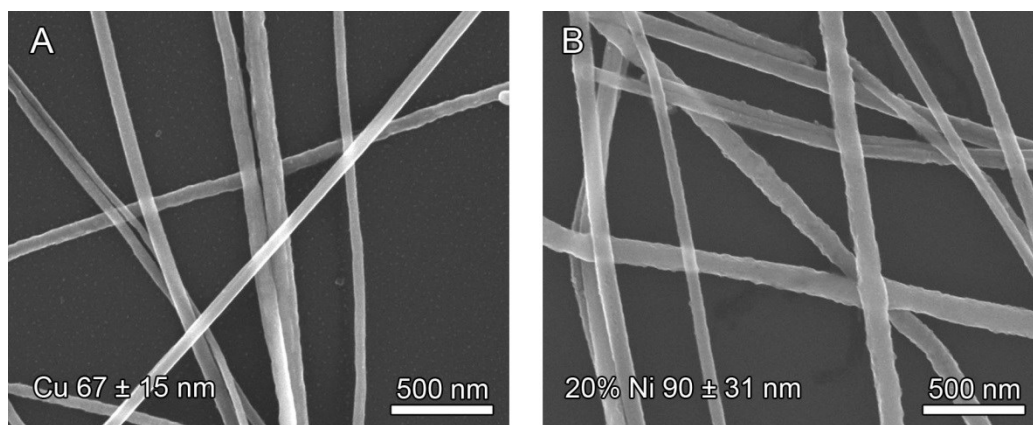


Figure 55: SEM images of A) CuNWs and B) 20% Ni coated CuNWs showing the diameter change without major morphological changes.

resulted in a 20% nickel coating on the CuNW film without seriously changing the smoothness of the wires.

A plot of the specular transmittance vs. sheet resistance for copper nanowire networks cleaned using acetic acid and networks of 20% nickel coated copper nanowires is shown in Figure 56A. This plot illustrates that the transmittance of the networks at a

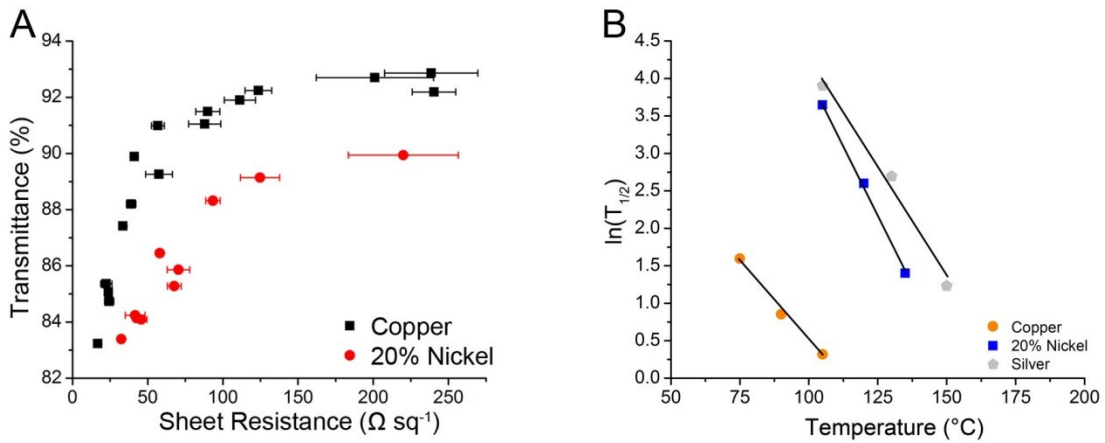


Figure 56: A) Plot of sheet resistance vs. transmittance for film processable CuNW and 20% Ni CuNW films. B) A modified Arrhenius plot of $\ln(k)$ vs. T showing the temperature-dependent stability of the nanowire films.

given sheet resistance decreases with the addition of nickel as we demonstrated earlier.

For example, at a sheet resistance of $125 \Omega \text{ sq}^{-1}$, the transmittance drops from 92 % to 89 % ($\lambda = 550 \text{ nm}$), which is again similar to our previous results.

While adding nickel to the copper nanowire networks results in a lower transmittance at a given sheet resistance, it does improve their resistance to oxidation. To test the resistance of cupronickel nanowires to oxidation, we put films of comparable transmittance (85 – 87 %T) in an oven heated between 75-150 $^{\circ}\text{C}$, and periodically measured their sheet resistance over time. Using these results, we again plotted $\ln(T_{1/2})$ versus T in Figure 56B to make a modified Arrhenius plot. This plot allowed us to estimate the time at which $\Delta R/R_0 = 1$ at room temperature (25 $^{\circ}\text{C}$). These times are 2, 655, and 250 days for networks of copper, 20% Ni:Cu, and silver nanowires, respectively. As

described before, these results apply only for dry air, and may change depending on the composition of the surrounding atmosphere or matrix. Compared to our previously published results, these films are not nearly as resistant to oxidation. This could be due to the new cleaning method, different starting nanowires, or differences in the room atmosphere. The 20% nickel coated copper nanowires are far less resistant to oxidation because we believe the nanowires are not being completely covered with nickel. Because the wires are pressed into the substrate, it seems likely the side of the wire making contact with the substrate does not have access to the nickel plating bath. During oxidation, air would still be able to get underneath the wires and cause the films to oxidize much quicker than our previously published results.

6. Summary and Conclusion

The replacement for ITO transparent conductors is well within our grasp. I have demonstrated that copper nanowire films are among the best alternatives to date, with higher transmittances at a given sheet resistance compared to films of AgNWs and CNTs (Figure 57). In contrast to ITO, CuNW films can be flexed 1000 times without

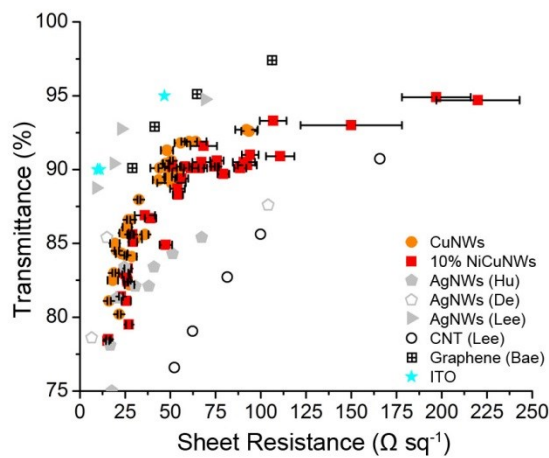
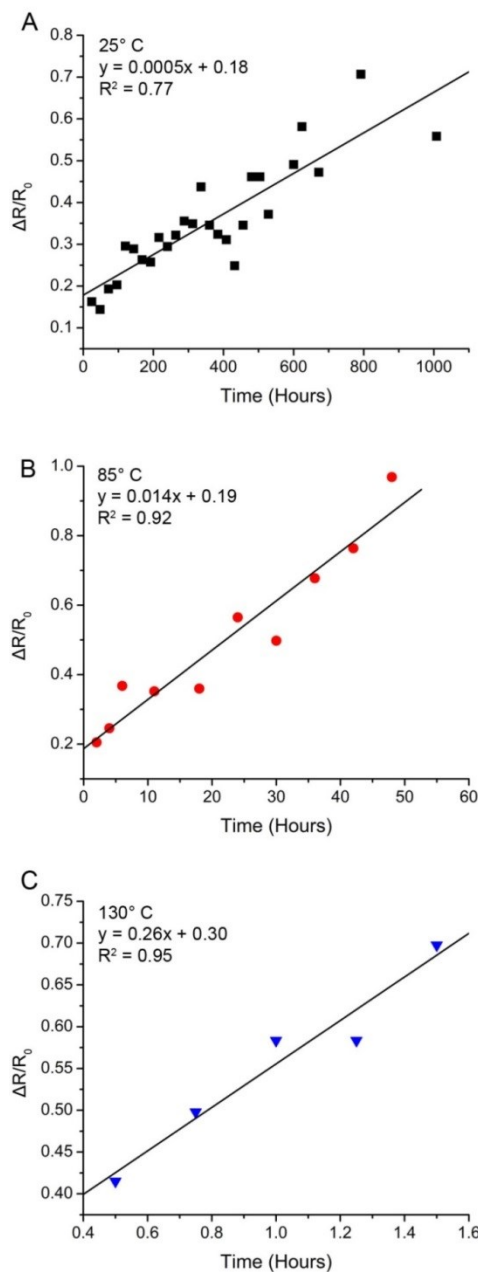


Figure 57: Plot of sheet resistance vs. transmittance comparing electrodes made with CuNWs,^{6, 7} NiCuNWs,⁷ AgNWs,^{38, 54, 56} CNT,²⁴ graphene,¹⁶ and ITO.

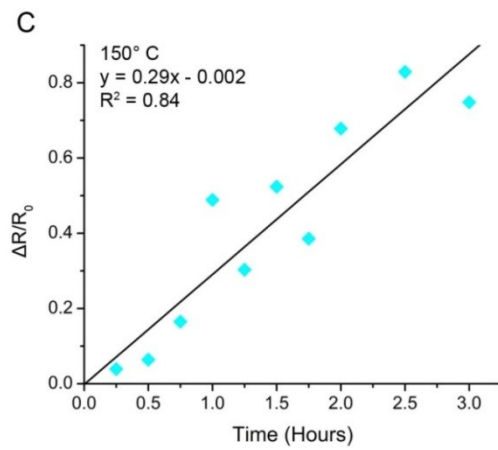
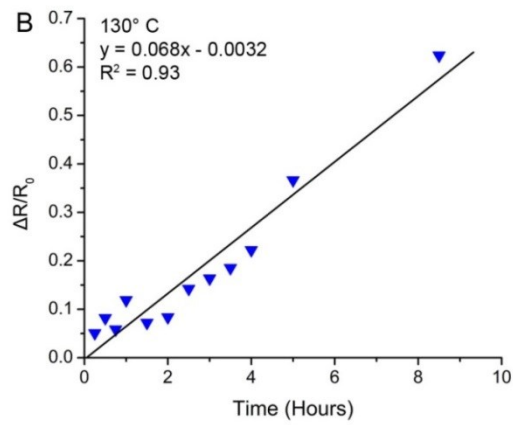
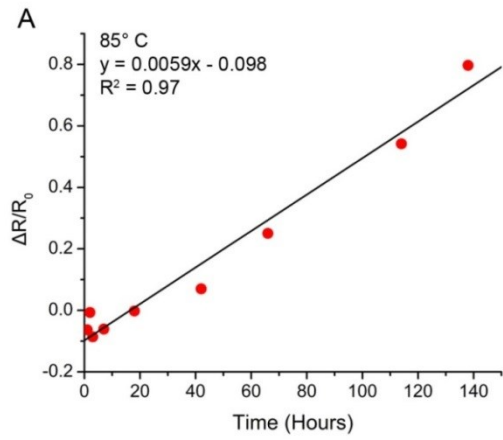
Degrading, and they are highly transparent in the near-infrared region. The CuNWs can also be coated with a layer of nickel to make them 1000 times more resistant to oxidation while giving them a more desirable grey color. Given that the properties of the CuNW and CuNiNW films are competitive with ITO films, and since both copper and nickel are 1000 times more abundant than silver and indium, I would expect these films to be

seriously considered in the production of lower-cost flexible displays, OLEDs, and thin-film photovoltaics.

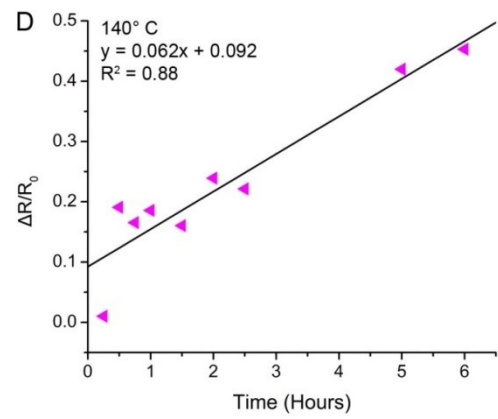
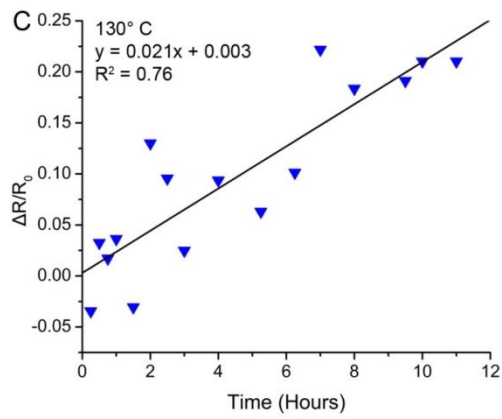
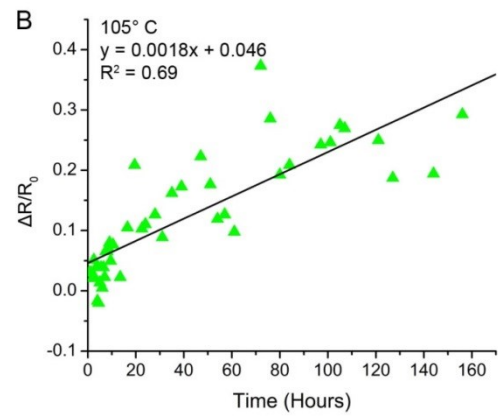
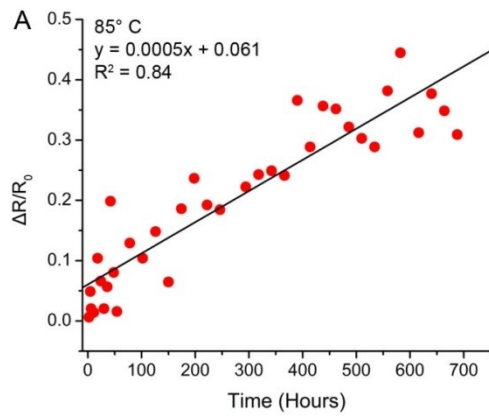
Appendix A: Oxidation Measurements of Cupronickel Nanowires at Different Temperatures⁷



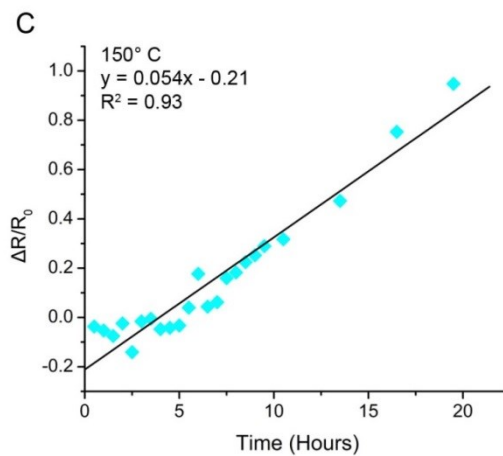
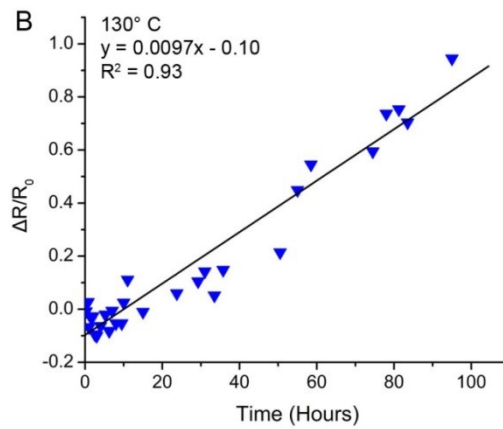
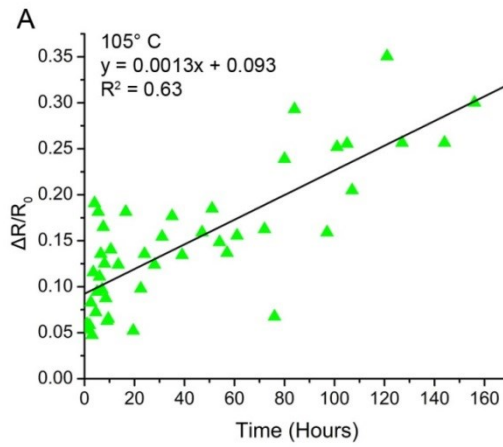
AB1: Plot of $\Delta R/R_0$ vs. time for copper nanowire films.



AB2: Plot of $\Delta R/R_0$ vs. time for silver nanowire films.



AB3: Plot of $\Delta R/R_0$ vs. time for 4:1 Cu:Ni nanowire films.



AB4: Plot of $\Delta R/R_0$ vs. time for 1:1 Cu:Ni nanowire films.

References

1. "Indium Tin Oxide and Alternative Transparent Conductor Markets" (NanoMarkets, LC, 2009).
2. K. Moskvitch. (BBC News Technology, 2012).
3. Slowbuddha. (www.ecofriendlydaily.com, 2011).
4. J. Feroso. (wired.com, 2008).
5. A. R. Rathmell, S. M. Bergin, Y.-L. Hua, Z.-Y. Li, B. J. Wiley, *The Growth Mechanism of Copper Nanowires and Their Properties in Flexible, Transparent Conducting Films*. *Adv. Mater.* **22**, (3558) 2010.
6. A. R. Rathmell, B. J. Wiley, *The Synthesis and Coating of Long, Thin Copper Nanowires to Make Flexible, Transparent Conducting Films on Plastic Substrates*. *Adv. Mater.* **23**, (4798) 2011.
7. A. R. Rathmell, M. Nguyen, M. Chi, B. J. Wiley, *Synthesis of Oxidation-Resistant Cupronickel Nanowires for Transparent Conducting Nanowire Networks*. *Nano Lett.* **12**, (3193) 2012/06/13, 2012.
8. S. M. Bergin, Y. H. Chen, A. R. Rathmell, P. Charbonneau, Z. Y. Li, B. J. Wiley, *The effect of nanowire length and diameter on the properties of transparent, conducting nanowire films*. *Nanoscale* **4**, (1996) 2012.
9. R. M. Mutiso, M. C. Sherrott, A. R. Rathmell, B. J. Wiley, K. I. Winey, *Nanowire Films for Transparent Conductors: Simulations of Sheet Resistance*. *Nano Lett.* submitted.
10. D. S. Hecht, L. Hu, G. Irvin, *Emerging Transparent Electrodes Based on Thin Films of Carbon Nanotubes, Graphene, and Metallic Nanostructures*. *Adv. Mater.* **23**, (1482) 2011.
11. U.S. Geological Survey, *Mineral Commodity Summaries. Indium.*, (2011).
12. C. K. Chiang, C. R. Fincher, Jr., Y. W. Park, A. J. Heeger, H. Shirakawa, E. J. Louis, S. C. Gau, A. G. MacDiarmid, *Electrical Conductivity in Doped Polyacetylene*. *Phys. Rev. Lett.* **39**, (1098) 1977.

13. H. Shirakawa, E. J. Louis, A. G. MacDiarmid, C. K. Chiang, A. J. Heeger, *Synthesis of electrically conducting organic polymers: halogen derivatives of polyacetylene, (CH)_x*. J. Chem. Soc., Chem. Commun. **16**, (578) 1977.
14. S. Kirchmeyer, K. Reuter, *Scientific importance, properties and growing applications of poly(3,4-ethylenedioxythiophene)*. J. Mater. Chem. **15**, (2077) 2005.
15. N. Q. Science, in *Graphene: Production, Properties, and Applications*. (NIST), vol. 2013.
16. S. Bae, H. Kim, Y. Lee, X. Xu, J.-S. Park, Y. Zheng, J. Balakrishnan, T. Lei, H. Ri Kim, Y. I. Song, Y.-J. Kim, K. S. Kim, B. Ozyilmaz, J.-H. Ahn, B. H. Hong, S. Iijima, *Roll-to-roll production of 30-inch graphene films for transparent electrodes*. Nat. Nano. **5**, (574) 2010.
17. X. Wan, G. Long, L. Huang, Y. Chen, *Graphene – A Promising Material for Organic Photovoltaic Cells*. Adv. Mater. **23**, (5342) 2011.
18. S. De, J. N. Coleman, *The effects of percolation in nanostructured transparent conductors*. MRS Bull. **36**, (774) 2011.
19. R. Po, C. Carbonera, A. Bernardi, F. Tinti, N. Camaioni, *Polymer- and carbon-based electrodes for polymer solar cells: Toward low-cost, continuous fabrication over large area*. Sol. Energy Mater. Sol. Cells **100**, (97) 2012.
20. D. S. Hecht, R. B. Kaner, *Solution-processed transparent electrodes*. MRS Bull. **36**, (749) 2011.
21. C. J. M. Emmott, A. Urbina, J. Nelson, *Environmental and economic assessment of ITO-free electrodes for organic solar cells*. Sol. Energy Mater. Sol. Cells **97**, (14) 2012.
22. Z. Wu, Z. Chen, X. Du, J. M. Logan, J. Sippel, M. Nikolou, K. Kamaras, J. R. Reynolds, D. B. Tanner, A. F. Hebard, A. G. Rinzler, *Transparent, Conductive Carbon Nanotube Films*. Science **305**, (1273) 2004.
23. C. Niu, *Carbon nanotube transparent conducting films*. MRS Bull. **36**, (766) 2011.
24. H. Z. Geng, K. K. Kim, K. P. So, Y. S. Lee, Y. Chang, Y. H. Lee, *Effect of acid treatment on carbon nanotube-based flexible transparent conducting films*. J. Am. Chem. Soc. **129**, (7758) 2007.

25. D. S. Hecht, A. M. Heintz, R. Lee, L. Hu, B. Moore, C. Cucksey, S. Risser, *High conductivity transparent carbon nanotube films deposited from superacid*. *Nanotechnology* **22**, (169501) 2011.
26. Y. Feng, X. Ju, W. Feng, H. Zhang, Y. Cheng, J. Liu, A. Fujii, M. Ozaki, K. Yoshino, *Organic solar cells using few-walled carbon nanotubes electrode controlled by the balance between sheet resistance and the transparency*. *Appl. Phys. Lett.* **94**, (123302) 2009.
27. M. Fahland, T. Vogt, W. Schoenberger, N. Schiller, *Optical properties of metal based transparent electrodes on polymer films*. *Thin Solid Films* **516**, (5777) 2008.
28. B. O'Connor, C. Haughn, K.-H. An, K. P. Pipe, M. Shtein, *Transparent and conductive electrodes based on unpatterned, thin metal films*. *Appl. Phys. Lett.* **93**, (223304) 2008.
29. R. B. Pode, C. J. Lee, D. G. Moon, J. I. Han, *Transparent conducting metal electrode for top emission organic light-emitting devices: Ca--Ag double layer*. *Appl. Phys. Lett.* **84**, (4614) 2004.
30. D. S. Ghosh, L. Martinez, S. Giurgola, P. Vergani, V. Pruneri, *Widely transparent electrodes based on ultrathin metals*. *Opt. Lett.* **34**, (325) 2009.
31. D. S. Ghosh, T. L. Chen, V. Pruneri, *High figure-of-merit ultrathin metal transparent electrodes incorporating a conductive grid*. *Appl. Phys. Lett.* **96**, (041109) 2010.
32. M. G. Kang, L. J. Guo, *Nanoimprinted Semitransparent Metal Electrodes and Their Application in Organic Light-Emitting Diodes*. *Adv. Mater.* **19**, (1391) 2007.
33. K. Myung-Gyu, P. Hui Joon, A. Se Hyun, X. Ting, L. J. Guo, *Toward Low-Cost, High-Efficiency, and Scalable Organic Solar Cells with Transparent Metal Electrode and Improved Domain Morphology*. *Journal of Selected Topics in Quantum Electronics, IEEE* **16**, (1807) 2010.
34. P. B. Catrysse, S. Fan, *Nanopatterned Metallic Films for Use As Transparent Conductive Electrodes in Optoelectronic Devices*. *Nano Lett.* **10**, (2944) 2010/08/11, 2010.
35. L. Hu, H. Wu, Y. Cui, *Metal nanogrids, nanowires, and nanofibers for transparent electrodes*. *MRS Bull.* **36**, (760) 2011.

36. J. van de Groep, P. Spinelli, A. Polman, *Transparent Conducting Silver Nanowire Networks*. Nano Lett. **12**, (3138) 2012.
37. J. Woerle, H. Rost, *Roll-to-roll production of transparent conductive films using metallic grids*. MRS Bull. **36**, (789) 2011.
38. J. Lee, P. Lee, H. Lee, D. Lee, S. S. Lee, S. H. Ko, *Very long Ag nanowire synthesis and its application in a highly transparent, conductive and flexible metal electrode touch panel*. Nanoscale **4**, (6408) 2012.
39. U.S. Geological Survey, *Mineral Commodity Summaries. Silver*. (2011).
40. U.S. Geological Survey, *Mineral Commodity Summaries. Copper*. (2011).
41. K. Fuchs, *The conductivity of thin metallic films according to the electron theory of metals*. Mathematical Proceedings of the Cambridge Philosophical Society **34**, (100) 1938.
42. R. B. Dingle, *The Electrical Conductivity of Thin Wires*. Proceedings of the Royal Society of London. Series A. Mathematical and Physical Sciences **201**, (545) 1950.
43. J. M. Ziman, *Electrons and Phonons*. (Clarendon Press, Oxford, 1960).
44. A. Bid, A. Bora, A. K. Raychaudhuri, *Temperature dependence of the resistance of metallic nanowires of diameter ≥ 15 nm: Applicability of Bloch-Grüneisen theorem*. Physical Review B **74**, (035426) 2006.
45. S. B. Soffer, *Statistical Model for the Size Effect in Electrical Conduction*. J. Appl. Phys. **38**, (1710) 1967.
46. J. R. Sambles, K. C. Elsom, T. W. Preist, *The resistivity of thin wires*. Journal of Physics F: Metal Physics **12**, (1169) 1982.
47. K. Critchley, B. P. Khanal, M. Ł. Górzny, L. Vigderman, S. D. Evans, E. R. Zubarev, N. A. Kotov, *Near-Bulk Conductivity of Gold Nanowires as Nanoscale Interconnects and the Role of Atomically Smooth Interface*. Adv. Mater. **22**, (2338) 2010.

48. R. L. Graham, G. B. Alers, T. Mountsier, N. Shamma, S. Dhuey, S. Cabrini, R. H. Geiss, D. T. Read, S. Peddetti, *Resistivity dominated by surface scattering in sub-50 nm Cu wires*. Appl. Phys. Lett. **96**, (042116) 2010.
49. M. M. Kolečnik, S. Hansel, T. Lutz, N. Kinahan, M. Boese, V. Krstić, *Resolving In Situ Specific-Contact, Current-Crowding, and Channel Resistivity in Nanowire Devices: A Case Study with Silver Nanowires*. Small **7**, (2873) 2011.
50. C. Durkan, M. E. Welland, *Size effects in the electrical resistivity of polycrystalline nanowires*. Physical Review B **61**, (14215) 2000.
51. A. F. Oskooi, D. Roundy, M. Ibanescu, P. Bermel, J. D. Joannopoulos, S. G. Johnson, *Meep: A flexible free-software package for electromagnetic simulations by the FDTD method*. Comput. Phys. Commun. **181**, (687) 2010.
52. P. B. Johnson, R. W. Christy, *Optical Constants of the Noble Metals*. Physical Review B **6**, (4370) 1972.
53. S. M. Bergin, Y.-H. Chen, A. R. Rathmell, P. Charbonneau, Z.-Y. Li, B. J. Wiley, *The effect of nanowire length and diameter on the properties of transparent, conducting nanowire films*. Nanoscale **4**, (1996) 2012.
54. S. De, T. M. Higgins, P. E. Lyons, E. M. Doherty, P. N. Nirmalraj, W. J. Blau, J. J. Boland, J. N. Coleman, *Silver Nanowire Networks as Flexible, Transparent, Conducting Films: Extremely High DC to Optical Conductivity Ratios*. ACS Nano **3**, (1767) Jul, 2009.
55. Y. C. Lu, K. S. Chou, *Tailoring of Silver Wires and their Performance as Transparent Conductive Coatings*. Nanotechnology **21**, (215707) May, 2010.
56. L. B. Hu, H. S. Kim, J. Y. Lee, P. Peumans, Y. Cui, *Scalable Coating and Properties of Transparent, Flexible, Silver Nanowire Electrodes*. ACS Nano **4**, (2955) May, 2010.
57. M. Žeželj, I. Stanković, *From percolating to dense random stick networks: Conductivity model investigation*. Physical Review B **86**, (134202) 2012.
58. P. Keblinski, F. Cleri, *Contact resistance in percolating networks*. Physical Review B **69**, (184201) 2004.

59. G. E. Pike, C. H. Seager, *Percolation and Conductivity: A Computer Study. I.* Phys. Rev. B **10**, (1421) 1974.
60. J. Li, S.-L. Zhang, *Conductivity exponents in stick percolation.* Physical Review E **81**, (021120) 2010.
61. Y. Sun, B. Gates, B. Mayers, Y. Xia, *Crystalline Silver Nanowires by Soft Solution Processing.* Nano Lett. **2**, (165) 2002/02/01, 2002.
62. Y. Sun, Y. Xia, *Large-Scale Synthesis of Uniform Silver Nanowires Through a Soft, Self-Seeding, Polyol Process.* Adv. Mater. **14**, (833) 2002.
63. Y. Sun, Y. Yin, B. T. Mayers, T. Herricks, Y. Xia, *Uniform Silver Nanowires Synthesis by Reducing AgNO₃ with Ethylene Glycol in the Presence of Seeds and Poly(Vinyl Pyrrolidone).* Chem. Mater. **14**, (4736) 2002/11/01, 2002.
64. S. E. Skrabalak, B. J. Wiley, M. Kim, E. V. Formo, Y. Xia, *On the Polyol Synthesis of Silver Nanostructures: Glycolaldehyde as a Reducing Agent.* Nano Lett. **8**, (2077) 2008.
65. Y. G. Sun, B. Mayers, T. Herricks, Y. N. Xia, *Polyol Synthesis of Uniform Silver Nanowires: A Plausible Growth Mechanism and the Supporting Evidence.* Nano Lett. **3**, (955) Jul, 2003.
66. B. Wiley, Y. Sun, Y. Xia, *Synthesis of Silver Nanostructures with Controlled Shapes and Properties.* Acc. Chem. Res. **40**, (1067) 2007.
67. K. E. Korte, S. E. Skrabalak, Y. Xia, *Rapid synthesis of silver nanowires through a CuCl- or CuCl₂-mediated polyol process.* J. Mater. Chem. **18**, (437) 2008.
68. X. Xu, X. Luo, H. Zhuang, W. Li, B. Zhang, *Electroless silver coating on fine copper powder and its effects on oxidation resistance.* Mater. Lett. **57**, (3987) 2003.
69. Y. Chang, M. L. Lye, H. C. Zeng, *Large-Scale Synthesis of High-Quality Ultralong Copper Nanowires.* Langmuir **21**, (3746) 2005/04/01, 2005.
70. Y.-Y. H. Chao, D. R. Kearns, *Electron spin resonance investigation of the soluble blue copper(II) hydroxide complex.* The Journal of Physical Chemistry **81**, (666) 1977/04/01, 1977.

71. J. Chen, T. Herricks, M. Geissler, Y. Xia, *Single-Crystal Nanowires of Platinum Can Be Synthesized by Controlling the Reaction Rate of a Polyol Process*. *J. Am. Chem. Soc.* **126**, (10854) 2004.
72. E. P. Lee, J. Chen, Y. Yin, C. T. Campbell, Y. Xia, *Pd-Catalyzed Growth of Pt Nanoparticles or Nanowires as Dense Coatings on Polymeric and Ceramic Particulate Supports*. *Adv. Mater.* **18**, (3271) 2006.
73. T. D. Daff, I. Saadoune, I. Lisiecki, N. H. de Leeuw, *Computer simulations of the effect of atomic structure and coordination on the stabilities and melting behaviour of copper surfaces and nano-particles*. *Surf. Sci.* **603**, (445) 2009.
74. M. I. Baskes, *Modified embedded-atom potentials for cubic materials and impurities*. *Physical Review B* **46**, (2727) 1992.
75. I. Galanakis, N. Papanikolaou, P. H. Dederichs, *Applicability of the broken-bond rule to the surface energy of the fcc metals*. *Surf. Sci.* **511**, (1) 2002.
76. Y. Wang, T. Herricks, Y. Xia, *Single Crystalline Nanowires of Lead Can Be Synthesized through Thermal Decomposition of Lead Acetate in Ethylene Glycol*. *Nano Lett.* **3**, (1163) 2003/08/01, 2003.
77. Y. Wang, X. Jiang, T. Herricks, Y. Xia, *Single Crystalline Nanowires of Lead: Large-Scale Synthesis, Mechanistic Studies, and Transport Measurements†*. *The Journal of Physical Chemistry B* **108**, (8631) 2004/06/01, 2004.
78. M. Singh, J. Wang, M. Tian, Q. Zhang, A. Pereira, N. Kumar, T. E. Mallouk, M. H. W. Chan, *Synthesis and Superconductivity of Electrochemically Grown Single-Crystal Aluminum Nanowires*. *Chem. Mater.* **21**, (5557) 2009/12/08, 2009.
79. K. S. Byung Hee Hong, Sung Chul Bae, Chi-Wan Lee, Sukmin Jeong, Kim, *Ultrathin Single-Crystalline Silver Nanowire Arrays Formed in an Ambient Solution Phase*. *Science* **294**, (348) 2001.
80. M. Hu, P. Hillyard, G. V. Hartland, T. Kosel, J. Perez-Juste, P. Mulvaney, *Determination of the Elastic Constants of Gold Nanorods Produced by Seed Mediated Growth*. *Nano Lett.* **4**, (2493) 2004/12/01, 2004.

81. X. Lu, M. S. Yavuz, H.-Y. Tuan, B. A. Korgel, Y. Xia, *Ultrathin Gold Nanowires Can Be Obtained by Reducing Polymeric Strands of Oleylamine–AuCl Complexes Formed via Auophilic Interaction*. *J. Am. Chem. Soc.* **130**, (8900) 2008/07/01, 2008.
82. N. Zettsu, J. M. McLellan, B. Wiley, Y. D. Yin, Z. Y. Li, Y. N. Xia, *Synthesis, stability, and surface plasmonic properties of rhodium multipods, and their use as substrates for surface-enhanced Raman scattering*. *Angewandte Chemie-International Edition* **45**, (1288) 2006.
83. S. Zhang, H. C. Zeng, *Solution-Based Epitaxial Growth of Magnetically Responsive Cu@Ni Nanowires*. *Chem. Mater.* **22**, (1282) 2010/02/23, 2010.
84. M. Mohl, P. Pusztai, A. Kukovecz, Z. Konya, J. Kukkola, K. Kordas, R. Vajtai, P. M. Ajayan, *Low-Temperature Large-Scale Synthesis and Electrical Testing of Ultralong Copper Nanowires†*. *Langmuir* **26**, (16496) 2010/11/02, 2010.
85. M. Jin, G. He, H. Zhang, J. Zeng, Z. Xie, Y. Xia, *Shape-Controlled Synthesis of Copper Nanocrystals in an Aqueous Solution with Glucose as a Reducing Agent and Hexadecylamine as a Capping Agent*. *Angew. Chem. Int. Ed.* **50**, (10560) 2011.
86. A. Halder, N. Ravishankar, *Ultrafine Single-Crystalline Gold Nanowire Arrays by Oriented Attachment*. *Adv. Mater.* **19**, (1854) 2007.
87. Z. Huo, C.-k. Tsung, W. Huang, X. Zhang, P. Yang, *Sub-Two Nanometer Single Crystal Au Nanowires*. *Nano Lett.* **8**, (2041) 2008/07/01, 2008.
88. N. s. Pazos-Pérez, D. Baranov, S. Irsen, M. Hilgendorff, L. M. Liz-Marzán, M. Giersig, *Synthesis of Flexible, Ultrathin Gold Nanowires in Organic Media*. *Langmuir* **24**, (9855) 2008/09/02, 2008.
89. C. Wang, Y. Hu, C. M. Lieber, S. Sun, *Ultrathin Au Nanowires and Their Transport Properties*. *J. Am. Chem. Soc.* **130**, (8902) 2008/07/01, 2008.
90. H. Feng, Y. Yang, Y. You, G. Li, J. Guo, T. Yu, Z. Shen, T. Wu, B. Xing, *Simple and rapid synthesis of ultrathin gold nanowires, their self-assembly and application in surface-enhanced Raman scattering*. *Chem. Commun.* **0**, (1984) 2009.
91. C. Wang, Y. Hou, J. Kim, S. Sun, *A General Strategy for Synthesizing FePt Nanowires and Nanorods*. *Angew. Chem. Int. Ed.* **46**, (6333) 2007.

92. B.-K. Pong, J.-Y. Lee, B. L. Trout, *First Principles Computational Study for Understanding the Interactions between ssDNA and Gold Nanoparticles: Adsorption of Methylamine on Gold Nanoparticulate Surfaces*. *Langmuir* **21**, (11599) 2005/12/01, 2005.
93. A. Kisner, M. Heggen, E. Fernández, S. Lenk, D. Mayer, U. Simon, A. Offenhäusser, Y. Mourzina, *The Role of Oxidative Etching in the Synthesis of Ultrathin Single-Crystalline Au Nanowires*. *Chemistry – A European Journal* **17**, (9503) 2011.
94. B. Wiley, T. Herricks, Y. G. Sun, Y. N. Xia, *Polyol synthesis of silver nanoparticles: Use of chloride and oxygen to promote the formation of single-crystal, truncated cubes and tetrahedrons*. *Nano Lett.* **4**, (1733) Sep, 2004.
95. Y. Xiong, Y. Xia, *Shape-Controlled Synthesis of Metal Nanostructures: The Case of Palladium*. *Adv. Mater.* **19**, (3385) 2007.
96. H. Hofmeister, S. A. Nepijko, D. N. Ievlev, W. Schulze, G. Ertl, *Composition and lattice structure of fivefold twinned nanorods of silver*. *J. Cryst. Growth* **234**, (773) 2002.
97. N. R. Jana, L. Gearheart, S. O. Obare, C. J. Murphy, *Anisotropic Chemical Reactivity of Gold Spheroids and Nanorods*. *Langmuir* **18**, (922) 2002/02/01, 2002.
98. A. Henglein, *Physicochemical properties of small metal particles in solution: "microelectrode" reactions, chemisorption, composite metal particles, and the atom-to-metal transition*. *The Journal of Physical Chemistry* **97**, (5457) 1993/05/01, 1993.
99. X. Hou, X. Zhang, Y. Fang, S. Chen, N. Li, Q. Zhou, *Synthesis of SERS active Au nanowires in different noncoordinating solvents*. *J. Nanopart. Res.* **13**, (2625) 2011/06/01, 2011.
100. X. Hou, X. Zhang, S. Chen, Y. Fang, N. Li, X. Zhai, Y. Liu, *Size-controlled synthesis of Au nanoparticles and nanowires and their application as SERS substrates*. *Colloids and Surfaces A: Physicochemical and Engineering Aspects* **384**, (345) 2011.
101. J. Y. Lee, S. T. Connor, Y. Cui, P. Peumans, *Solution-Processed Metal Nanowire Mesh Transparent Electrodes*. *Nano Lett.* **8**, (689) Feb, 2008.

102. W. Gaynor, J. Y. Lee, P. Peumans, *Fully Solution-Processed Inverted Polymer Solar Cells with Laminated Nanowire Electrodes*. *ACS Nano* **4**, (30) Jan, 2009.
103. B. E. Hardin, W. Gaynor, I. K. Ding, S.-B. Rim, P. Peumans, M. D. McGehee, *Laminating solution-processed silver nanowire mesh electrodes onto solid-state dye-sensitized solar cells*. *Org. Electron.* **12**, (875) 2011.
104. J. Jiu, M. Nogi, T. Sugahara, T. Tokuno, T. Araki, N. Komoda, K. Suganuma, H. Uchida, K. Shinozaki, *Strongly adhesive and flexible transparent silver nanowire conductive films fabricated with a high-intensity pulsed light technique*. *J. Mater. Chem.* **22**, (23561) 2012.
105. W. Hu, X. Niu, L. Li, S. Yun, Z. Yu, Q. Pei, *Intrinsically stretchable transparent electrodes based on silver-nanowire-crosslinked-polyacrylate composites*. *Nanotechnology* **23**, (344002) 2012.
106. F. Xu, Y. Zhu, *Highly Conductive and Stretchable Silver Nanowire Conductors*. *Adv. Mater.* **24**, (5117) 2012.
107. S. Yun, X. Niu, Z. Yu, W. Hu, P. Brochu, Q. Pei, *Compliant Silver Nanowire-Polymer Composite Electrodes for Bistable Large Strain Actuation*. *Adv. Mater.* **24**, (1321) 2012.
108. Z. Yu, Q. Zhang, L. Li, Q. Chen, X. Niu, J. Liu, Q. Pei, *Highly Flexible Silver Nanowire Electrodes for Shape-Memory Polymer Light-Emitting Diodes*. *Adv. Mater.* **23**, (664) 2011.
109. Y. Wang, T. Feng, K. Wang, M. Qian, Y. Chen, Z. Sun, *A facile method for preparing transparent, conductive, and paper-like silver nanowire films*. *J. Nanomaterials* **2011**, (1) 2011.
110. X. Ho, J. N. Tey, W. Liu, C. K. Cheng, J. Wei, *Biaxially stretchable silver nanowire transparent conductors*. *J. Appl. Phys.* **113**, (044311) 2013.
111. D. Zhang, R. Wang, M. Wen, D. Weng, X. Cui, J. Sun, H. Li, Y. Lu, *Synthesis of Ultralong Copper Nanowires for High-Performance Transparent Electrodes*. *J. Am. Chem. Soc.* **134**, (14283) 2012/09/05, 2012.
112. P. Lee, J. Lee, H. Lee, J. Yeo, S. Hong, K. H. Nam, D. Lee, S. S. Lee, S. H. Ko, *Highly Stretchable and Highly Conductive Metal Electrode by Very Long Metal Nanowire Percolation Network*. *Adv. Mater.* **24**, (3326) 2012.

113. P. E. Lyons, S. De, J. Elias, M. Schamel, L. Philippe, A. T. Bellew, J. J. Boland, J. N. Coleman, *High-Performance Transparent Conductors from Networks of Gold Nanowires*. *The Journal of Physical Chemistry Letters* **2**, (3058) 2011/12/15, 2011.
114. C. Celle, C. Mayousse, E. Moreau, H. Basti, A. Carella, J.-P. Simonato, *Highly flexible transparent film heaters based on random networks of silver nanowires*. *Nano Res.* **5**, (427) 2012/06/01, 2012.
115. J. Spechler, C. Arnold, *Direct-write pulsed laser processed silver nanowire networks for transparent conducting electrodes*. *Appl. Phys. A* **108**, (25) 2012/07/01, 2012.
116. Y. Ahn, Y. Jeong, Y. Lee, *Improved Thermal Oxidation Stability of Solution-Processable Silver Nanowire Transparent Electrode by Reduced Graphene Oxide*. *ACS Applied Materials & Interfaces* **4**, (6410) 2012/12/26, 2012.
117. T.-G. Chen, B.-Y. Huang, H.-W. Liu, Y.-Y. Huang, H.-T. Pan, H.-F. Meng, P. Yu, *Flexible Silver Nanowire Meshes for High-Efficiency Microtextured Organic-Silicon Hybrid Photovoltaics*. *ACS Applied Materials & Interfaces* **4**, (6857) 2012/12/26, 2012.
118. T. L. Belenkova, D. Rimmerman, E. Mentovich, H. Gilon, N. Hendler, S. Richter, G. Markovich, *UV induced formation of transparent Au-Ag nanowire mesh film for repairable OLED devices*. *J. Mater. Chem.* **22**, (24042) 2012.
119. L.-H. Chen, P. Lin, M.-C. Chen, P.-Y. Huang, C. Kim, J.-C. Ho, C.-C. Lee, *Silver nanowire-polymer composite electrode for high performance solution-processed thin-film transistors*. *Org. Electron.* **13**, (1881) 2012.
120. C.-H. Chung, T.-B. Song, B. Bob, R. Zhu, H.-S. Duan, Y. Yang, *Silver Nanowire Composite Window Layers for Fully Solution-Deposited Thin-Film Photovoltaic Devices*. *Adv. Mater.* **24**, (5499) 2012.
121. C.-T. Hsieh, D.-Y. Tzou, C. Pan, W.-Y. Chen, *Microwave-assisted deposition, scalable coating, and wetting behavior of silver nanowire layers*. *Surf. Coat. Technol.* **207**, (11) 2012.
122. C.-C. Chen, L. Dou, R. Zhu, C.-H. Chung, T.-B. Song, Y. B. Zheng, S. Hawks, G. Li, P. S. Weiss, Y. Yang, *Visibly Transparent Polymer Solar Cells Produced by Solution Processing*. *ACS Nano* **6**, (7185) 2012/08/28, 2012.

123. D.-S. Leem, A. Edwards, M. Faist, J. Nelson, D. D. C. Bradley, J. C. de Mello, *Efficient Organic Solar Cells with Solution-Processed Silver Nanowire Electrodes*. *Adv. Mater.* **23**, (4371) 2011.
124. J. Ajuria, I. Ugarte, W. Cambarau, I. Etxebarria, R. Tena-Zaera, R. Pacios, *Insights on the working principles of flexible and efficient ITO-free organic solar cells based on solution processed Ag nanowire electrodes*. *Sol. Energy Mater. Sol. Cells* **102**, (148) 2012.
125. L. Yang, T. Zhang, H. Zhou, S. C. Price, B. J. Wiley, W. You, *Solution-Processed Flexible Polymer Solar Cells with Silver Nanowire Electrodes*. *ACS Applied Materials & Interfaces* **3**, (4075) 2011/10/26, 2011.
126. D. Y. Choi, H. W. Kang, H. J. Sung, S. S. Kim, *Annealing-free, flexible silver nanowire-polymer composite electrodes via a continuous two-step spray-coating method*. *Nanoscale* **5**, (977) 2013.
127. A. Afal, S. Coskun, H. E. Unalan, *All solution processed, nanowire enhanced ultraviolet photodetectors*. *Appl. Phys. Lett.* **102**, (043503) 2013.
128. I. N. Kholmanov, S. H. Domingues, H. Chou, X. Wang, C. Tan, J.-Y. Kim, H. Li, R. Piner, A. J. G. Zarbin, R. S. Ruoff, *Reduced Graphene Oxide/Copper Nanowire Hybrid Films as High-Performance Transparent Electrodes*. *ACS Nano*, 2013.
129. T. Kim, A. Canlier, G. H. Kim, J. Choi, M. Park, S. M. Han, *Electrostatic Spray Deposition of Highly Transparent Silver Nanowire Electrode on Flexible Substrate*. *ACS Applied Materials & Interfaces* **5**, (788) 2013/02/13, 2012.
130. T. Akter, W. S. Kim, *Reversibly Stretchable Transparent Conductive Coatings of Spray-Deposited Silver Nanowires*. *ACS Applied Materials & Interfaces* **4**, (1855) 2012/04/25, 2012.
131. A. K. Anuj R. Madaria, Chongwu Zhou, *Large scale, highly conductive and patterned transparent films of silver nanowires on arbitrary substrates and their application in touch screens*. *Nanotechnology* **22**, (7) 2011.
132. V. Scardaci, R. Coull, P. E. Lyons, D. Rickard, J. N. Coleman, *Spray Deposition of Highly Transparent, Low-Resistance Networks of Silver Nanowires over Large Areas*. *Small* **7**, (2621) 2011.

133. S. Sorel, U. Khan, J. N. Coleman, *Flexible, transparent dielectric capacitors with nanostructured electrodes*. Appl. Phys. Lett. **101**, (103106) 2012.
134. V. Scardaci, R. Coull, J. N. Coleman, *Very thin transparent, conductive carbon nanotube films on flexible substrates*. Appl. Phys. Lett. **97**, Jul, 2010.
135. V. Scardaci, R. Coull, P. E. Lyons, D. Rickard, J. N. Coleman, *Spray Deposition of Highly Transparent, Low-Resistance Networks of Silver Nanowires over Large Areas*. Small **7**, (8) 2011.
136. R. Zhu, C.-H. Chung, K. C. Cha, W. Yang, Y. B. Zheng, H. Zhou, T.-B. Song, C.-C. Chen, P. S. Weiss, G. Li, Y. Yang, *Fused Silver Nanowires with Metal Oxide Nanoparticles and Organic Polymers for Highly Transparent Conductors*. ACS Nano **5**, (9877) 2011/12/27, 2011.
137. J. Kim, I. Maeng, J. Jung, H. Song, J.-H. Son, K. Kim, J. Lee, C.-H. Kim, G. Chae, M. Jun, Y. Hwang, S. J. Lee, J.-M. Myoung, H. Choi, *Terahertz time-domain measurement of non-Drude conductivity in silver nanowire thin films for transparent electrode applications*. Appl. Phys. Lett. **102**, (011109) 2013.
138. L. Hu, G. Zheng, J. Yao, N. Liu, B. Weil, M. Eskilsson, E. Karabulut, Z. Ruan, S. Fan, J. T. Bloking, M. D. McGehee, L. Wagberg, Y. Cui, *Transparent and conductive paper from nanocellulose fibers*. Energy & Environmental Science **6**, (513) 2013.
139. M. Hu, J. Gao, Y. Dong, K. Li, G. Shan, S. Yang, R. K.-Y. Li, *Flexible Transparent PES/Silver Nanowires/PET Sandwich-Structured Film for High-Efficiency Electromagnetic Interference Shielding*. Langmuir **28**, (7101) 2012/05/08, 2012.
140. A. Sánchez-Iglesias, B. Rivas-Murias, M. Grzelczak, J. Pérez-Juste, L. M. Liz-Marzán, F. Rivadulla, M. A. Correa-Duarte, *Highly Transparent and Conductive Films of Densely Aligned Ultrathin Au Nanowire Monolayers*. Nano Lett. **12**, (6066) 2012/12/12, 2012.
141. E. C. Garnett, W. Cai, J. J. Cha, F. Mahmood, S. T. Connor, M. Greyson Christoforo, Y. Cui, M. D. McGehee, M. L. Brongersma, *Self-limited plasmonic welding of silver nanowire junctions*. Nat Mater **11**, (241) 2012.
142. S. Guo, *The creation of nanojunctions*. Nanoscale **2**, (2521) 2010.

143. J. S. Kang, J. Ryu, H. S. Kim, H. T. Hahn, *Sintering of Inkjet-Printed Silver Nanoparticles at Room Temperature Using Intense Pulsed Light*. J. Electron. Mater. **40**, (2268) 2011/11/01, 2011.
144. H. S. Kim, S. R. Dhage, D. E. Shim, H. T. Hahn, *Intense pulsed light sintering of copper nanoink for printed electronics*. Applied Physics a-Materials Science & Processing **97**, (791) Dec, 2009.
145. J. Ryu, H.-S. Kim, H. T. Hahn, *Reactive Sintering of Copper Nanoparticles Using Intense Pulsed Light for Printed Electronics*. J. Electron. Mater. **40**, (42) 2011/01/01, 2011.
146. J. H. Lee, P. Lee, D. Lee, S. S. Lee, S. H. Ko, *Large-Scale Synthesis and Characterization of Very Long Silver Nanowires via Successive Multistep Growth*. Crystal Growth & Design **12**, (5598) 2012/11/07, 2012.
147. V. V. Diev, K. Hanson, J. D. Zimmerman, S. R. Forrest, M. E. Thompson, *Fused Pyrene–Diporphyrins: Shifting Near-Infrared Absorption to 1.5 μm and Beyond*. Angew. Chem. Int. Ed. **49**, (5523) 2010.
148. J. D. Zimmerman, V. V. Diev, K. Hanson, R. R. Lunt, E. K. Yu, M. E. Thompson, S. R. Forrest, *Porphyrin-Tape/C60 Organic Photodetectors with 6.5% External Quantum Efficiency in the Near Infrared*. Adv. Mater. **22**, (2780) 2010.
149. J. D. Zimmerman, E. K. Yu, V. V. Diev, K. Hanson, M. E. Thompson, S. R. Forrest, *Use of additives in porphyrin-tape/C60 near-infrared photodetectors*. Org. Electron. **12**, (869) 2011.
150. X. H. Chen, L. Lu, K. Lu, *Electrical resistivity of ultrafine-grained copper with nanoscale growth twins*. J. Appl. Phys. **102**, (083708) 2007.
151. *Copper-nickel alloys: Basic engineering data*. (International Nickel Company, New York, 1970).
152. J. E. Castle, M. Nasserian-Riabi, *The oxidation of cupronickel alloys—I. XPS study of inter-diffusion*. Corros. Sci. **15**, (537) 1975.
153. A. Yabuki, S. Tanaka, *Oxidation behavior of copper nanoparticles at low temperature*. Mater. Res. Bull. **46**, (2323) 2011.

154. A. R. H. Fisher, *J. Inst. Met* **89**, (65) 1960-1961.
155. O. K. B. E. Hopkins, *The Oxidation of Metals and Alloys*. (Butterworths Scientific Publications, London, 1953).
156. K. L. Chavez, D. W. Hess, *A Novel Method of Etching Copper Oxide Using Acetic Acid*. *J. Electrochem. Soc.* **148**, (G640) January 1, 2001, 2001.
157. J. F. Rohan, G. O'Riordan, J. Boardman, *Selective electroless nickel deposition on copper as a final barrier/bonding layer material for microelectronics applications*. *Appl. Surf. Sci.* **185**, (289) 2002.
158. F. Z. Kong, X. B. Zhang, W. Q. Xiong, F. Liu, W. Z. Huang, Y. L. Sun, J. P. Tu, X. W. Chen, *Continuous Ni-layer on multiwall carbon nanotubes by an electroless plating method*. *Surf. Coat. Technol.* **155**, (33) 2002.

Biography

Born: Aaron Robert Rathmell December 30, 1985 in Lewisburg, PA to Jeffrey and Julia Rathmell.

Education

Ph.D. Duke University 2008-2013

Major: Chemistry (Nanoscience Certificate)

Advisor: Dr. Benjamin Wiley

Dissertation: Metal Nanowires: Synthesis, Processing, and Structure-Property Relationships in the Context of Flexible Transparent Conducting Films

B.S. Millersville University 2004-2008

Major: Chemistry

Advisor: Dr. Edward Rajaseelan

Thesis: Imidazole Based N-Heterocyclic Carbene Complexes

Teaching Experience

Teaching Assistant Duke University

Organic Chemistry Laboratory and Recitation Instructor 2008-2009

Awards and Fellowships

MRS Graduate Student Silver Award 2013

Kathleen Zielek Fellowship, *Duke University* 2013

MRSEC Fellow, *Duke University* 2011 - 2013

Paul M. Gross Fellowship, *Duke University* 2011

GP Nanoscience Fellow, *Duke University* 2010

Publications

1. **Rathmell, A. R.**; Bergin, S. M.; Hua, Y. L.; Li, Z. Y.; Wiley, B. J. *The Growth Mechanism of Copper Nanowires and their Properties in Flexible, Transparent Conducting Films*. *Adv. Mater.* 2010, 22, 3558-3563.

2. **Rathmell, A. R.;** Wiley, B. J. *The Synthesis and Coating of Long, Thin Copper Nanowires to make Flexible, Transparent Conducting Films on Plastic Substrates*. *Adv. Mater.* 2011, 23, 4798-4803.
3. Xu, J., Wilson, A. R., **Rathmell, A. R.**, Howe, J., Chi, M., Wiley, B. J. *Synthesis of Au-Pd Nanoflowers through Nanocluster Assembly*. *ACS Nano*. 2011, 5, 6119-6127.
4. Bergin, S. M., **Rathmell, A. R.**, Chen, Y., Charbonneau, P., Li, Z., Wiley, B. J. *The Effect of Nanowire Length and Width on the Properties of Transparent Conducting Films*. *Nanoscale*. 2012, 4, 1996-2004.
5. **Rathmell, A. R.**, Nguyen, M., Chi, M., Wiley, B. J. *Synthesis of Oxidation-Resistant Cupronickel Nanowires for Transparent Conducting Nanowire Networks*. *Nano Lett.* 2012, 12, 3913.

Publications in Preparation

1. **Rathmell, Aaron;** Wiley, Benjamin. *Room Temperature Synthesis of Copper and Cupronickel Nanowire Networks and Their Applications in Solar Cells*.
2. Wu, Jianghong; Zeng, Jianfeng; **Rathmell, Aaron;** Zhao, Xuanhe; Wiley, Benjamin. *Reversible Sliding in Networks of Nanowires*. (submitted to NanoLetters)
3. Ye, Shengrong; **Rathmell, Aaron;** Wiley, Benjamin. *Controlled Growth of Ultra Skinny Copper Nanowires and Their Incorporation into Transparent Conductors*.
4. Mutiso, Rose; Sherrott, Michelle; **Rathmell, Aaron;** Wiley, Benjamin; Winey, Karen. *Thin-Film Nanowire Networks for Transparent Conductor Applications: Simulations of Sheet Resistance and Percolation Thresholds*. (submitted to NanoLetters)
5. Copper Nanowire Network Perspective, an invitation from Advanced Materials.

Presentations

1. *The Synthesis and Coating of Long, Thin Copper Nanowires to make Flexible Transparent Conducting Films on Plastic Substrates*. A. R. Rathmell and B. J. Wiley. 3rd Annual Triangle Soft Matter Workshop at UNC Chapel Hill, NC, August 22, 2011.
2. *The Synthesis and Coating of Long, Thin Copper Nanowires to make Flexible Transparent Conducting Films on Plastic Substrates*. A. R. Rathmell and B. J. Wiley. 2011 FIP Symposium at Duke University NC, October 10, 2011.
3. *Synthesis of Oxidation-Resistant Cupronickel Nanowires for Transparent Conducting Nanowire Networks*. A.R. Rathmell, M. Nguyen, M. Chi, and B. J. Wiley. 2012 Gordon

Research Conference: Noble Metal Nanoparticles at Mount Holyoke College, MA, June 2012.

4. *Flexible, Transparent, Conducting Networks of Copper Nanowires*. A. R. Rathmell and B. J. Wiley. 2013 MRS Spring Meeting, San Francisco, CA, April 2013.